# Process time optimization of robotic remote laser cutting by utilizing customized beam patterns and redundancy space task sequencing

Villumsen, Sigurd

*DOI (link to publication from Publisher):*
10.5278/vbn.phd.engsci.00080

*Publication date:*
2016

*Document Version*
Publisher's PDF, also known as Version of record

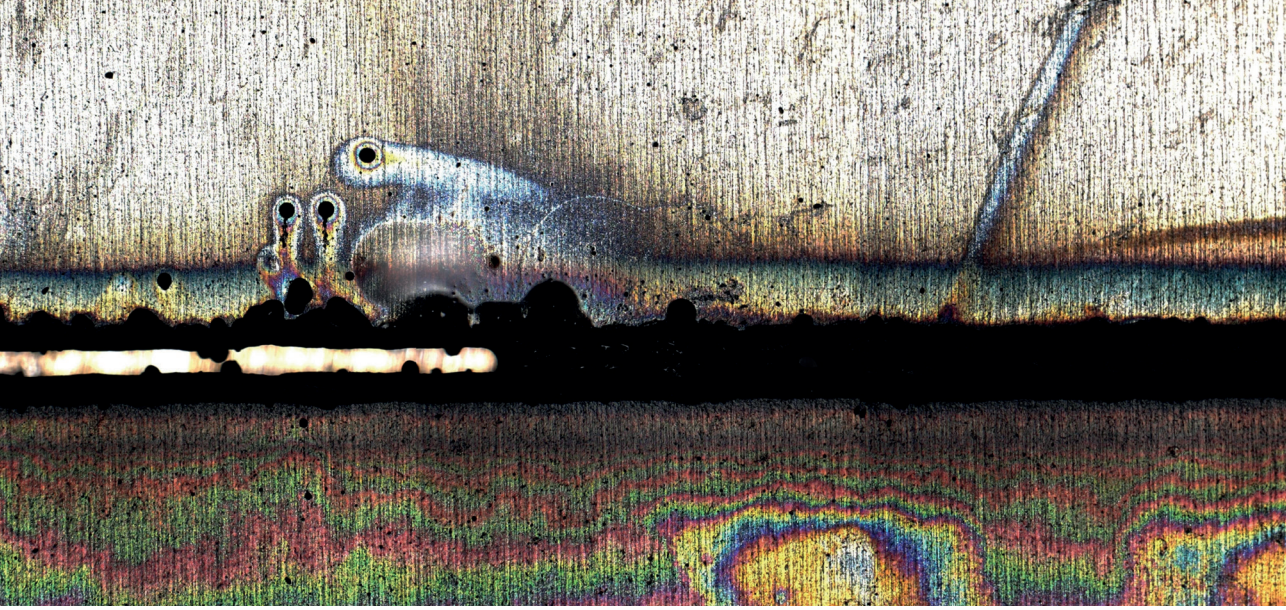

# PROCESS TIME OPTIMIZATION OF ROBOTIC REMOTE LASER CUTTING BY UTILIZING CUSTOMIZED BEAM PATTERNS AND REDUNDANCY SPACE TASK SEQUENCING


**BY**
**SIGURD LAZIC VILLUMSEN**


DISSERTATION SUBMITTED 2016


AALBORG UNIVERSITY
DENMARK

# Process time optimization of robotic remote laser cutting by utilizing customized beam patterns and redundancy space task sequencing

Ph.D. Dissertation

Sigurd Lazic Villumsen

Dissertation submitted March, 2016

Dissertation submitted: March, 2016

PhD supervisor: Associate Prof. Morten Kristiansen
Aalborg University

PhD committee: Associate Professor Benny Endelt (chairman)
Aalborg University

Senior Researcher András Kovács
Hungarian Academy of Sciences (MTA SZTAKI)

Professor Henrik G. Petersen
University of Southern Denmark

PhD Series: Faculty of Engineering and Science, Aalborg University

ISSN (online): 2246-1248
ISBN (online): 978-87-7112-539-9

Published by:
Aalborg University Press
Skjernvej 4A, 2nd floor
DK – 9220 Aalborg Ø
Phone: +45 99407140
aauf@forlag.aau.dk
forlag.aau.dk



Printed in Denmark by Rosendahls, 2016

# Preface

This dissertation is written as a part of the ROBOCUT project which is partly funded by the Danish National Advanced Technology Foundation (Højteknologifonden - HTF) [52] and several industrial partners. These include IPU [53], Grundfos [34], Ib Andresen Industries [51], Micronix. Furthermore two foreign partners are involved, KUKA Roboter GMBH [103] and Volvo [95].

The dissertation presents the obtained results from the research conducted as a part of the Ph.D. scholarship AAU. No. 915-11091 with the working title:

*PhD Stipend in Integration, Control and Process Optimization of Laser Cutting Systems.*

The work presented herein was carried out at the Department of Mechanical and Manufacturing Engineering at Aalborg University from February 2012 to March 2016. This dissertation is constructed as a collection of papers with several sections dedicated to unpublished results.

# Acknowledgements

During the course of this project I have received a great deal of help and support from several persons which I would like to thank.

First of all, I would like to thank my academic supervisor, Associate Professor Morten Kristiansen for all his help and suggestions during the course of this entire project.

I would also like to thank Steven F. Smith and the other staff of the Intelligent Coordination and Logistics Laboratory, Carnegie Mellon University, Pittsburgh, USA for their hospitality and encouragement when I stayed in Pittsburgh.

Furthermore I would like to thank Flemming O. Olsen and the rest of the staff at IPU, Copenhagen for their support and their technical expertise.

I would also like to express a special thanks to my colleagues at the Department of Mechanical and Manufacturing Engineering for all their help.

Also, I would like to thank my wife Danica and my daughter Frida for their love and support during this process.

Finally, I would like to thank any future children as well, so that they won't get jealous when they see that Frida got a place in the acknowledgments and they didn't.

Sigurd Lazic Villumsen
Aalborg, March 28, 2016

# Abstract

This dissertation is written as a part of the ROBOCUT project which concerns the development of a new laser cutting technology. The technology seeks to increase the performance of traditional and remote laser cutting by using beam shaping technologies. The resulting customized beam patterns are obtained by using a diffractive optical element (DOE).

The main work of this dissertation falls within three areas of focus.

The first area of focus covers the development of a flexible laser processing laboratory for cutting with customized beam patterns. A laboratory was created with a single mode fiber laser used mainly for DOE cutting and an industrial robot and XY table for positioning the laser beam. Furthermore, software interfaces to all pieces of auxiliary equipment were created. An iterative learning control (ILC) algorithm was implemented on the control system in an effort to increase the accuracy of the positioning system. The implemented algorithm was capable of reducing the tracking error by a factor of almost 2.

The second area of focus covers the establishment of a benchmark with which the performance of the ROBOCUT technology could be evaluated. It was chosen to evaluate the performance of the ROBOCUT technology based on the remote fusion cutting technology. It was shown through several experimental series that ROBOCUT cutting performed significantly better when concerning stability than RFC. This increase in stability did however come at the cost of speed, as the ROBOCUT cutting was conducted at approximately 20% of the cutting speed of RFC. This reduced speed is however due to the low duty cycle of the cutting process, which was also in the range of 20%.

The third and final area of focus concerns the development of a framework for task sequencing and path planning that can be used with the developed DOE based cutting technology. The developed framework was based on sampling the redundant axes of the laser cutting system and transforming the sequencing problem into a generalized traveling salesman problem (GTSP) which

was solved by the open source GTSP solver GLKH. To ensure the connectivity of robot configurations a path planning algorithm based on probabilistic road maps approach was developed. A simulation has been carried out on a workpiece which showed that the algorithm minimized the time spent on reconfiguration between the cutting tasks on the workpiece.

**Keywords:** Laser cutting, Remote laser cutting; Beam shaping; Single mode fiber laser; Task sequencing; Sequencing of laser processes; Robot redundancy; Iterative learning;

# Resumé

Denne afhandling er skrevet som en del af ROBOCUT projektet som omhandler udviklingen af en ny laserskæreteknologi. Målet for denne teknologi er at øge ydeevnen for traditionel laserskæring ved at anvende stråleformgivningsteknologier. De resulterende strålemønstre er opnået ved at anvende diffraktive optiske elementer (DOE).

Det udførte arbejde falder i tre fokusområder.

Det første fokusområde omhandler udviklingen af et fleksibelt laser processerings laboratorie, hvor skæring med strålemønstre kan opnås. Et laboratorie blev udviklet med en single mode fiber laser til DOE skæringer, en industriel robot og et XY bord til stråle positionering. Desuden blev software interfaces udviklet til alt eksternt udstyr. For at undersøge systemets fleksibilitet blev det valgt at implementere en machine learning algoritme på kontrolsystemet. En iterative learning control (ILC) algoritme blev implementeret for at øge nøjagtigheden af systemet. Den implementerede algoritme var i stand til at reducere følgefejlen med en faktor to.

Det andet fokusområde omhandler udviklingen af et referencepunkt med hvilket ROBOCUT teknologien kan evalueres. Det blev valgt at basere referencepunktet på remote fusion cutting (RFC). Igennem flere forsøgsserier blev det vist at ROBOCUT teknologien ydede signifikant bedre end RFC med hensyn til stabilitet. Den øgede stabilitet er dog opnået på bekostning af den maksimale skærehastighed, som viste sig at være på ca. 20 % af skærehastigheden for RFC. Denne reduktion af skærehastighed skal dog ses i lyset af at ROBOCUT skæringerne blev udført med en pulseret laser med en duty cycle på ca. 20%.

Det tredje og sidste fokusområde omhandler udviklingen af algoritmer til sekvensering af laserskæreopgaver og baneplanlægning, som kan bruges med den udviklede DOE baserede skæreteknologi. De udviklede algoritmer blev baseret på at sample de redundante akser for laserskæresystemet og derved transformere sekvenseringsproblemet til et generaliseret traveling salesman problem

(GTSP), som blev løst med open source GTSP solveren GLKH. For at sikre at de samplede robotkonfigurationer kan nå hinanden var det nødvendigt at udvkle en baneplanlægningsalgoritme. Denne algoritme var baseret på probabilistic roadmaps. En simulering er blevet foretaget på et emne, som viste at de udviklede algoritmer minimerede den anvendte tid på omkonfigureringer af systemet mellem skæreopgaver.

# Dissertation Details

| | |
|---|---|
| **Dissertation Title:** | Process time optimization of robotic remote laser cutting by utilizing customized beam patterns and redundancy space task sequencing |
| **Ph.D. Student:** | Sigurd Lazic Villumsen |
| **Supervisor:** | Associate Professor Morten Kristiansen, Aalborg University |

The main body of this dissertation consist of the following published papers.

- Paper **A** [123] Sigurd Villumsen, Steffen Nordahl Joergensen and Morten Kristiansen, "Flexible Laser Metal Cutting An Introduction to the ROBO-CUT Laser Cutting Technique," Proceedings of the 7th World Conference on Mass Customization, pp. 217-228, 2014.
- Paper **B** [129] Sigurd Villumsen and Casper Schou, "Optimizing Tracking Performance of XY Repositioning System with ILC," Recent Advances in Mechanism Design for Robotics. Proceedings of the 3rd IFToMM Symposium on Mechanism Design for Robotics, vol.33, pp. 207-217, 2015.
- Paper **C** [125] Sigurd Villumsen and Morten Kristiansen, "Angular Stability Margins for the Remote Fusion Cutting Process" Physics Procedia (2015) 15th Nordic Laser Materials Processing Conference , vol.78 , pp. 89 - 98, 2015.
- Paper **D** [124] Sigurd Villumsen and Morten Kristiansen, "Theoretical Limits of Accuracy of Industrial Robots with Scanner Heads for Remote Laser Cutting," Proceedings of the 2nd AAU Workshop on Robotics 2013.[1]

In addition to the main papers, contributions have also been made in the following publication.

[1] Publication of the proceedings pending.

- Paper **E** [66] Morten Kristiansen, Sigurd Villumsen and Flemming O. Olsen, "Modelling of the Remote Fusion Cutting Process Based on Experiments", Physics Procedia (2015) 15th Nordic Laser Materials Processing Conference, vol.78, pp. 110 - 119, 2015.

In addition to the above published papers the following papers have been made ready for submission to upcoming conferences or journals. These unpublished papers can be found in the appendix.

- Paper **F** [127] Sigurd Lazic Villumsen, Stephen F. Smith and Morten Kristiansen, "PRM based path planning along end effector path for redundant robotic laser processing machinery with scanner mirrors," Unpublished.

- Paper **G** [126] Sigurd Lazic Villumsen, Stephen F. Smith and Morten Kristiansen, "A framework for task sequencing for redundant robotic remote laser processing equipment based on redundancy space sampling", Unpublished.

Also an abstract has been submitted and accepted for presentation at the 9th international conference on Photonic Technologies 2016 (LANE 2016).

- Paper **H** [128] Sigurd Lazic Villumsen, Morten Kristiansen and Flemming O. Olsen, "On the stability of remote laser cutting with customized beam patterns", Abstract accepted for LANE 2016.

This dissertation has been submitted for assessment in partial fulfillment of the PhD degree. The dissertation is based on the submitted or published scientific papers which are listed above. Parts of the papers are used directly or indirectly in the extended summary of the dissertation. As part of the assessment, co-author statements have been made available to the assessment committee for all published papers and are also available at the Faculty. The dissertation is not in its present form acceptable for open publication but only in limited and closed circulation as copyright may not be ensured.

# Contents

# Nomenclature

**Other**

| | |
|---|---|
| $\odot$ | Denotes element wise multiplication of two vectors |
| $\propto$ | Proportional to. |

**Laser processing**

| | |
|---|---|
| $\alpha$ | The travel angle, which is the angle of the incident beam in the direction of the cut as defined in appendix III |
| $\beta$ | The Work angle, which is the angle of the incident beam in the direction perpendicular to the direction of the cut as defined in appendix III |
| $\lambda$ | The wavelength of the laser beam. |
| $\theta_h$ | The half angle of divergence, which is half the angle of divergence of the beam. |
| $D_0$ | The beam waist diameter, which is the diameter of the beam at its narrowest point. |
| $D_{col}$ | The collimated beam width in a laser cutting head. |
| $d_{foc}$ | The focal length of the cutting head. The focal length gives the distance from the focusing lens to the beam waist. |
| $M^2$ | The laser beam quality factor. Describes the ratio of the divergence angle for a theoretical Gaussian beam and a given beam with the same minimum waist diameter. |

**Robotics**

| | |
|---|---|
| $\delta$ | The focus adjustment distance of a scanner cutting head. |
| $\phi_k$ | The deflection angle of a scanner mirror, where k denotes the scanner mirror number. |

$\psi$ The rotation angle of the DOE rotator device.

$\sigma$ The path variable. A variable defined over a contour in such a way that as a path is traversed from start to end point the path variable is traversed from from 0 to 1 ($\sigma \in [0, 1]$)

$\theta_i$ The joint angle associated with joint i of the industrial robot.

$f(q)$ The forward kinematic equations mapping joint space to task space by the formula p=f(q)

$p$ The end effector position defined in task space

$q$ The joint vector of the mechanical manipulator. For a full ROBOCUT setup with scanner mirrors and beam rotator it is composed of the variables $\theta_1$-$\theta_6$, $\psi$, $\phi_1$ $\phi_2$ and $\delta$

$t^b_{P_a}$ A prediction of the reconfiguration duration $d^b_a$ based on a calculation involving the weighted joint displacement of each joint.

$W_S$ A joint speed weight array calibrated to the robotic system

$X, Y, Z$ The Cartesian coordinates of a point. Often used in combination with a set of angles to describe a frame assignment.

**Task sequencing**

$\mathbb{T}$ A set of tasks that needs to be conducted on a work piece.

$Ck$ A processing contour. This contour defines the geometry of the laser process that needs to be carried out.

$d_{\mathbb{T}}(S)$ The total cycle time of a work piece. It is calculated as the sum of all inter task durations and all process durations ($dP_{\boldsymbol{t}} + dI_{\boldsymbol{t}}$)

$d^{\boldsymbol{t}_b}_{\boldsymbol{t}_a}$ The intertask time between task $\boldsymbol{t}_a$ and $\boldsymbol{t}_b$.

$d_{\boldsymbol{t}_i}$ The processing time of the task $\boldsymbol{t}_i$ on a workpiece.

$d^b_a$ The duration of the reconfiguration between two points a and b

$dI_{\boldsymbol{t}}$ The total intertask time which denotes the total time spent reconfiguring the mechanical manipulator between tasks without actually cutting. $(\sum_{i=S(1)}^{S(N-1)} \left(d^{\boldsymbol{t}_{i+1}}_{\boldsymbol{t}_i}\right) + d^{\boldsymbol{t}_{S(1)}}_{\boldsymbol{t}_{S(N)}})$

$dP_{\boldsymbol{t}}$ The total processing time of the all tasks $\boldsymbol{t}$ on a workpiece.$(\sum_{i=S(1)}^{S(N)} (d_{\boldsymbol{t}_i}))$

$l_a^b$ The Cartesian length between two points a and b

$P_{I_{MAX}}$ A vector containing the 1/max joint speeds

$R_d(N)$ The number of Hamilton circuits in a directed graph with N nodes. This can be calculated by $R_d(N) = \frac{(N-1)!}{2}$

$R_u(N)$ The number of Hamilton circuits in an undirected graph with N nodes. This can be calculated by $R_u(N) = (N-1)!$

$S$ A sequence vector containing a permutation of the numbers from 1 to N where N is the number of tasks on the work piece.

$S*$ This vector is used as an index vector to create the task sequence that yields the minimum robot reconfiguration time.

$\boldsymbol{t}$ Task, a processing contour combined with processing parameters. When a task is defined the contour defines its geometry and the parameters defines the process type e.g. cutting or welding

# Chapter 1

# The ROBOCUT project and dissertation overview

In the following chapter a quick overview of the dissertation will be given. It will be composed of a brief introduction to the HTF project - ROBOCUT under which this dissertation is written. This will lead to a description of three areas of focus in section 1.1 which will be treated throughout this document. In section 1.2 a description of the scientific contributions will be given. Furthermore, a reading guide is provided in section 1.3.

## 1.1 The ROBOCUT project and dissertation main contributions

The main objective of the ROBOCUT project is to develop a new robot-based laser cutting technology which has the potential to outperform state-of-the-art laser cutting. The main concept behind the process is that the ejection of molten material out of the cutting kerf can be improved by changing the shape of the laser beam by utilizing beam shaping. In this project this will be done with a diffractive optical element which is capable of changing the Gaussian intensity profile of the laser beam into a desired shape. By using such an optical elements a beam pattern can in theory be tailor made to change the behavior of the process with regards to e.g. melt flow. The scientific work conducted on the ROBOCUT project has been divided between Aalborg University and IPU in such a way that IPU has mainly conducted research on developing the necessary beam patterns and Aalborg University has done the experimental work and worked on the development of control and task sequencing algorithms. This has entailed that the work presented in this dissertation will be within three areas which can be described as:

1. Developing and commissioning a flexible laser processing laboratory for the ROBOCUT technology
2. Analyzing the ROBOCUT and the remote fusion cutting process
3. Developing a framework for task sequencing and path planning

These three areas of focus will briefly be described in the following sections for further reference. This leads to an overview of the scientific contributions and a reading guide for this dissertation.

### 1.1.1 Developing and commissioning of ROBOCUT test facilities

As the ROBOCUT project requires the insertion of a diffractive optical element in the laser beam path, and as a special laser is required to obtain the necessary beam patterns, no laser processing facilities existed that could accommodate the requirements. This has entailed that much effort has been put into specifying requirements for, developing and commissioning a laser laboratory that can accommodate the special requirements of the ROBOCUT technology. Focus has been on developing a laser laboratory where flexibility is of the highest importance with regards to control systems and to the process possibilities. The developed laboratory is currently in full operation and several publications have already been made with various fields of laser processing. Besides the papers on which this dissertation is founded several publications have been made based on experimental data obtained in this laboratory e.g. [28, 38, 40, 65].

### 1.1.2 Analysis of the ROBOCUT cutting process and remote fusion cutting

In the second area of focus much effort has been put into creating a backlog of experiments with which it is possible to benchmark the obtained results from the ROBOCUT process. This backlog mainly consists of a series of parameter studies on remote fusion cutting as the melt ejection principle of the ROBOCUT technology can be seen as a refinement of the principle governing the melt ejection of this process.

### 1.1.3 Framework for task sequencing and path planning

The third and final focus area of this dissertation is devoted to developing a framework for task sequencing and path planning for remote robotic laser cutting systems mounted with scanner mirrors. The developed framework is easily adapted to the special requirements of the ROBOCUT project and directly implements robot redundancy in the solution space searched for optimal task sequences.

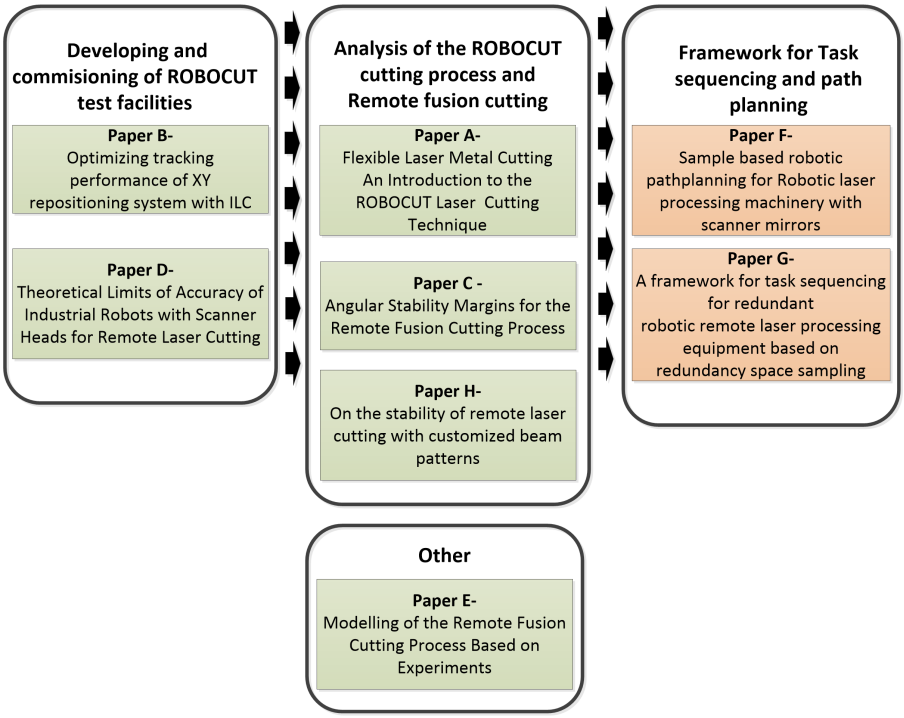


**Fig. 1.1:** The main contributions of this dissertation.

## 1.2 Scientific contributions

Within these three areas of focus several results have been obtained which have been condensed into a set of scientific papers. Figure 1.1 shows a visualization of where these papers are situated in the three focus areas described in the previous sections. Furthermore, the figure illustrates the work flow of the dissertation from specifying laboratory requirements over laser benchmarking to the development of laser task sequencing algorithms. The five first papers have been published (A,B,C,D and E) and presentations have been made at peer-reviewed national and international conferences. Two papers (F and G) are scheduled to be submitted to conferences / journals in the spring 2016. At the time of writing the process of finding suitable outlets for publishing is ongoing. Finally, Paper H, has been submitted in the form of an abstract to a conference scheduled to be held in 2016.

## 1.3 Reading guide

The dissertation is divided into three parts, a main body consisting of the chapters 1-6 which summarizes the work conducted as a part of this dissertation. This is followed by the appendices which are numbered I-IV. These are then again followed by the papers which can be seen in chapters A-H. The textual composition of the main body will generally reflect the division between the three focus areas described in section 1.1. It will be composed of several chapters which will be briefly presented below. The general structure of the dissertation can furthermore be seen from figure 1.2

- **Chapter 2**
  Contains a more thorough introduction to the ROBOCUT project and the state-of-the-art of remote laser cutting. One summary will be presented in this section showing the initial results obtained by the ROBOCUT cutting technology. This leads to a description of the current state-of-the-art for task sequencing of remote laser processing systems. This again leads to a description of a set of research objectives and requirements for the further work.

- **Chapter 3**
  Covers the first area of focus described in section 1.1 - the development and commissioning of a flexible laser processing laboratory for the ROBOCUT project. A description of the used hardware components will be given with a short introduction to the used laser processing parameters. Two paper summaries will be presented in this chapter, one concerning the implementation of a machine learning control algorithm on the XY table, and one concerning an assessment of the repeatability of laser scanner mounted cutting heads on industrial robots.

- **Chapter 4**
  Covers the conducted work within the second focus area described in section 1.1 - the analysis of ROBOCUT cutting and remote fusion cutting. In this chapter an automatic measurement system for laser cuts is presented. This leads to a set of results obtained by conducting remote fusion cutting. These results will be presented in a summary. This finally leads to a section which is devoted to showing the currently unpublished results obtained from benchmarking the ROBOCUT technology against RFC.

- **Chapter 5**
  Covers the third and final focus area - the development of algorithms for automatic task sequencing and robot path planning for remote laser processing systems. An analysis of the problem will be presented and a

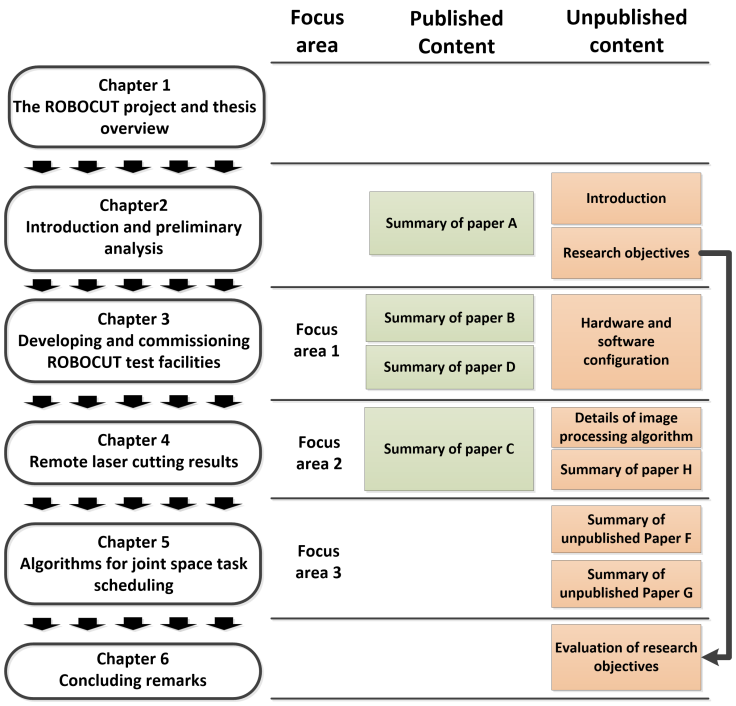


**Fig. 1.2:** An overview of the composition of the chapters of this dissertation

solution is chosen based on sampling based robot path planning. Two paper summaries will be presented, one concerning the development of maps connecting entry and exit robot configurations over a contour and one concerning the development of a task sequencing algorithm based on these maps.

- **Chapter 6**
  Contains an evaluation of the conducted work based on the research objectives presented in section 2.1. Some concluding remarks will be presented with some additional thoughts with regards to future work.

# Chapter 2

# Introduction and preliminary analysis

As suggested by the title of this dissertation the main objective is to optimize the time it takes to cut a given part with remote laser cutting. This time is dependent on two factors, how fast the cutting process itself can be conducted and how well the motions of the mechanical positioning system has been planned. In this dissertation both of these factors will be analyzed and taken into account. To increase the cutting speed of the process the use of customized beam patterns will be investigated. To optimize the motion planning of the mechanical system the problem of task sequencing is analyzed. In this chapter an introduction to the field of traditional and remote laser cutting will be given along with a description of the state-of-the-art of task sequencing within the field of laser processing. This is done to define the context within which the further analysis of the problem can be conducted.

The chapter will be structured in the following way: In section 2.1 traditional laser cutting and remote laser cutting will be described. In section 2.2 the idea of beam customization will be introduced and a more in depth introduction to the ROBOCUT principle will be given. Then in section 2.3 various methods for beam shaping will be introduced, along with the one used in the ROBOCUT project. This is further discussed in 2.3.1 which contains a summary of the initial results obtained by using customized beam patterns for laser cutting. In section 2.4 the problem of task sequencing for robot based remote laser cutting systems is discussed. This will lead to a set of research objectives which are presented in section 2.5.

## 2.1 Laser cutting

The following section will describe the current state-of-the-art of laser cutting. Starting with the use of traditional laser cutting and moving to remote cutting technologies. Lasers are used for many purposes throughout the industry such as communication, materials processing, semiconductor production, printing and eye surgery. With a market share of 29% of the total revenue in the global laser market, materials processing is the second largest application for fiber lasers, only surpassed by communication applications with a market share of 32 % [121]. Furthermore, industrial laser systems represented 14% of the global machine tool sales in 2014 [78]. Laser cutting is the dominating process for lasers with a power of 1 kW or higher [72].

### 2.1.1 Traditional laser cutting

Since the first Oxygen assisted laser cut was achieved in 1967 [117] the field of laser cutting, and laser processing in general, has seen a great deal of development. The number of applications has expanded from metal to many other materials such as wood [75], carbon fiber reinforced plastics [1] and even ceramics [120]. The core laser cutting process itself has however not changed much since 1967. The principle of the process is simple, a focused high power laser beam is moved over the workpiece that needs to be cut. The intensity of the beam will cause the material of the workpiece to melt, evaporate and sublimate (phase transition from solid directly to vapor state). In standard laser metal cutting the governing phase transition is melting. If the molten material is not removed from the cutting kerf it will start to resolidify as soon as the laser beam is turned off or has been moved away. This solidification will then close the cutting kerf and thus a proper separation will not be obtained. This entails that one of the key elements to obtaining fast high quality cuts is to achieve a highly efficient melt ejection. In traditional laser cutting this is achieved by applying a cutting gas through a gas nozzle [13,99,109]. The cutting gas enters the cutting kerf and blows away the material. The gas can either be an inert gas that prevents oxidation of the metal e.g. nitrogen or argon or it can be others e.g. oxygen or compressed air that has the potential to increase the generated heat input by oxidizing the molten metal (Iron) [55, 90]. If an inert gas is used the process if often labeled fusion cutting and if oxygen is used it is called combustion cutting. A conceptual traditional laser cutting setup can be seen from figure 2.1. From this figure it is seen that the cutting gas enters the cutting head through a gas hose and is ejected through a nozzle. A large part of it enters the cutting kerf but some escapes due to the distance between the cutting head and the sheet surface. The escaping gas entails that a lower gas pressure is obtained on the workpiece surface, which again means that the gas flow through the cutting kerf is reduced. If the gas flow becomes too small

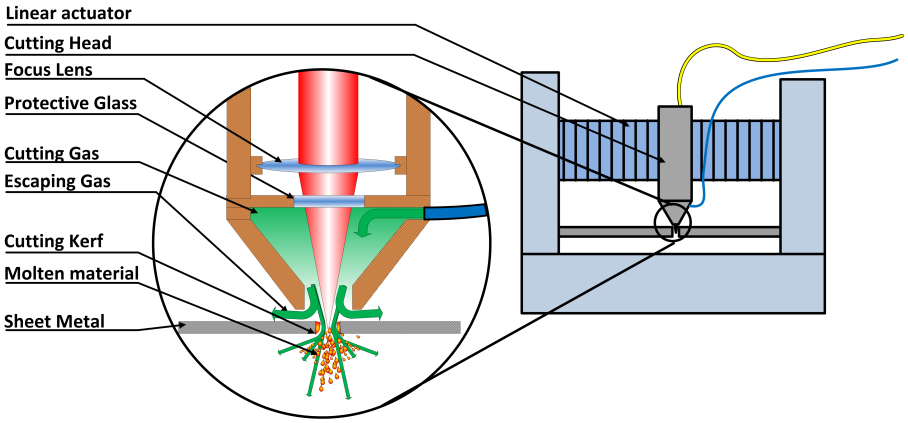


**Fig. 2.1:** A setup for traditional laser cutting. Notice the use of a cutting gas to eject the molten material from the cutting kerf.

the achievable cutting speeds can be significantly limited. On figure 2.1 one actuation systems has been depicted - an XY-table. An XY table system is often found in the industry for flatbed laser cutters, here it is often used to move the cutting head due to significant mass of the steel plates that needs to be cut. Robotic systems are used for more complex 3D tasks. A system composed of both a robot and an XY table is rarely found in the industry due to the combined cost. It is however very useful for research purposes as it offers a great deal of flexibility. The XY table can be used to emulate a traditional flatbed laser cutter or e.g. a moving conveyor while the robot can perform tasks on a moving object or remain stationary.

The processing speeds of traditional laser cutting are generally high due to the cutting gas assisted melt ejection. One of the drawbacks is however that the close proximity of the gas nozzle increases the risk of collisions between the cutting head and the workpiece. When considering the cutting speed one could mention that in [130] a 5kW fiber laser is used to cut 10mm of stainless steel at a rate of 1.6 m/min (Nitrogen cutting). For 1mm SST sheets, speeds of more than 30m/min can be achieved [98]. Also in [63] 2mm SST is cut with a speed of 17m/min. These high speeds are however often unobtainable as the cutting of parts generally requires many accelerations and decelerations. Furthermore, the laser power of e.g. fiber lasers has continued to grow which entails that lasers with powers reaching 100 kW are commercially available [30] This entails that in most cases the processing speed of a given work piece is no longer given by the laser itself, but by the actuators moving the cutting head [76]. To overcome some of these drawbacks much research has been conducted within the field of remote laser processing.

### 2.1.2 Remote laser cutting

In remote laser cutting the laser cutting head is no longer positioned close to the workpiece, instead it is positioned above it. This remote position inherently reduces the risk of tool workpiece collisions, but inhibits the use of a cutting gas for melt ejection. This entails that the molten material needs to be ejected from the cutting kerf by other means than a cutting gas. The remote cutting head position makes it possible to reposition the beam simply by changing the angle of the cutting head. The process is often sped up by means of an optical system that can deflect the beam efficiently by e.g. scanner mirrors or various forms of rotating mirror prisms. Mirror prisms are often used for moving the beam over a predefined path which makes them suitable for various kinds of surface treatments. Scanner mirror systems are often used for cutting and welding as they are flexible and allow very fast beam repositions exceeding >720 m/min [134].

A remote cutting setup based on scanning mirrors can be seen from figure 2.2 where mirrors are used to deflect the beam. For simplicity some components of the cutting head are not shown on the figure e.g. collimating lens and focus adjustment. In section 3.3.3 cutting head designs are discussed in more detail. As described briefly, the melt ejection in remote cutting, cannot be

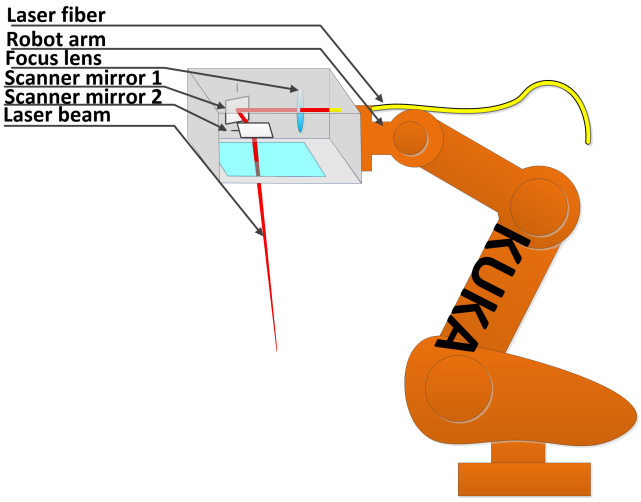


**Fig. 2.2:** A sketch of a remote laser cutting setup. The remote position reduces the risk of tool workpiece collisions and allows fast repositioning of the laser beam.

achieved by the use of a cutting gas due to the remote position of the cutting head. Currently there are two processes by which the molten material can be removed, these are remote ablation cutting (RAC) and remote fusion cutting

(RFC) [134]. In the following these technologies will be described and evaluated based on several parameters such as speed, required equipment and a set of quality parameters such as kerf width, burr formation, heat affected zone (HAZ) and edge quality.

### Remote ablation cutting

In remote ablation cutting (RAC) the melt ejection is achieved by scanning a highly focused high power laser over a contour repeatedly [134]. Due to the short exposure and the high intensity the beam evaporates much material inside the cutting kerf. This evaporated material expands and builds up a gas pressure that ejects any molten material out of the cutting kerf. On each pass the beam removes only the surface layer of the metal. When enough passes are conducted the kerf meets the bottom of the sheet and a cut is obtained. This process can be seen from figure 2.3. RAC is generally considered to be a fast

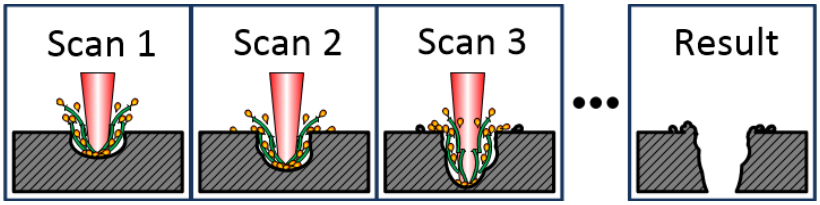


**Fig. 2.3:** Shows the principle of remote ablation cutting of sheet metal (grey). The laser beam (red) melts the metal (orange) and creates a vapor pressure (green arrows). The melt is ejected by means of the vapor and to some extent solidifies as burr on the top of the cutting kerf. [123]

cutting process for cutting thin plates but the speed quickly decreases with the thickness. In [134] it is reported that scan speeds exceeding 360m/min can be used for cutting. However, for sheets with a thickness larger than 50 $\mu$ more than one scan is necessary. For 0.5 mm approximately 8 scans are necessary yielding a total speed of approximately 45 meters/min. This combined with the acceleration capabilities of the scanner systems shows the real strength of remote cutting. One of the main drawbacks of such systems is however that scanning cutting heads are necessary as the process relies on very fast scan speeds. Furthermore the accuracy of the system needs to be extremely high as every scan needs to enter the cutting kerf which is less than $100\mu m$ wide. Due to the very fast travel speed of the laser, the HAZ is very small and mainly present in the top of the kerf where the laser is present for all scans [96]. One of the characteristics of the process is the presence of burr on top of the workpiece due to the depositioning of ejected metal from the cutting kerf. In [96] burr heights of approximately 90 $\mu m$ is reported for 1mm S235 steel, but with almost perpendicular edges.

### Remote fusion cutting

Another remote cutting process is remote fusion cutting. In remote fusion cutting a laser beam in the kW range, focused to a diameter of approximately $600\mu m$, is moved over a workpiece. Due to the intensity of the beam the material melts and evaporates. The evaporation of metal on the top side of the workpiece, and the pressure generated by the intensity of the beam inside the cutting kerf expels the molten material. The melt ejection principles are however not completely understood yet [134]. But the governing dynamics are often seen as being similar to the ones for keyhole laser welding. This is due to the fact that for RFC the beam diameter and laser power results in intensities on the workpiece in the range of $10^6 W/cm2$ which entails that the intensity is in the range of keyhole welding. In keyhole welding the high intensities of the laser beam evaporates a deep cavity called a keyhole in the material. One of the characteristics of keyhole welding is that the molten material runs around the keyhole as the weld proceeds [19]. This is depicted on figure 2.4 The material flow around the beam is furthermore combined

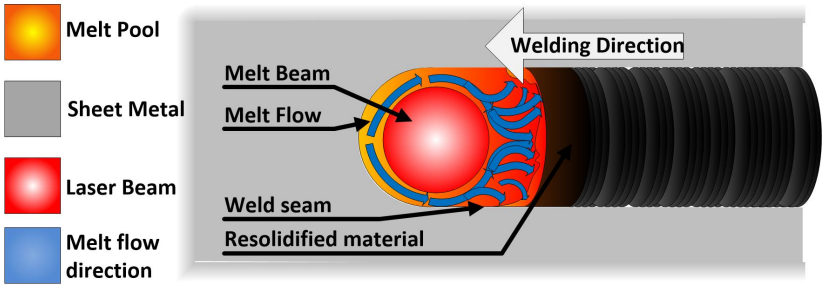


**Fig. 2.4:** The material flow of keyhole laser welding. Notice the material flow around the beam

with another downwards material flow which is currently being investigated by the research community through high speed videos [27]. It is inferred that if parameters are chosen wisely these material flows can be harnessed to eject the molten material out of the cutting kerf. This can be seen from figure 2.5. The experiments conducted in RFC all show that the flow of material is towards the bottom of the cutting kerf just as with traditional laser cutting. The main force acting upon the melt is thus not gravity as the melt ejection direction is just as prominent for workpieces processed upside down. This is illustrated in figure 2.6 which shows a sideways view of figure 2.5. The main drawbacks of RFC, when compared to RAC, is the slow cutting speeds for thin sheets and the large heat affected zone (HAZ). In [134] a series of RFC results are presented. The results are conducted with 4-8kW of laser power. These results show that processing speeds ranging from 4-12 meters/min for sheets with thicknesses between 0.75 mm and 4 mm could be obtained. The main problem is however

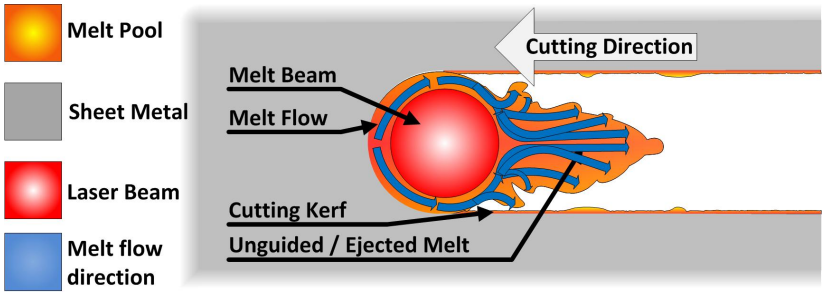


**Fig. 2.5:** The material flow of remote fusion cutting. Notice the material flow around the beam and the unblocked kerf trailing behind it

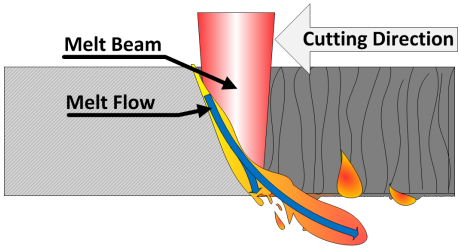


**Fig. 2.6:** A sideways view of the material flow of remote fusion cutting. Notice the material flow downwards out of the cutting kerf

still the HAZ. An increased HAZ is a severe drawback as the internal metallic structure changes within the HAZ, which entails that additional processing steps might be necessary to prevent e.g. changes in hardness and increased risks of ruptures [118]. The cutting kerf has a width of more than 600 $\mu$ m for S235 steel which entails that much material is lost while cutting [96]. Furthermore, all the molten material also entails that the edges are almost round instead of being perpendicular, as the edges are essentially composed of molten material. This entails that the roughness is extremely low for RFC. Also no burr is generated on the top or bottom of the workpiece. Another benefit is however that the process does not require a scanning system as was the case for RAC.

### Efficiency of remote cutting technologies

Form the above sections it is clear that remote ablation cutting in many ways is capable of competing with traditional laser processes when considering the cutting speed for thin metal sheets. The cutting speed does however quickly decrease with sheet thickness. Remote fusion cutting is capable of cutting thicker sheets, but with reduced speed and a larger heat effected zone. However, when these processes are compared to traditional laser cutting it becomes evident

that they are both quite inefficient. In [86, 134] it was shown that RFC with a 4 KW laser can cut 3 mm stainless steel sheets. In [64] a weaker laser (3 kW) is used to cut plates more than three times as thick, and at much faster speeds when an external cutting gas is applied. In [29] a 3 kW fiber laser is used for cutting 25 mm of stainless steel, however with much slower speeds. In table 2.1 several parameters for comparison between the processes are listed. The values

| | **RFC** | **RAC** | **Traditional** ($CO_2$) |
|---|---|---|---|
| Speed (1mm ST, 3kW laser power) | N/A (10m/min 0.5mm SST [125]) [a] | 12m/min [47] | 16 m/min ( [63] 800W SM fiber) [b] |
| Maximum thicknesses | 4mm [108] @8kW disc laser | 2 mm [96] @ 3kW single mode fiber laser | More than 50mm @ 2kW $+O_2$ [91] |
| Required laser power | >3 kW | 1kW SM | N/A |
| Kerf width (1mm ST) | 600 $\mu$ m | <100 $\mu$ m | 300$\mu$ m |
| Burr formation | None | <80 $\mu$ m (top) | Low |
| HAZ | Very large | Very small | Very small |
| Edge perpendicularity | Round | 20 $\mu$ m | 30 $\mu$ m |
| Required laser equipment | Fiber or disc laser | Single mode fiber laser | $CO_2$ laser |
| Required mechanical equipment | Any positioning system | Scanner mirror positioning system | Any positioning system |

**Table 2.1:** A summary of the capabilities of various laser processing. [a] RFC generally needs more power than 3kW, but for 0.5 mm 10m/min has been achieved in [125]. [b] 3kW is generally not necessary for traditional laser cutting 16 m/min has been reported for 800W single mode fiber laser.

in the above table are taken from the scientific literature. Industrial systems utilizing 4kW fiber lasers exist showing cutting speeds in the range of 60 m/min in 1 mm metal(material unspecified) [106]. To increase the efficiency of remote cutting systems one might consider the use of beam modification to control the melt ejection principles even further. This has the potential to increase both the quality of the cuts and the speed of the process. In the following sections the use of beam modification will be discussed, which leads to the presentation of the ROBOCUT project.

## 2.2 Cutting with customized beam patterns - ROBOCUT

As described in chapter 1, the goal of the ROBOCUT project is to create a robot-based laser cutting technology for sheet metal (0.15mm-6.3mm as defined in [131]) which has the potential to outperform the state-of-the-art of laser cutting. The main idea behind the ROBOCUT technology is that the speed and quality of a laser cut is generally determined by the process ability to

expel molten material from the cutting kerf. If the melt ejection is insufficient the molten material resolidifies on the sides of the cutting kerf and a cut will not be obtained. As discussed in the previous sections remote fusion cutting is generally considered inefficient when compared to more traditional cutting and RAC for thinner sheets. The main concept of the ROBOCUT process originates from the thought that if it is possible, in remote fusion cutting, to induce a flow of molten metal out of the cutting kerf, then this flow can also be modified by customizing the intensity profile of the laser beam. Instead of having a round beam, around which the melt flows as depicted in figure 2.5 and 2.6, a customized beam intensity profile is used to direct the molten material out of the cutting kerf. Such a concept can be seen from figure 2.7. From this

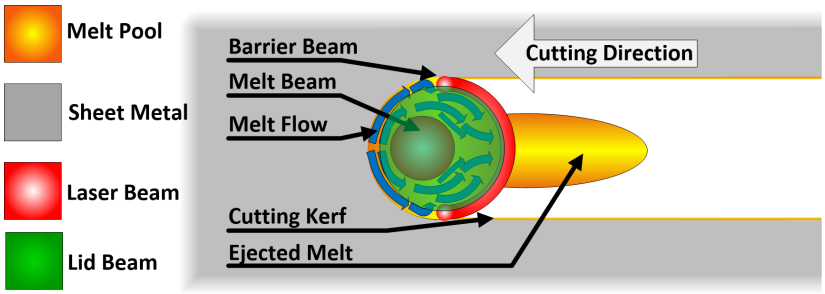


**Fig. 2.7:** The material flow of ROBOCUT cutting. Notice the material flow around the beam guided by the barrier beam

figure it is seen that the normally round laser beam used for RFC has been replaced by a beam composed of three sections, a melt beam, a barrier beam and a lid beam. The general idea is that the melt beam carries the majority of the laser power, and melts and evaporates the material which flows around the beam as in RFC, but when it meets the barrier beam it is pushed towards the center of the kerf and the lid beam pushes it towards the bottom. Figure 2.8 shows this from the side. The key element of the ROBOCUT project is the

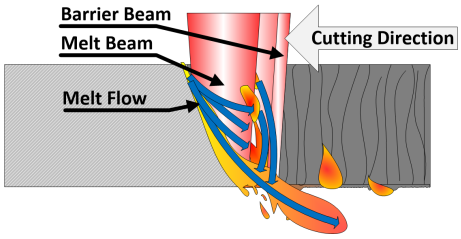


**Fig. 2.8:** A sideways view of the material flow of ROBOCUT cutting. Notice the material flow downwards and around the barrier beam.

generated beam profile. A preliminary assessment of the ROBOCUT potential

shows that one of the main strengths lies in its versatility - it can be used for virtually any sheet thickness. Furthermore the main idea behind it is that it can be used in combination with a cutting gas to increase the speed of traditional cutting or as a remote process. The following naming convention will be used to distinguish between these two ROBOCUT processes.

- ROBOCUT traditional cutting - RTC
- ROBOCUT remote cutting - RRC

As the main focus of this dissertation is on remote laser cutting RRC will mainly be treated. Much of the preliminary work has however been done on the RTC process. The potential of the RTC technology can be seen from figure 2.9(a) and 2.9(b).
From these figures it is seen that the speeds have been assessed to be higher

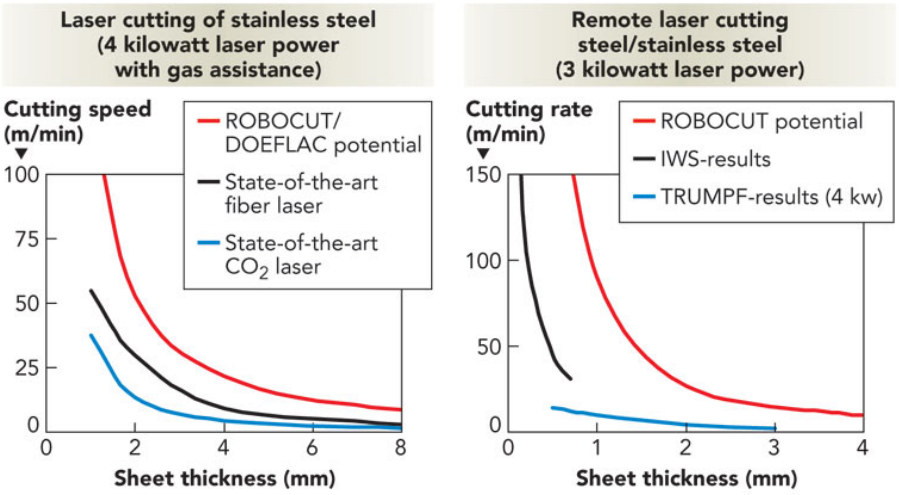


(a) The potential of the ROBOCUT technology when conducted without the use of a cutting gas. In this case the melt ejection is entirely generated by the beam intensity in the cutting kerf.

(b) The potential of the ROBOCUT technology when combined a cutting gas. Here the melt is ejected in by the applied cutting gas and by the internally generated pressure from the intensity of the beam

**Fig. 2.9:** Graphs of the potential of the ROBOCUT project. These figures and a further discussion on the potential can be found in [88] and [86]. Here it should be noted that "IWS-result" is a reference to remote ablation cutting results from IWS [47] and TRUMPF-results are remote fusion cutting results from TRUMPF [108].

than for both RAC and RFC. The efficiency of the ROBOCUT technology will however depend on the efficiency of a given beam pattern. As beam shaping is the core of the technology the following section gives a brief description of various methods of beam shaping.

## 2.3 Beam shaping technologies

Various technologies for beam shaping exists which has the potential to obtain the beam patterns used for the ROBOCUT project. The main task of beam shaping can be said to be to distribute the beam intensity so that it resembles a predefined profile. Various technologies exists for intensity shaping, some of which will be presented in the following sections. They will be evaluated based on their flexibility, the quality of the produced patterns and their cost.

#### High-speed laser scanning

High-speed laser scanning is based on the same scanning technology used for RAC described in section 2.1.2. If the area of the scanned contour is very small and a pattern is scanned fast and repeatedly this could be seen as a beam pattern formed by the average power distribution in the cutting kerf. This type of intensity shaping might be called artificial as the scanned beam keeps the same intensity while the average intensity changes. This also entails that this type of scanning technology introduces changes in the temperature gradient on the cutting kerf and it can thus change the dynamics of the cutting process. This can however be beneficial as it can stimulate the melt ejection when cutting which can be seen in the case of RAC. Often these systems are used for other processes such as laser hardening [110] and welding [82]. One of the advantages of such a process would be that the repositioning system could be combined with the beam shaping system, which might reduce costs and the need for introducing other technologies. The flexibility of such a beam shaping technology is high as it is possible to change a produced pattern simply by changing the programming of the scanner head. In theory any pattern can be obtained within the tolerances of the scanner mirrors. The fact that the pattern is produced as an average intensity can however influence the melt ejection.

#### Beam splitting and the use of multiple laser sources

When conducting beam splitting a laser beam is split into several beams which can be aligned individually on the focus plane of the work piece. By arranging these beams it is possible to generate various beam patterns consisting of a series of laser spots. The patterns which can be obtained by these technologies are however limited by the used number of beam splitters and aligning these beams can be difficult depending on the proposed pattern. The proof of concept cuts conducted at the start of the ROBOCUT project was achieved by using 1 melt beam and 8 beams for melt guidance and cut edge trimming [89]. For simple patterns multiple beams or multiple laser sources can be used. Scaling to more intricate patterns will however be difficult to achieve.

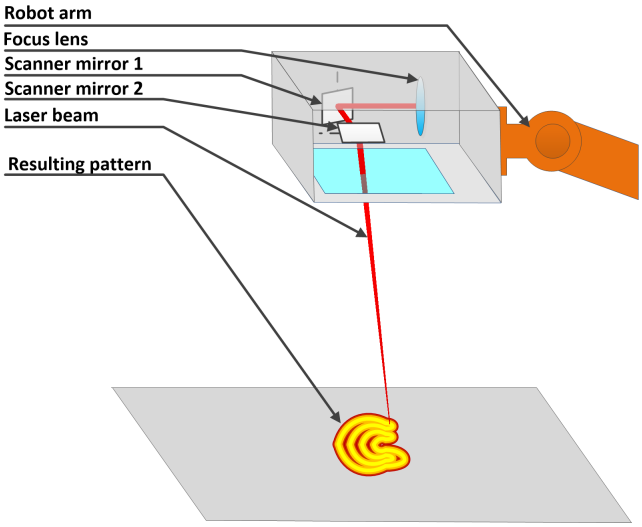


**Fig. 2.10:** Conceptual setup of high speed scanning system for beam shaping. By scanning the beam rapidly over a surface the average intensity of the beam can be modified to yield any pattern.

### Diffractive optical element

Diffractive optical elements uses a thin micro structure to alter the phase of the light transmitted through it. This phase pattern, can manipulate the beam to achieve a large range of beam intensity profiles. By using such an optical elements a beam pattern can in theory be tailor made to a given process. The DOE works by changing the phase of the laser beam wave front. As the beam wave front passes through a focusing lens these changes leads to a change in beam intensity. This is illustrated in figure 2.11. One of the drawbacks of this approach is that an additional optical component is added in the beam path. This again entails that a customized processing head is necessary for such an option. Furthermore the presence of additional optical components might cause thermal lensing, a phenomena where the accumulated heat in an optical components makes the component expand. As such components are cooled on the sides the center region expands more than the sides. This can potentially cause the DOE to act as an additional focusing lens yielding a focus offset depending on its temperature. Diffractive optical elements have, since the ROBOCUT project was initiated, seen a great deal of interest from the research community. In [56] it is reported that by using diffractive optical elements it is possible to reduce the amount of cutting gas significantly. In [122] a DOE is used to create customized beam patterns for smoothing out weld bead profiles to achieve smoother surfaces. By using one melt beam and two smoothing beams a significant improvement in weld toe angle was achieved. In [38] it is

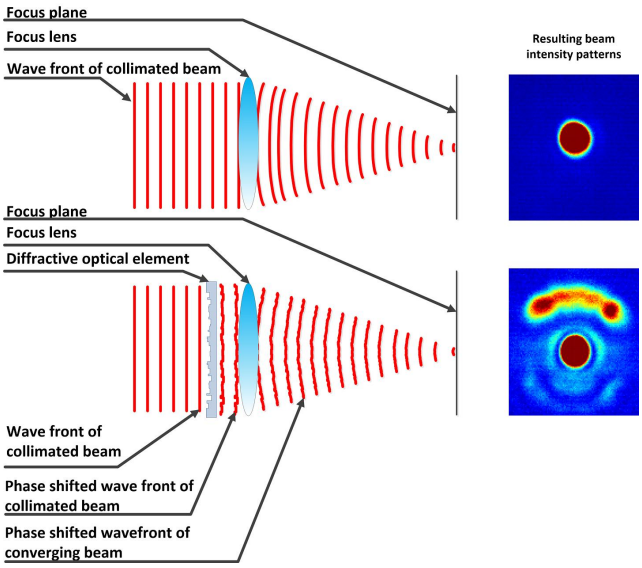


**Fig. 2.11:** Beam shaping by using diffractive optical elements.

shown that by applying beam shaping through the use of a DOE it is possible to increase the control over the size and depth of the weld pool for laser welding.

### Others

Other forms of beam shaping exists such as micro lens arrays [49, 73] and gratings. These have however not been considered for this project.

### Chosen technology for ROBOCUT

In this project it has been chosen to use DOEs as the means of beam shaping, as it offers a way to generate very intricate beam patterns by the use of various software suites. This, combined with their high power capabilities, means that they have the greatest potential of providing a pattern which can increase the performance of various cutting processes. It has also been chosen to omit a scanner based beam shaping as the dynamics of the wobbling laser beam might influence the cut quality. DOEs can generally be reflective or transmissive. Figure 2.12 shows three representations of a transmissive DOE. On figure 2.12(a) the pattern of the diffractive optical element is shown. On figure 2.12(b) this pattern has been etched into a disc forming a diffractive optical element. On figure 2.12(c) the resulting intensity pattern can be seen. Notice that the mapping between figure 2.12(a) and 2.12(c) is not trivial and one cannot determine the resulting intensity profile simply by inspecting the DOE pattern.

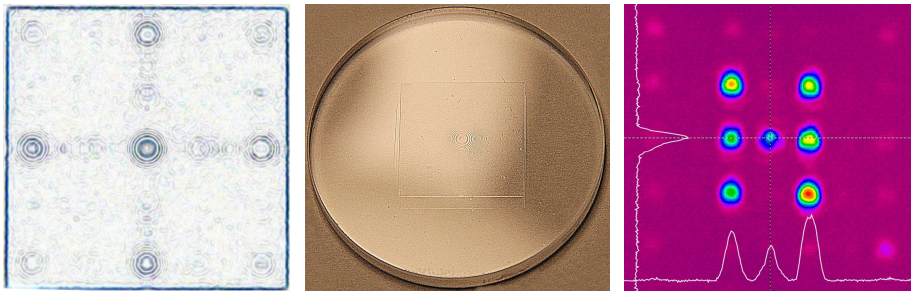

(a) The computer generated phase pattern to be implemented to achieve the intended intensity profile. The generated pattern can be interpreted as a height map of the DOE. The resulting beam intensity pattern cannot be seen from the image as the mapping between the phase pattern shown above and the intensity profile is not trivial.

(b) The finished optical element. Notice the resemblance of the pattern shown here and the one shown on 2.12(a). It should be noted that the above image has been sharpened and image processed to bring out the pattern. When seen with the naked eye, the patter is all but invisible except when seen in a proper light

(c) The resulting intensity pattern obtained when the diffractive optical element is inserted in the beam path. Notice that this pattern is purely used as an example and has been designed for welding and not cutting. The measurements are obtained by using the equipment described in [41]. Courtesy of Klaus Schütt Hansen, IPU, [53]

**Fig. 2.12:** Three images of a diffractive optical element. On the left an etching pattern for a DOE is seen. In the middle picture the finished DOE is seen, and on the right side an intensity profile is seen.

In the following section the first paper produced as a part of this Ph.D. will be summarized as it contains a set of preliminary results for the first iteration of cutting with a customized beam shape. Further results related to the ROBOCUT technology will be given in chapter 4.

### 2.3.1 Summary of paper C: Flexible Laser Metal Cutting - An Introduction to the ROBOCUT Laser Cutting Technique

The following section contains a summary of the paper "Flexible Laser Metal Cutting - An Introduction to the ROBOCUT Laser Cutting Technique".

#### Objectives

1. To present the concept of the ROBOCUT technology to a wider audience.
2. To investigate its applicability to flexible manufacturing

3. To investigate the beam quality of the single mode fiber laser at Aalborg University

4. To present the, at the time being, capabilities of the ROBOCUT technology

### 2.3.2 Summary

Laser cutting and welding are flexible processes which can be used for many applications in the industry. As they can cut workpieces based on CAD/CAM data and has a high precision and cleanliness they can be characterized as one of the processes revolutionizing mass production [36, 113]. Due to changes in consumer demand [50, 105] it can also be characterized as an enabling technology for mass customization of parts.

When conducting laser cutting, one of the main bottlenecks for obtaining

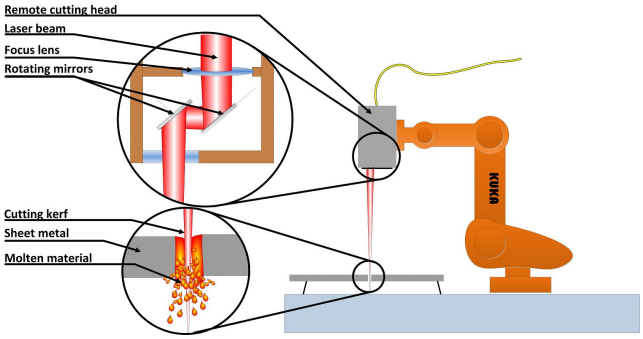


**Fig. 2.13:** An industrial robot mounted with a laser cutting head for remote laser cutting [123].

good quality cuts and achieving high processing speeds is the melt ejection efficiency. If the molten material is expelled from the cutting kerf in an efficient manner high speeds can be achieved. In laser cutting the molten material is often expelled by applying a cutting gas through a gas nozzle that blows the molten material out of the cutting kerf. This type of melt ejection is highly efficient and yields good quality. However, the cutting gas is expensive and the nozzle needs to be positioned close to the surface of the workpiece to ensure that the cutting gas expels the material from the kerf. The position of the cutting head increases the risk of collisions between the workpiece and cutting head. Furthermore it has been assessed that the limiting factor with regards to processing speed is no longer the laser power but the limitations of the linear actuators repositioning the beam [76]. This has entailed that research is currently being conducted within the field of remote cutting. In remote cutting the laser cutting head is positioned e.g. 1 m above the workpiece. This remote

position has the advantage of reducing collisions and ensures that the beam can be moved simply by tilting the cutting head. However, the melt ejection cant be achieved by applying a cutting gas as the gas nozzle cant be positioned close to the workpiece. Instead the melt ejection is generated by pressure phenomena in the cutting kerf. An illustration of such a setup can be seen from figure 2.13.
Remote cuts are however still conducted by beams with round intensity profiles as can be seen from figure 2.14(a). The main idea behind the ROBOCUT technology, as described in [86, 87, 89] is to change the shape of this beam to increase the efficiency of the melt ejection. An example of a beam intensity profile can be seen from figure 2.14(b). Here it is seen that the beam is divided into three parts, a melt beam that melts and evaporates the material, a barrier beam that directs the melt out of the cutting kerf and finally a lid beam that uniformly generates a gas pressure that expels the molten material.

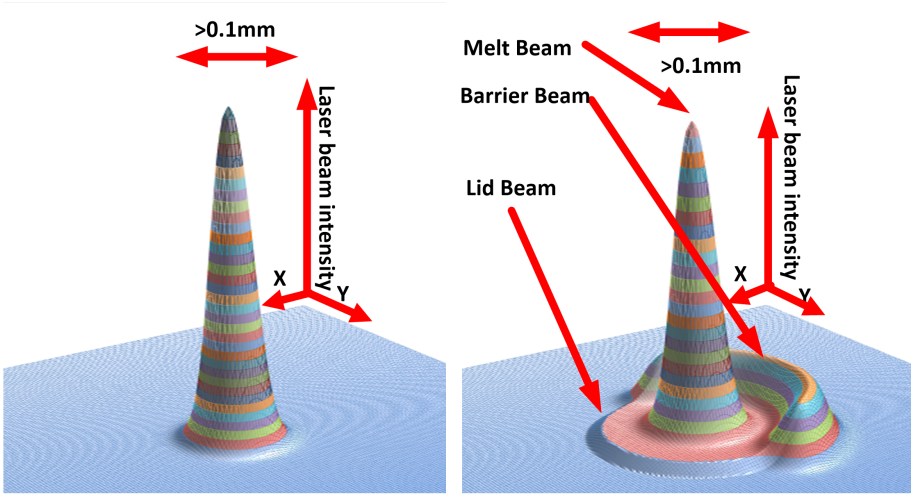


(a) A conceptual illustration of the beam intensity for a laser beam with a beam parameter product=1, which indicates that the intensity can be seen as a Gaussian distribution. This entails that the intensity is highest in the center point and gradually fades with the distance from center. Single mode fiber lasers have an intensity profile very similar to a Gaussian.

(b) A conceptual illustration of a ROBOCUT beam intensity profile where the beam is divided into various functional areas. The lid beam, the barrier beam and the melt beam.

**Fig. 2.14:** Illustrations of two beam profiles, a typical beam from a single mode fiber laser and a customized cutting beam from the ROBOCUT project [123].

These beam patterns can also be combined with traditional cutting to achieve

the combined melt ejection of an applied cutting gas and the internally generated pressure. The main advantage of using these tailored beam patterns instead of a round beam is that the cutting gas, can be directly generated in the cutting kerf by evaporating the metal. By doing so it can be ensured that a good melt ejection can be obtained, even in narrow cutting kerfs. As a narrow cutting kerf entails that the laser needs to melt less material this could lead to an increases in cutting speed when compared to RFC and RAC. On this basis a preliminary estimation of the cutting potential has been conducted by [87] where it is assessed that speeds can be almost doubled compared to standard laser cutting when the internal gas generation is combined with a standard cutting gas. In the following some preliminary results from the ROBOCUT project will be presented.

**Results**

The constructed DOE is measured by using a beam analysis device constructed for the laser laboratory as described in [41]. By using this device a series of intensity profiles of the beam can be generated in several focus levels. The analyzed beam of the single mode fiber laser can be seen from Fig 2.15(a). The intensity profile is here truncated in such a way that low power levels are visible. The beam has has a close approximation of a Gaussian beam which is necessary as the resulting beam patterns after the DOE is dependent on the beam quality of the beam. Figure 2.15(b) shows the resulting beam pattern when the beam is transmitted through the constructed DOE. It is seen that the beam is still centered and that a highly intense melt beam is formed in the center. The barrier beam seems quite uniform as well, with some higher intensities on the edges of the barrier shape. The two images are truncated to show similar intensity values so that they are comparable with regards to beam intensity. Notice that the resulting beam pattern is wider than the original and close to 400 $\mu m$ from one end of the barrier beam to the other.
To determine the effect of utilizing the beam presented in 2.15(b) several cuts were made. These cuts showed that the presence of the DOE influences the cutting process. The result obtained without DOE can be seen from 2.16(a) and the result with DOE can be seen from 2.16(b). Both cuts are done with Nitrogen as cutting gas at a pressure of 5 bar in 1 mm stainless steel (SST EN X4CrNi18-10) with a focal length of 300 mm and with 800W laser power.
From these two figures it is seen that the cutting kerf obtained by the ROBOCUT cut is approximately three times as wide as the standard cut. This is due to the increased width of the beam pattern, which again means that the intensity is spread over a too large area and thus a wider cutting kerf is created, which leads to reduced cutting speed. This entails that more research should be put into generating more efficient beam patterns.

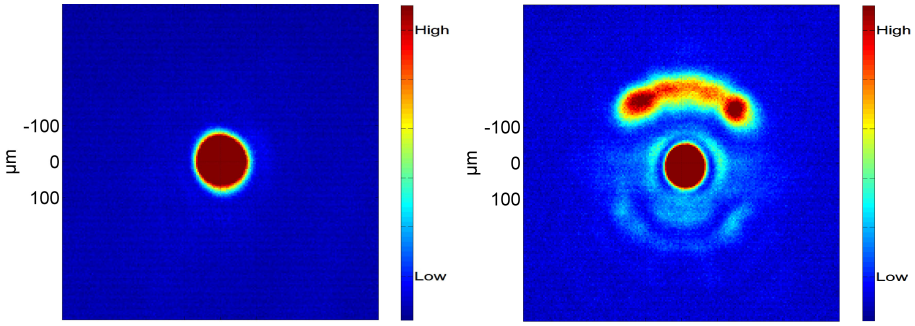


(a) The beam intensity of the 3kW single mode fiber laser purchased for the ROBOCUT project. Notice the round shape which resembles the proposed Gaussian distribution

(b) The beam intensity profile of the proposed ROBOCUT design pattern. Notice the barrier and melt beam from figure 2.14(b). The lid beam is however hidden in the background noise due to intensity truncation in to the measurement system.

**Fig. 2.15:** Measurements of the obtained beam profiles. Notice the round shape of the beam intensity for the single mode fiber laser and the modified beam on the right [123].

### Future research

As the obtained cutting results with the presented beam pattern indicate that too much material is melted it is necessary to continue doing research into new beam patterns. Furthermore more studies should indicate to what extent the ROBOCUT principle can improve the results when conducting remote cutting.

Now that the concepts the ROBOCUT project has been introduced along with the most commonly used remote laser cutting technologies the following section will treat the problem of sequencing tasks for such remote laser processes.

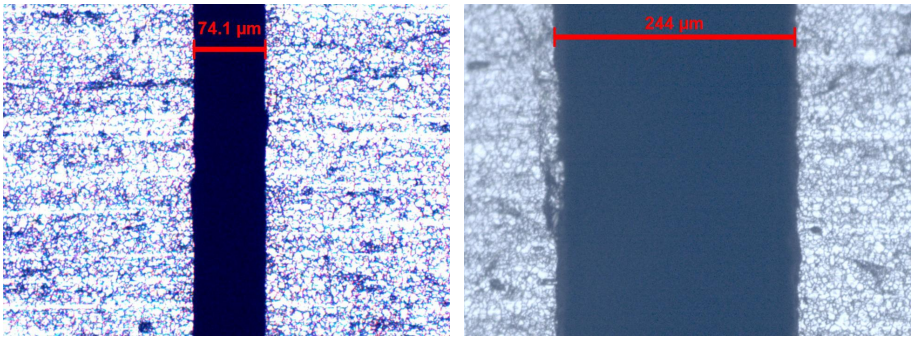


(a) The resulting cutting kerf obtained by traditional laser cutting with a round symmetrical beam.

(b) The resulting cut obtained by a the ROBOCUT beampattern shown in 2.15(b)

**Fig. 2.16:** The resulting cuts obtained by two beams. Notice the increased width of the cutting kerf for the ROBOCUT beam [123].

## 2.4 Task sequencing and integrated path planning for robot based remote laser processing systems

In the following the concept of task sequencing will be described in further detail, as it is the third and final area of focus of this dissertation. Furthermore it constitutes the second factor mentioned in the title of this dissertation. The task of optimizing the processing time of a part by considering the problem of task sequencing. This section will describe the current state-of-the-art for task sequencing for robotic systems. The results presented here will lay the foundation of the analysis seen in chapter 5.
When considering the process of laser cutting, it is clear that it involves much more than the laser cutting process itself. As described in section 2.3.1 laser cutting is often a component in larger CAD/CAM systems used for mass production of parts. Figure 2.17 shows a conceptual overview of such a system. In the CAD step a part is designed based on a set of requirements and a general idea of the product and in the CAM step these designs are realized by programming various pieces of equipment. The CAD step is often conducted in general CAD programs such as e.g. solidworks or Autocad. When considering CAM several steps are shown, process selection, selecting process parameters, task sequencing and path planning, code generation and finally execution. All of these steps are directly linked to the capabilities of the processes and machinery needed for the realization of the designed part. The distinction is however a bit blurry as CAD systems often offers CAM plugins which enables them to

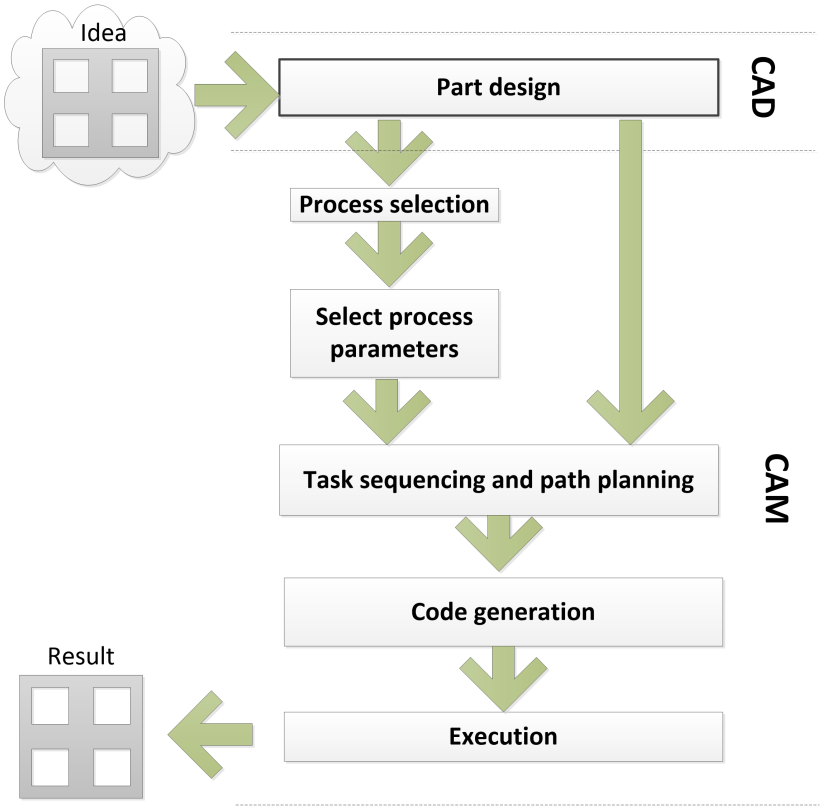


**Fig. 2.17:** A conceptual drawing of the steps involved in the development and manufacturing of a part for a production system.

interface with various pieces of equipment [114].

When considering process selection and selecting process parameters it concerns the act of choosing appropriate processes and appropriate process parameters to achieve the features and requirements given in the design. Even if a design is made with a given process in mind, it is clear that it can be interchanged with another if it is capable of performing the same operation e.g. cutting with the same quality. The selection of process parameters depend on knowledge of the selected process and its capabilities. Often many parameters needs to be found that are dependent on the material type, thickness and available equipment. These two steps feeds the details of the chosen process and relevant processing data forward to the task sequencing planner.

Task sequencing and path planning is necessary when a part needs to be cut in several locations or it needs to be both cut and welded. By utilizing sequenc-

ing algorithms it is possible to obtain a sequence of processes that minimizes a specified cost function. Such a function could be the processing time of the part, but it could also consider quality parameters such as the warping of the metal due to the heat input of the laser. An important point here is however that the task sequence is very dependent on the equipment on which the tasks are going to be executed.

Code generation is the process of generating code for the various pieces of equipment required to perform the processes selected previously. When considering 2D laser cutting the execution code is often given in G-codes with e.g. M functions specifying specific laser behavior [9]. For robotic systems trajectories are often given in native ROBOT languages such as KUKA KRL or Adept V+. For other components such as scanner mirrors dedicated control boxes exist that needs reference signals from control systems.

Execution is the final step which executes the code generated in the previous step. By executing this code the part is produced as per the design created in the CAD step. The described production flow is however quite simplified as the process is often iterative so that the design is changed depending on the obtained result and the available equipment.

In the following sections a state-of-the-art of the problem of task sequencing is presented. It will start with a short a short literature review discussing the degrees of freedom of various laser processing systems in section 2.4.1. This leads to a description of a series of frameworks treating the problem of task sequencing and path planning for remote laser processes in section 2.4.2. Furthermore a series algorithms for task sequencing for other applications will be presented in section 2.4.3.

### 2.4.1 Mechanical systems for laser processing

When considering the problem of task sequencing for remote laser processes, the mechanical system of a laser processing cell is one of the key elements. A quick literature survey has revealed that, when considering laser processing a wide range of mechanical systems are used for guiding the laser beam over the work piece. Table 2.2 shows an overview of the used DOF presented in the scientific literature. From this table it is seen that the mechanical systems varies from 2 to 10 DOF. It is also seen that, when considering remote laser processing systems, industrial robots are often used in combination with scanner heads. The use of a remote laser processing in combination with an industrial robot has in fact been presented in several papers [43, 59], and seen a great deal of success especially within the automotive industry [57, 81].
Often an industrial robot has 6 joints as it has a workspace within which all

| Paper | Application | DOF | Actuated system | Redundant |
|---|---|---|---|---|
| [38] | Multi beam 2D Laser Welding | 2 | XY - table | No |
| [28] | 3D laser hybrid welding | 6 | Industrial robot | Yes |
| [18] | 2D Laser cutting | 2 | XY - table | No |
| [31] | 3D Laser cutting | 6 | Industrial robot | No |
| [101] | Remote 3D laser welding | 6 | Industrial robot | Yes |
| [61] | Remote 3D laser welding | 7 | Industrial robot and scanner head | Yes |
| [42] | Remote ablation cutting | 9 | Industrial robot and scanner head | Yes |
| [42] | Remote ablation cutting and remote laser welding | 9 | Industrial robot and scanner head | Yes |
| [125] | Remote 3D fusion cutting | 6 | Industrial robot | Yes |
| | Remote 3D ROBO-CUT cutting | 6 | Industrial robot | No |
| | Remote 3D ROBO-CUT cutting | 7 | Industrial robot and beam rotator | Yes |
| | Remote 3D ROBO-CUT cutting | 10 | Industrial robot, beam rotator and scanner head | Yes |

**Table 2.2:** A list of several publications with the used Degrees of freedom involved in the setup.

positions can be reached in all orientations. The scanner heads is composed of a series of actuated mirrors that can move the laser beam on the workpiece by means of reflection. Often these mirrors are accompanied by a focus compensation module. This entails that for remote processing a scanner cutting head can have as many as 3 DOF. This entails that the 6 DOF from the ROBOT is added to the 3 DOF of the scanner heads giving a system with 9 DOF. If it furthermore is envisioned that the DOE of the ROBOCUT technology requires a rotation device to rotate the beam a ROBOCUT cutting head can have as many as 4 DOF. This results in a kinematic chain composed of as many as 10 DOF.

These long kinematic chains can be seen as a great asset as they render the mechanical system redundant in terms of the laser processing task that needs to be conducted on the workpiece [16]. This entails that a given pose in the

workspace of the robot can be reached with an infinity of robot configurations. In fact, when considering 3D laser processing with a round beam a traditional 6 DOF industrial robot can also be considered to be redundant as cutting head rotations around the axis of beam propagation will not affect the process. This entails that virtually all laser processes involving remote laser processing with a mechanical positioning system with more than 5DOF can be considered to be redundant. The use of redundant mechanical systems can generally be seen as a great advantage as it allows for optimizing the robot trajectories with respect to many parameters such as; collision avoidance [32], avoiding singular points in a trajectory, [84] and to reduce the required joint torques for a given trajectory [48]. The drawbacks are however that each joint introduces inaccuracies into the system [124]. These inaccuracies will propagate through the system and effect the end effector accuracy. Furthermore, each joint will result in a higher cost of the system, both from an acquisition point of view, but also when considering maintenance.

Finally, the many joints and thus the infinite set of robot configurations entails that programming of such systems increase in complexity. For remote laser processing this has increased to a level where traditional online programming is becoming infeasible, both due to the many DOF of the mechanical system, but also due to the fact that the robot tool flange is situated at a distance from the work piece, which makes manual robot positioning difficult for an operator [101]. This entails that algorithms for task sequencing and path generation for the mechanical system are needed for optimizing processing paths. Several frameworks has been presented in the scientific literature which will be discussed in the following section.

### 2.4.2 Task sequencing for remote laser welding

The trend towards offline programming for remote laser processing described in the previous section is mainly seen for remote laser welding (RLW). In the following a set of frameworks for task sequencing of RLW will be presented.

In [101] an automated RLW system for conventional optics is presented. By using augmented-reality for user interface presentation directly on a work piece weld seams are generated. By using a simple traveling salesman problem (TSP) solver an initial path is generated, this path is then modified by changing the laser incident angle. The TSP solver is based on Cartesian space distance, and the modification algorithm is based on the position of the cutting head in Cartesian space.

In [42–44, 83] a planning system is presented for both laser remote ablation cutting (RAC) and laser welding. The system works by identifying regions

around each task that enables the cutting head to reach the cutting kerf. These are circular regions denoted scan circles. A suitable robot path is then found within these scan circles and a corresponding scanner head path is then found. The scan circles are connected by straight lines and paths are connected by using the traveling salesman algorithm. The benefits of using this algorithm is that it decouples the scanner head and the robot. This again entails that an implementation can be done easily as the control units of the scanner systems and the robot are two separate units. The algorithm enables the use of processes that requires multiple passes such as the RAC algorithm. By utilizing scan circles it is however limited to 2D shapes, and as paths are connected by straight lines optimality cannot be guaranteed. Also the working field of the laser is limited to a circle and the level of redundancy of the robot and scanner system is not utilized to its full extent.

In [116] an approach to planning of RLW tasks for an articulated robot mounted with scanner mirrors is presented. It is based on defining clusters of points in the robot workspace that allows for welding of the seam in a task. One cluster is defined for each task and a GTSP solver connects these clusters by the shortest path. This algorithm utilizes the redundancy of the robot and scanner mirrors to minimize the processing time. The main drawback of the GTSP approach is however that it requires the start and end configuration of a task to be the same. Furthermore it does not take Kino dynamic constraints into consideration as it is unclear whether or not a given start or end configuration can be used when traversing the entire path.

In [61, 62] an integrated approach to rough cut path planning and task sequencing for RLW with scanner mirrors is presented. Access volumes are defined around start and endpoints of weld seams with the shape of truncated cones. These truncated cones are defined by the allowable incident angle of the laser beam and by the allowable focus range. By using a tabu search algorithm combined with a path planning heuristic that computes a close-to-optimal scanner path for each candidate task sequence. Redundancy is handled by fixing a joint to "mid-range" value.

In [25, 26] a set of algorithms is presented for solving the optimization problems related to each step of the work flow involved in remote laser welding. The presented work is based on the previously presented work in [61, 62]. In this framework a series of steps generates a collision free path. First all weld stitches are tested for accessibility, then a collision free scanner path is found in Cartesian space. Then the workpiece and fixture is positioned relative to the welding robot. The inverse kinematics are used to calculate robot joint configurations and the path is adjusted in a trajectory planning step. Finally collision detection is carried out. The generated path is then transformed to a

robot program and a simulation is conducted displaying key parameters.

### 2.4.3 Task sequencing for other applications

Besides the frameworks dedicated to the task of sequencing tasks in remote laser welding several other frameworks exists for other processes. In the following several other approaches will be presented.

In [2] the general problem of sequencing tasks, finding robot configurations and optimizing the resulting trajectories is treated in three components. The first component considers the problem of finding a sequence of points on task contours and their entry points by solving a traveling salesman problem with neighborhoods. In the second component the problem of finding robot configurations is treated by solving a touring-a-series-of-polygons problem (TPP). This is also done in the third component which treats the task of optimizing the robot trajectory. A welding example is given in which close to optimal paths are generated. The mechanical system is however simpler than for e.g. RLW.

In [18] a task sequencing framework is presented for flatbed traditional laser cutting. This paper incorporates many laser specific considerations such as piercing, pre-cut and sharp angles. The presented algorithm outperforms commercially available sequencing algorithms. The resulting system is however only 2D which entails that the mechanical system is simple compared to the ones for remote laser cutting and welding.

In [35] it is proposed to solve a TSP problem for goals located on a rotating table accessed by an industrial robot, by treating the combined mechanical system as one redundant system. By segmenting the goals into clusters a sequence is obtained. Then for each cluster two goals are determined as connectors for the previous and following clusters in the sequence. After that the TSP is solved with the Lin Kernighan heuristic in each cluster. The distance measure of the TSP problem is the Cartesian distance between nodes in the graph. Collision free paths are obtained by using the redundancy of the system.

In [22] an algorithm for robot task sequencing inspired by the fruit picking industry is presented. It concerns a near-minimum-time task-planning algorithm for fruit-harvesting robots. In this paper a TSP is solved in order to finding a minimum path. A cost matrix is calculated by using geodesics in the inertia space of the robot in order to minimize the cycle time while considering both robot kinematics and dynamics. However, the algorithm does not take

obstacle collisions into account.

In [132] an algorithm for task sequencing of welding tasks on a work piece is considered. The algorithm focuses on optimizing both productivity, in the cycle time sense, and quality, in the sense of distortion. In this paper the tasks are divided into two groups, one dealing with tasks with a high impact on quality and one group with the remaining points. The traveling salesman problem is solved by two approaches. Tasks in the group with low distortion impact are solved by the Elastic Net Method (ENM) [20] and the remaining points are solved by a genetic algorithm to reduce work piece distortion. The task is solved in 2D due to the complexity of the underlying model.

In [60] a task sequencing algorithm is presented for robotic painting system. The work presented herein is based on the development of scheduling models for the painting task which are capable of taking quality into account, in the sense of sagging and paint dust, while still evaluating a multitude of robot configurations. Two models are proposed, a dispatching rule scheduler and a constraint optimization scheduler. The proposed method decouples the scheduling problem from the motion planning stages. The work herein can be generalized to other processes, but relies on a finite set of solutions to the inverse kinematics.

### 2.4.4 Task sequencing for ROBOCUT

The frameworks and algorithms described for remote laser welding in section 2.4.2 have generally shown promising results. However, they generally treat the redundant nature of the large kinematic chains indirectly by defining Cartesian regions such as scan circles or access volumes within which solutions are found. These geometrical constructs should however be seen as a mapping of the redundancy space of the kinematic system which doesn't take all degrees of redundancy into account. The benefit is that solutions can be found faster by e.g. fixing joint values, the main drawback is however that the many levels of redundancy are not taken into account in the optimization procedure. With the introduction of the non-round beam of the ROBOCUT process it becomes even more difficult to keep a geometrical representation of the redundancy space. The algorithms presented in section 2.4.3 generally treat systems which are not redundant in nature. This entails that, on one hand more complicated task sequencing rules can be derived for e.g. quality but on the other hand the solutions are not applicable to the task of remote laser processing. This entails that the problem of task sequencing and path planning will be needed to be addressed.

## 2.5 Dissertation research objectives

Now that the goal and context of the ROBOCUT project has been presented in the previous sections the research objectives of this dissertation can be defined. The research objectives will be based on the description of the ROBOCUT technology from section 2.1-2.4. These research objectives will define the context within which this dissertation is written.

In section 1.1 it was discussed that the main contributions of this dissertation will fall within three areas of focus.

1. Developing and commissioning a flexible laser processing laboratory for the ROBOCUT technology
2. Analyzing the ROBOCUT remote cutting and the remote fusion cutting process
3. Developing a framework for task sequencing and path planning

In the following a set of research objectives will be defined and divided between these three areas of focus.

**Developing and commissioning a flexible laser processing laboratory for the ROBOCUT technology**

As discussed in section 2.3 the core technological difference between the ROBOCUT technology and other cutting technologies is the use of customized beam patterns for cutting. The beam intensity profile is altered by using a diffractive optical element which needs to be positioned in the beam path. This has the immediate consequences that the developed laboratory in which the processing is evaluated needs to be capable of conducting DOE laser processing. This concerns not only the task of modifying mechanical components such as cutting heads but also to the development of control system for these devices. Furthermore, as the potential cutting speed of the ROBOCUT technology is assessed to be in the range where scanner cutting heads are applicable (see section 2.2) some effort should be put in to investigating the applicability of such systems

- Develop a flexible laser processing laboratory for laser processing with DOE patterns.
- Develop a control architecture for the mechanical actuators with a flexible interface that allows for the implementation of advanced control algorithms.
- Investigate the applicability of using scanner mirrors for ROBOCUT remote cutting

As described in chapter 1 this area of focus is covered in chapter 3.

### Analyzing the ROBOCUT and the remote fusion cutting process

Another consequence of using diffractive optical elements in the beam path is that the beam intensity profile can change simply by changing the DOE. As the beam patterns of the ROBOCUT project are a work in progress it is necessary to develop a flexible laser processing laboratory that can evaluate the performance of a given DOE pattern. This evaluation should be based on knowledge of similar processes. As discussed in section 2.2 the ROBOCUT technology should be seen as both a remote process (RRC) and as a gas assisted process (RTC). This dissertation will mainly concern the development of the RRC process. As the RRC process can be seen as a refinement of the RFC process (see section 2.2) it is necessary to have a thorough understanding of the parameter windows within which RFC can be conducted. Such knowledge can be treated as a baseline with which ROBOCUT cutting can be evaluated. This leads to the following three research objectives.

- Develop a method and metric for fast evaluation of the stability of conducted laser cutting experiments.
- Determine the process windows within which RFC can be conducted with respect to parameters such as focus region, processing speed and incident angle.
- Evaluate the potential of ROBOCUT remote cutting by comparing experimental results to the RFC experiments.

As described in chapter 1 this area of focus is covered in chapter 4.

### Developing a framework for task sequencing and path planning

Furthermore, the introduction of cutting with customized beam patterns has the consequence that the beam can no longer be considered as being round. This means that the beam orientation becomes important which again entails that it needs to be included in the motion planning procedure.

- Develop an algorithm for generating paths for the remote laser cutting system that allows it to reconfigure itself while still cutting the specified contour.
- Investigate and develop algorithms for path sequencing for workpieces that requires multiple cuts, which takes the robot redundancy into account

As described in chapter 1 this area of focus is covered in chapter 5.

In the following chapters the obtained results within these three areas of focus will be presented and summarized.

# Chapter 3

# Developing and commissioning the ROBOCUT laboratory

As presented in section 1.3 this dissertation is composed of three areas of focus. This chapter covers the first focus area, the development and commissioning the ROBOCUT laser laboratory. As discussed in section 2.2 the ROBOCUT technology uses a diffractive optical element (DOE) inserted in the beam path to achieve a customized beam pattern. As no adequate laboratories have been identified nationally a new laser laboratory needs to developed and commissioned that can accommodate the needs for the ROBOCUT technology. In section 2.5 three research objectives were presented regarding this task:

- Develop a flexible laser processing laboratory for laser processing with DOE patterns.
- Develop a control architecture for the mechanical actuators with a flexible interface that allows for the implementation of advanced control algorithms.
- Investigate the applicability of using scanner mirrors for remote cutting

In the following sections these research objectives will be described and evaluated. Two scientific papers has been written as a part of this process which will be included as summaries.

The chapter will be organized in the following way: In section 3.1 a series of requirements for the laser laboratory will be presented based on the analysis of the state-of-the-art of traditional and remote laser processing which was

presented in chapter 2. This will lead to a description of the laboratory. This description will be divided into three areas which will be treated in different sections. In section 3.2 the laser source and optical components are described. In section 3.3 the mechanical platform will be described. In section 3.4 the software platform will be described. Finally, an evaluation of the resulting system will be carried out in section 3.5.

## 3.1 Analysis of Requirements

In the following section an analysis of the requirements for the flexible laser processing laboratory will be presented. It will be based on the information described in chapter 2. But before the requirements are described a short section describing a set of important laser processing parameters will be given as they are directly related to the development of the system requirements.

### 3.1.1 Parameters used in laser materials processing

As discussed in chapter 2.1 laser processing is conducted by moving a laser cutting head, delivering a high intensity laser beam, over a workpiece. Figure 3.1 shows a conceptual view of the optical path of a cutting head. From this

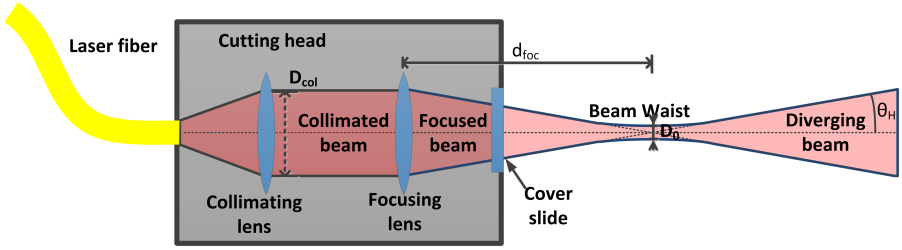


**Fig. 3.1:** The main optical components of a laser cutting head

figure it is seen that a laser beam is delivered to the cutting head by means of a fiber. When the beam exits the fiber it diverges. A collimating lens is then inserted to make the beam parallel and a focusing lens focuses it. The beam is sent out of the cutting head through a protective cover, the cover slide, and continues towards the work piece. Four parameters have been marked on the figure,

- $D_{col}$, collimated beam width, which is the beam diameter of the collimated beam diameter
- $D_0$,the beam waist diameter, which is the diameter of the beam at its narrowest point

- $d_{foc}$, the focal length, which is the distance from the focusing lens to the beam waist
- $\theta_h$ the half angle divergence, which is half the angle of divergence of the beam.

The beam intensity is often measured in power / area, and often in the units of $w/cm^2$. As the area of the beam decreases the intensity increases as the same amount of power is concentrated in a smaller area. This entails that in the beam waist the highest intensity is obtained, which is often wanted when doing laser materials processing. This leads to another parameter, the Rayleigh length $Z_R$, which is a quantity which is defined as the distance from the beam waist, in the direction of beam propagation, where the cross section area of the beam is doubled. The Rayleigh length can, for a Gaussian beam, be calculated by:

$$Z_R = \frac{\pi \cdot (D_0/2)^2}{\lambda} \tag{3.1}$$

Where $\lambda$ is the wavelength of the laser. The beam diameter can be calculated along the beam path by using the formula [115]:

$$D(z) = D_0 \cdot \sqrt{1 + \frac{4 \cdot M^2 \lambda \cdot z}{\pi \cdot D_0^2}^2} \tag{3.2}$$

where D(z) is the beam diameter at position z, $M^2$ is the beam propagation factor, $z$ is the distance from the beam waist in the beam direction. Of these parameters $M^2$ describes the divergence angle ratio between a theoretical Gaussian beam and a beam with the same minimum waist diameter. This entails that it can be seen as a measure of the focusability of the beam and thus a quality parameter. This parameter is generally related to the laser source and its construction. The beam waist diameter can be calculated by [115]:

$$D_0 = \frac{4 \cdot M^2 \lambda \cdot d_{foc}}{\pi D_{col}} \tag{3.3}$$

Where $D_{col}$ is the collimated beam diameter, and $d_{foc}$ is the focal length of the resulting focused beam. By inserting equation 3.3 into 3.2 the following beam propagation equation is obtained.

$$D(z) = \frac{4 \cdot M^2 \lambda \cdot d_{foc}}{\pi D_{col}} \cdot \sqrt{1 + \frac{4 \cdot M^2 \lambda \cdot z}{\pi \cdot (\frac{4 \cdot M^2 \lambda \cdot d_{foc}}{\pi D_{col}})^2}^2} \tag{3.4}$$

From these equations it can be seen that the beam propagation and beam waist diameter is controlled by several parameters. Where $M^2$ and $\lambda$ is generally related to the laser source, $D_{col}$ and $d_{foc}$ is related to the cutting head. The

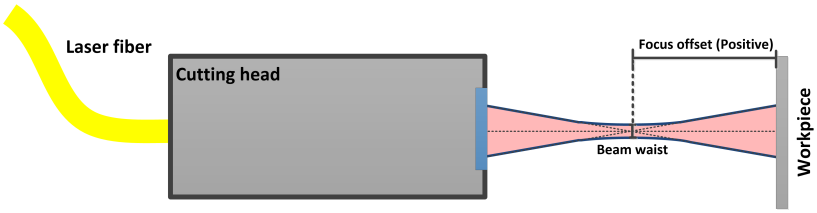


**Fig. 3.2:** The definition of focus used throughout in this dissertation

highest intensities are obtained when having a laser source with an $M^2$ close to 1, a wavelength as short as possible, a focal length as short as possible and a collimated beam width as large as possible. It should here be noted that the minimum beam diameter is of high importance for the ROBOCUT project as it also dictates the detail level of the generated beam patterns.

The beam waist is generally also denoted as the focus area of the beam. This area is often used for laser processing as it has the highest intensity. However, for other processes such as remote fusion cutting (RFC) or heat treatment it is necessary to work with a beam of a certain diameter. To ensure this for a single mode fiber laser it is necessary to work in an area where the beam is defocused. This entails that a definition is needed for defining to what extent the beam is out of focus. It has been chosen to use the distance from the beam waist to the surface of the work piece as a measure of where on the beam profile a process is achieved. This can be seen from 3.2. From this figure it is seen that positive focus values are obtained when the beam waist is located above the surface of the work piece. This entails that negative focus values are obtained when the beam waist lies underneath the surface of the work piece.

Now that a set of laser processing definitions have been given the requirements for the system will be presented. It has been chosen to divide the requirements for the laboratory into three categories dealing with various parts of the complete system. These categories are:

- Laser source and optical components
- Mechanical platform
- Software platform

In the following the requirements within these categories will be described individually starting with the requirements for the laser source and optical components.

### 3.1.2 Requirements for the laser source and the optical components

The first set of requirements deals with the laser source itself. The requirements listed below are mainly derived from the process descriptions given in section 2.

- **Power**
  3-4kW
  As described in table 2.1 in section 2.1.2 remote fusion cutting has been done with 4kW of laser power. As the ROBOCUT technology uses DOE's to obtain a more efficient melt ejection it should require less power than RFC to obtain stable cuts.

- **Beam Quality**
  $M^2$ as close to 1 as possible
  As discussed in section 3.1.1 the $M^2$ value determines how the beam propagates. As the quality of the created intensity patterns are linked to the $M^2$ value it is necessary that it is as close to 1 as possible.

- **Beam waist diameter**
  $D_0$ as small as possible.
  The smaller $D_0$ the higher the detail level of the resulting intensity pattern.

- **Beam Guidance**
  Fiber transmission
  As the ROBOCUT technology is robot based it is a requirement that the transmission of laser power from the source to the processing head is conducted by means of a fiber and not by mirrors. This has been chosen to increase the flexibility of the set-up and to lower the maintenance requirements.

- **Modes of operation**
  CW and pulsed
  The main idea behind the ROBOCUT project is to create a steady flow of molten material out of the cutting kerf by using a continuous wave laser source. This is what is generally used in laser metal cutting and welding as it keeps a consistent kerf and seam quality. Pulsed mode would however also be of interest as it can introduce oscillations in the melt flow boosting the melt ejection.

The next set of requirements are related to the cutting heads and other optical components of the system.

- **Diffractive optical element**
  It is a requirement that an optical element can be inserted in the collimated beam path
  When conducting ROBOCUT laser cutting it is necessary that a diffractive optical element can be inserted in the beam path. This needs to be done in the collimated beam path to ensure the integrity of the resulting beam intensity.

- **Cutting gas**
  The cutting head needs to be capable of delivering reactive and inert gasses (e.g. Oxygen and nitrogen) to the work piece with a controllable pressure between 0-20 bar
  As traditional laser cutting is conducted with a cutting gas it is necessary that the cutting head can be used with the traditional cutting gasses used in the industry.

- **Several focal lengths**
  It is required that the acquired cutting head(s) can accommodate different focusing lenses to allow for several focal lengths.
  From equation 3.3 it can be seen that a trade-off exists between obtaining long focal lengths for remote processing and obtaining small beam waist diameters for traditional laser processing. This entails that it is a requirement that the cutting head can accommodate several focal lengths.

- **Remote scanning**
  It is a requirement that the system can be upgraded with a scanner system
  In section 2.2 a graph showing the potential of the ROBOCUT with regards to processing speed was presented. From this it was noted that the potential cutting speed of the ROBOCUT process exceeds 150 m/min. This can generally only be realized with the use of scanner mirrors, especially when dealing with complicated work pieces.

It should be noted that the above list is not exhaustive as many simple requirements with regards to e.g. the geometry of the cutting head has been omitted. Also requirements with regards to the optical components such as the damage threshold for lenses and cover slides has been omitted.

### 3.1.3 Requirements for the Mechanical platform

In the following the requirements for the mechanical system will be specified. The requirements described here are generally based on section 2.4. It is envisioned that the majority of cutting will be conducted on non-curved surfaces (2D). It has however also been specified that the ROBOCUT project is robot

based which indicates the need for 3D cutting capabilities. This entails that two sets of requirements have been established, one concerning 2D cutting, and one concerning the robot enabling the system to perform 3D laser processing.

- **DOF**
  3 - Translation in the X and Y direction and beam rotation
  As described in section 2.1.1 traditional laser cutting is often conducted on an XY repositioning system. The non-round beam of the ROBOCUT does however require that the beam pattern needs to be aligned with the cutting direction. This entails that a beam rotating device is necessary.

- **Focus offset**
  An additional translational axis is required for offsetting the focus of the beam
  To further increase the flexibility of the laboratory it has been chosen to add a requirement for an additional axis for changing the focus of the laser beam. The axis does however not have to be motorized as focus should remain constant when cutting.

- **Velocity**
  Translational speed 60 m/min
  In section 2.1.2 several laser processes were described. It was also mentioned that commercial products exists which can realize cutting speeds exceeding 60 m/min [106]. It has been chosen to use the 60 m/min (1m/s) as a requirement for the laboratory.

- **Acceleration**
  Translational acceleration $10m/s^2$
  It has been chosen to specify the acceleration of the system by specifying that the maximum speed of 1m/s needs to be obtained on a distance of 5 cm. This is equivalent to specifying an acceleration of $10m/s^2$.

- **Accuracy**
  Static accuracy 0.1 mm
  Dynamic accuracy 5mm
  As the main objective of the laboratory is to evaluate the cutting potential of the ROBOCUT technology and not to be a part of a production chain, its ability to track a trajectory of small importance.

When regarding the requirements for the robot conducting 3D laser cutting the following set of requirements have been specified.

- **Robot**
  Articulated with more than 5 DOF
  This has been set as a requirement as the robot should be capable positioning the beam at any position and at any angle within the work

envelope. If a 5 DOF robot is chosen this implicitly entails that a beam rotation device needs to be used for aligning the beam with the cutting direction.

- **Reach**
  >2m
  As the reach of the robot limits the maximum size of the objects that can be processed the minimum reach of the robot needs to be defined. As the ROBOCUT consortium is composed of several manufacturers dealing with various sizes of workpieces it is impossible to determine a robot that is applicable in all cases. It has been chosen require a reach of at least 2 meters as it is enough to reach above a car (Case considered for Volvo) and as it is enough to process various steel profiles form Ib Andresen industries [51].

- **Payload**
  >80 kg
  The robot needs to be capable of carrying the cutting head and other pieces of equipment. It has been assessed that the cutting head weighs approximately 20 kg. It is furthermore envisioned that a high speed camera (also approximately 20 kg) might have to be mounted simultaneously on the robot. As the robot might have to carry additional pieces of equipment such as various tool flanges, the minimum required payload is set to 80 kg.

- **Speed**
  1 m/s
  The requirements for speed can be seen in the previous section for 2D cutting.

- **Operating environment**
  Industrial metal processing
  Even though the robot is acquired as a part of laboratory it is required that the robot should be capable of operating in with the same tasks in the industry. This is done to ensure the reliability of the system.

### 3.1.4 Requirements for the Software platform

The following section contains the main requirements for the software platform which is used to control the actuators and sensors of the entire laboratory.

- **Software and hardware interfaces**
  It is a requirement that the system can interface to the acquired hardware components used in the project. This includes the XY table, the cutting head sensors, the laser source, beam measurement equipment and the robot.

- **Real time capabilities**
  To control the motion of the various actuators and to synchronize the laser output with this motion it is necessary that the control system has real-time data processing capabilities.

- **CAM interpreter**
  The system is required to be capable of interpreting G-codes.
  This has been chosen as G-codes are one of the most widely used ways of controlling CAM systems ranging from private 3D printers to large scale industrial flatbed laser cutters.

- **Options for programming**
  To increase the flexibility of the laboratory and to be able to implement more advanced control algorithms an interface for high-level programming such as C#, Java or Python is also a requirement.

- **Upgradeable** It is required that the software platform is upgradeable when considering its hardware interfaces.
  This is required as the pieces of equipment the system needs to control and read data from will change as more equipment is acquired. To ensure that the system is not limited by decisions taken in the early stages of the project it is necessary to ensure that the system can be upgraded.

Now that the requirements have been established for the system the following sections will describe the optical, mechanical and software system developed.

## 3.2 Laser source and optical components

Based on the requirements specified in the previous section the optical components of the test facilities can be specified starting with the laser source.

### 3.2.1 Laser source

As discussed in the previous section the chosen laser source should comply with the following requirements:

- **Power**: 3-4kW
- **Beam Quality**: $M^2$ as close to 1 as possible.
- **Beam waist diameter**: $D_0$ as small as possible.
- **Beam Guidance**: Fiber transmission
- **Modes of operation**: CW and pulsed

Table 3.1 shows an overview of the resulting beam intensities obtained by various laser sources with the same power rating, focal length and collimated beam diameter. This table is adapted from [65]. From this it is seen that both $CO_2$

| Parameter | | Laser type | | | | |
|---|---|---|---|---|---|---|
| | | $CO_2$ | Nd:YAG Disc (DP) | | MM fiber | SM fiber |
| Power | [kW] | | | 1 | | |
| Focal length ($d_{foc}$) | [mm] | | | 200 | | |
| Collimated beam diameter ($D_{col}$) | [mm] | | | 12 | | |
| Wavelength ($\lambda$) | [$\mu$ m] | 10.6 | 1.064 | 1.030 | 1.070 | 1.076 |
| Beam quality factor ($M^2$) | | 1.8 | 35.4 | 12.2 | 7.3 | 1.1 |
| Beam waist diameter $D_0$ | [$\mu$ m] | 409 | 800 | 267 | 167 | 26 |
| Intensity | $\left[\frac{kW}{mm^2}\right]$ | 8 | 2 | 18 | 46 | 1879 |

**Table 3.1:** A table showing the resulting beam intensity for 5 commonly used industrial laser types with the same power rating, collimated beam diameter and focal length. Notice that intensity wise the single mode fiber laser outperforms all others by a significant margin

lasers and single mode fiber lasers have $M^2$ parameters close to one. The larger wavelength of the $CO_2$ laser does however entail that the resulting $D_0$ is much larger than for SM fiber lasers. This again results in beam intensities much larger than for $CO_2$ lasers. To obtain the required detail level of the patterns and to avoid the mirror guidance of the $CO_2$ laser the only option is the single mode fiber laser. It has been chosen to use an IPG YLS-3000 SM laser which is a 3kW single mode fiber laser. The main drawback of this is that single mode fiber lasers are very expensive when compared to e.g. multi-mode fiber lasers. Furthermore when conducting traditional laser cutting a too narrow cutting kerf is not necessarily better as it can inhibit the melt ejection, which makes it difficult to utilize the high beam intensities. Results have however been published which indicates that cutting with single mode fiber lasers can possibly increase the maximum achievable cutting speeds by traditional industrial lasers by as much as a factor of two [65].

### 3.2.2 Cutting heads

It was in section 3.1.2 discussed that the system should be capable of conducting traditional laser cutting. Furthermore it was discussed that with an upgrade the system should be capable of conducting scanner based remote cutting. As remote scanning cutting heads are actuated devices they will be treated in the

section concerning the mechanical system discussed in section 3.3.3. In the following section the traditional cutting heads will be discussed.

### Traditional cutting heads

In section 3.1.2 it was described that the cutting head needs to comply with the following requirements:

- **DOE:** It is a requirement that an optical element can be inserted in the collimated beam path
- **Gas nozzle:** The cutting head needs to be capable of delivering reactive and inert gasses (e.g. Oxygen and nitrogen) to the work piece with a controllable pressure between 0-20 bar
- **Focal lengths:** It is required that the cutting head can accommodate different focusing lenses to allow for several focal lengths.

As existing cutting heads cannot accommodate these requirements it is necessary to either construct a new cutting head from scratch or to modify existing solutions. As there is a lot of know-how involved in the development of cutting heads it has been chosen to base them heads on modified commercially available systems. As the size of the DOE induced beam pattern is dependent on the focal length of the cutting head, a design allowing for a change of focus lens is necessary. To reduce the amount of mechanical components, and to reduce the setup time between experiments with different focal lengths it has been chosen to create a cutting head based on a modular design, which can be seen on figure 3.3. Here it is seen that a collimation module collimates the beam

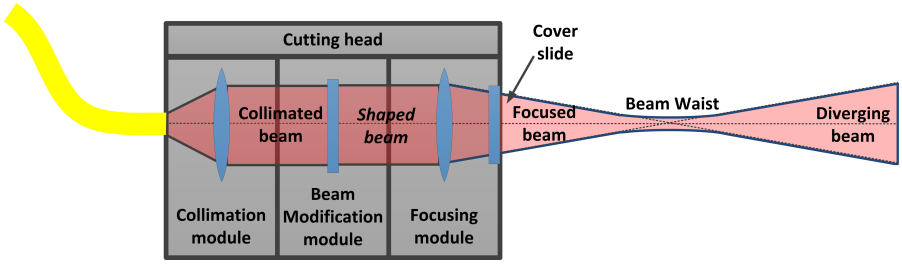


**Fig. 3.3:** Modular approach to the cutting head.

coming from the laser fiber. Then the beam propagates to the beam shaping module, where the DOE changes the phase pattern of the incoming beam to yield a customized beam shape. After the beam shaping modules the beam propagates to the focusing module where an interchangeable lens focuses the

beam on the work piece. Two beam modification modules have been made, one which is used for fixed DOE positioning in the beam path, and one which includes a motorized DOE rotator. When considering the focusing modules it is difficult to specify optimum focal lengths for the modules as the use of customized beam shapes for laser cutting is a new field of study. From equation 3.3 it can be seen that a trade-off exists between obtaining long focal lengths for remote processing and obtaining small beam waist diameters for generating smaller patterns. Four focus modules have been chosen for the initial setup, which yields focal lengths of 780 mm, 470mm, 300mm and 200mm. If other focal lengths needs to be considered at a later stage of the project the modular approach will ensure that they can simply be purchased separately. The resulting beam parameters obtained by these focus modules can be seen from table 3.2. From this table, and from equation 3.4 it is seen that as the focal length

YLS-3000-SM cutting head focus modules

| Parameter | Module 1 | Module 2 | Module 3 | Module 4 |
|---|---|---|---|---|
| Manufacturer | HighYag | HighYag | Optoskand | Optoskand |
| Focal length[mm] | 780 | 470 | 300 | 200 |
| $D_0$ [mm] | 0.116 | 0.070 | 0.045 | 0.030 |
| $D_{col}$ [mm] | 11.05 | 11.05 | 11.05 | 11.05 |
| $\theta_h$ [m °] | 14.2 | 23.5 | 36,8 | 55,2 |

**Table 3.2:** A summary of the parameters for the four acquired laser cutting head focus modules. Notice that as the focal length goes up the minimum beam diameter increases.

increases, the minimum beam diameter also increases. This entails that a $M^2$ as close to one as possible is necessary to achieve high intensities for large focal lengths. Figure 3.4 shows a plot of the beam diameter as a function of the distance from focus. From this it is seen that a short focal length has a very small beam diameter, it is however also seen that it is much more sensitive to focus variations and thus the accuracy of the positioning system.

To ensure that the system is not dependent on a single manufacturer of cutting heads it has been chosen to acquire two cutting heads from different manufacturers, one from Optoskand for the 200 mm and 300 mm focal length and a HighYag BIMO cutting head for 780 mm and 470 mm focal lengths. Both cutting heads have been modified with a static DOE module and adapters for the motorized DOE rotator. These developed components can be seen from figure 3.5.

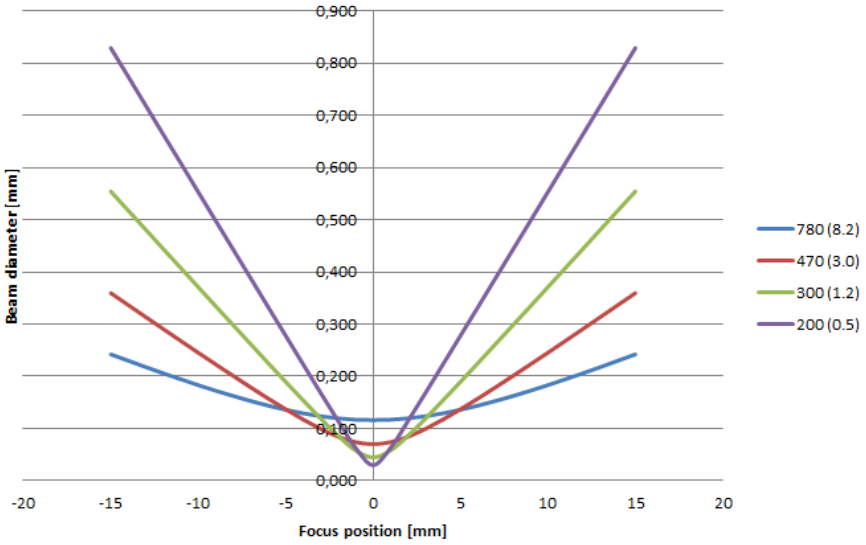


**Fig. 3.4:** The obtainable focus with the acquired cutting heads. By using equation 3.4 the beam diameter can be found for the four cutting heads. The four colors (Blue Red Green and purple) denotes the focal lengths of the four cutting heads (780 mm, 470 mm, 300 mm and 200 mm respectively). The number in parenthesis denotes the Rayleigh length for the given cutting head. A similar has previously been published in [64]

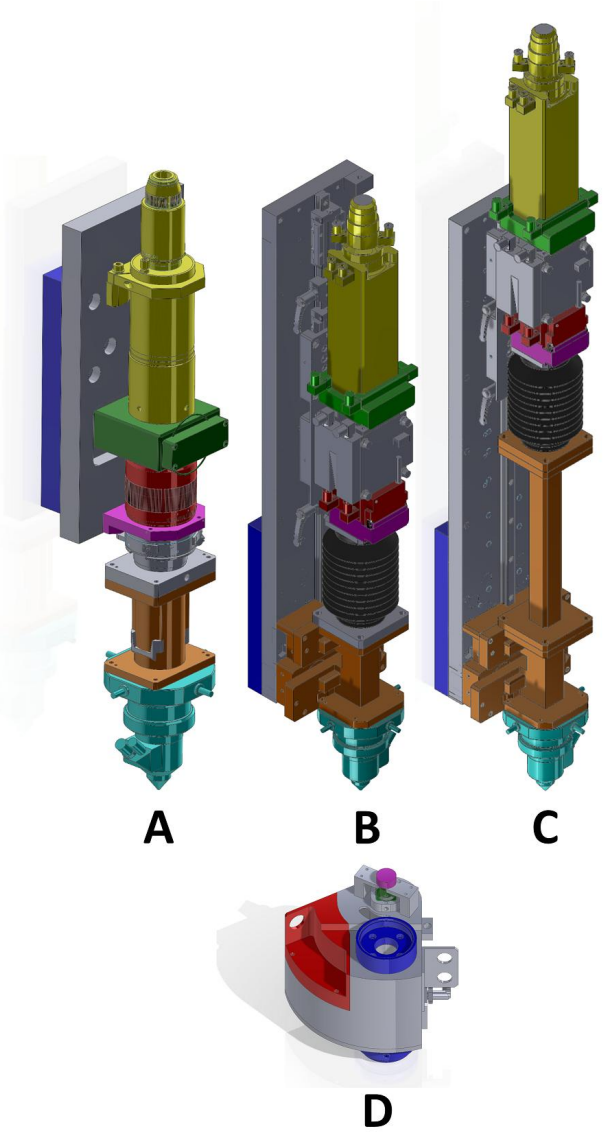


**Fig. 3.5:** The two cutting heads modified with a DOE module in the collimated beam path. A depicts the Optoskand head, B depicts the compact HighYag head and C depicts the applied extension for the HighYag head. D depicts the motorized beam rotator device. The colors on figure A,B and C shows the beam collimation unit (yellow), the beam shaping module (green), the focus module (red), adaptor pieces (orange) and gas nozzle (turquoise). On D Green depicts the rotating actuator, purple depicts the encoder, red depicts the lid used when exchanging DOEs and Blue the connection flanges.

It should however be noted that these cutting heads are all designed with the task of traditional laser cutting in mind as it can be seen from the presence of the gas nozzle. By removing the gas nozzle remote cutting and welding experiments can however be conducted, although without scanner mirrors.

## 3.3 Mechanical platform

Now that the laser source and optical components have been determined the mechanical platform can be specified in further detail. The mechanical system is composed of the actuators repositioning the laser beam with respect to the work piece. As described in section 2.2 the ROBOCUT technology covers two different cutting processes ROBOCUT remote cutting (RRC) and ROBOCUT traditional cutting (RTC). In RTC the generated gas from the evaporated material boosts the melt ejection of the applied cutting gas. In RRC no external cutting gas is applied and remote cutting is achieved. This entails that the mechanical set-up should be capable of conducting gas assisted 2D laser cutting, gas assisted 3D laser cutting and 3D Remote laser cutting. These capabilities can be realized in many ways, e.g. by an industrial robot alone. This is in many ways an appealing solution as it offers a very flexible and reliable mechanical platform. It would furthermore ensure that the programming can be conducted via a common and simple interface. It has however been chosen to expand such a set-up with an XY table. Such a set-up can be seen on figure 3.6. The figure shows an industrial robot mounted with a tool flange on which

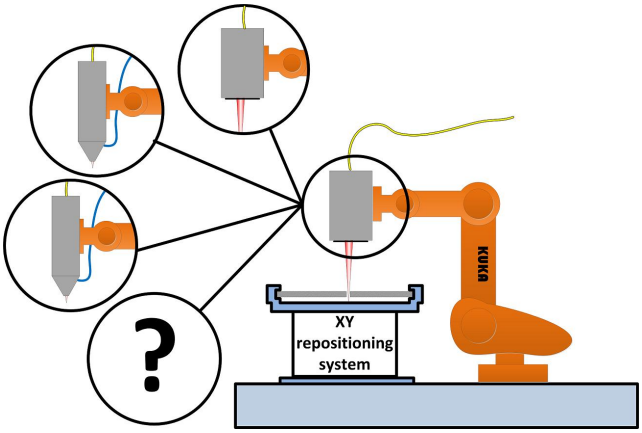


**Fig. 3.6:** A laser processing setup composed of two repositioning systems and a set of interchangeable cutting heads.

several cutting heads can be attached. An XY table is positioned below which can be used for fast 2D repositioning of a work piece. When conducting 2D cutting the XY-table is moved while the robot remains stationary and when

conducting 3D cutting the XY table remains stationary while the robot performs the motions. By mounting the laser cutting head on the robot it can be positioned with the flexibility of the industrial robot. This entails that the focus and incident angle of the laser beam on the work piece can be changed easily. Also, when 2D cutting is conducted the cutting head can be mounted on a static tool flange (Not shown on the figure) which entails that the industrial robot can be used as a mount for other pieces of measurement equipment such as high-speed cameras which makes it easy to focus directly on the processing zone. Furthermore the XY table can emulate the behavior of a conveyor and processing on moving objects can be conducted by the robot. In section 3.1.3 it was chosen to create two sets of requirements, one for 2D cutting and one for robot cutting on curved surfaces. These are listed below:

**Requirements for robot cutting**

- **Robot configuration**: Articulated with more than 5 DOF
- **Reach** :>2m
- **Payload** :>80 kg
- **Speed**: 1 m/s
- **Operating environment rating** : Industrial metal processing

**Requirements for 2D cutting**

- **DOF**: 3 - Translation in the X and Y direction and beam rotation
- **Focus offset**: An additional translational axis is required for offsetting the focus of the beam
- **Acceleration**: Translational acceleration $10m/s^2$
- **Accuracy**:
  Static accuracy 0.1 mm
  Dynamic accuracy 5mm

Furthermore it was described that the system should be capable of supporting scanner based remote laser processing heads:

- **Scanner cutting head :** It is a requirement that the system can be upgraded with a scanner system

In the following the mechanical platform will be described. It should however be noted that many of the key technological parameters for the chosen components have been omitted to increase the readability.

### 3.3.1 Industrial robot

Based on the requirements it has been chosen to acquire a KUKA QUANTEC KR 120 R2500 pro for the laser processing laboratory. It has a reach of 2.5 meters and a rated payload of 120 kg. From the official website [33] it is recommended for 30 different applications including laser cutting, laser welding, waterjet cutting, arc welding and machining. It is, with its high accuracy counterpart KUKA KR 120 R2700 extra HA, a common choice in materials processing research [68–70]. The robot has a pose repeatability of ±0.06 mm (ISO 9283). In contrast the high accuracy counterpart has a repeatability of ±0.05 mm. The high accuracy robot was however unavailable at the time of purchase. The difference in accuracy is however very limited and the accuracy of the KUKA KR 120 R2500 pro is still within the requirements described for 2D cutting which entails that all accuracy requirements can be taken into consideration. The robot, with a set of dimensions can be seen from figure 3.7. When considering the speed requirement of 1m/s it is not directly specified

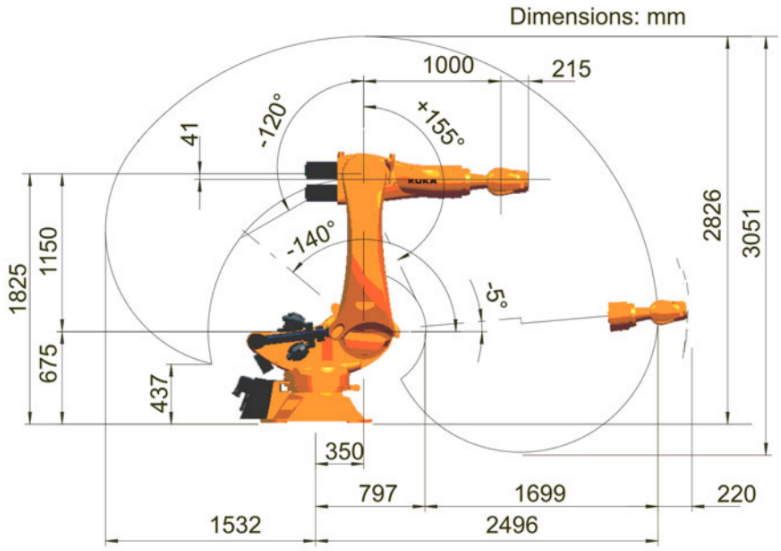


**Fig. 3.7:** Shows the KUKA robot with joint limits and link lengths [33]

in the robot specification, as the Cartesian speed depends on the joint configuration of the robot. Instead maximum joint speeds are given which can be converted to Cartesian velocities. The maximum joint speeds can be seen from table 3.3. To assess if speeds of 1m/s can be obtained, a quick calculation is performed. From table 3.3 it can be seen that the speed of joint 1 alone is 136°/s. If the robot is in the initial configuration, as seen on figure 3.7 then the center of the robot wrist will be 1350mm from the robot base horizontally.

| Axis | Range of motion | Speed with rated payload |
|---|---|---|
| 1 | ±185° | 136°/s |
| 2 | −5° to −140° | 130°/s |
| 3 | +155° to −120° | 120°/s |
| 4 | ±350° | 292°/s |
| 5 | ±125° | 258°/s |
| 6 | ±350° | 284°/s |

**Table 3.3:** A table showing the maximum and minimum angles of the robot joints. Also, the maximum joint speeds can be seen from the table.

This entails that a maximum speed in this configuration can be calculated as:

$$v = \frac{2 \cdot \pi \cdot 1.350m}{360°} \cdot 136°/s = 3.2m/s \tag{3.5}$$

which is well beyond the required 1m/s. More information with regards to the robot can be found in appendix I or in the robot specification [33].

### 3.3.2 XY table and auxiliary axes

Now that the industrial robot has been specified it is necessary to determine the specifications for the XY-table. To reduce the workload it has been chosen to hire a subcontractor to develop an XY table that can perform as specified by the requirements. The resulting system can be seen from figure 3.8.
From this figure it is seen that the system is composed of two sliders, which

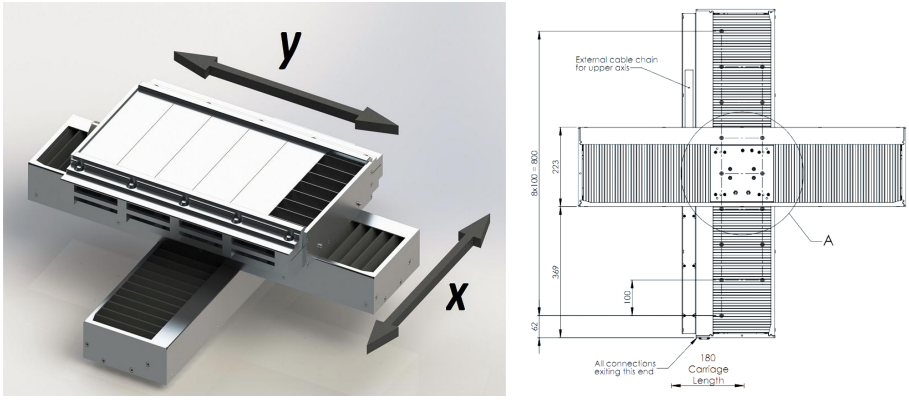


(a) Shows a cad drawing of the XY table acquired from Q-Sys

(b) A technical drawing of the XY system from Q-sys

**Fig. 3.8:** The XY table used in the laboratory, on the left figure a CAD drawing of the system is shown and on the right a technical drawing of the dimensions can be seen.

moves the stage in the X and Y direction. From figure 3.8(b) it is seen that the stroke is about 800mm-180mm=620mm in both the X and Y direction. The system is powered by two LC-050-100 linear actuators from Anorad [5] which are controlled by two kinetix 3 servo drives from Allen-Bradley [3]. Physically, the XY table is mounted on a heavy granite table to reduce vibrations. Besides the XY table specified above a stationary cutting head flange is mounted on a linear actuator which is mounted above the XY table forming an extra Z axis. This Z axis has been included to have a fast and easy way of performing z axis adjustments. This Z axis is driven by a Bosch Rexroth Indradrive CS [102].
Now that the non-robot axes have been described the concept of a mechanically actuated cutting head for remote laser processing will be discussed in further detail.

### 3.3.3 Remote cutting heads

In section 2.2 two graphs were presented showing the potential of the ROBOCUT cutting technology. From these figures it is seen that the cutting process has the potential to yield speeds exceeding 150m/min or 2.5 m/s. When this is combined with fast accelerations it depicts one of the problems with the mechanical repositioning systems for laser processing, namely that the laser power/processing potential of state-of-the-art laser sources are no longer the limiting factor when considering laser processing. Instead it has changed to be the mechanical actuators controlling the systems. By including scanner mirrors in the mechanical set-up it is possible to relocate the laser beam over the work piece at very high speeds reaching more than 360 m/min [134]. The low inertia of the scanner mirrors furthermore enables them to have excellent acceleration properties, which ensures that they can process complicated contours. This entails that by using scanner mirrors the mechanical system can accommodate very fast processes over very complicated contours. The presence of scanner mirrors can however also help the repositioning of the beam between tasks, effectively minimizing the task spent on repositioning the robot from one task to another. This entails that the possibility of utilizing scanner technology with the ROBOCUT technology is an option that shouldn't be ignored.

Several off-the-shelf scanner mirror components and complete scanner units exists that can be used for e.g. remote laser welding. However, not all scanner based remote cutting heads can be adapted to include a DOE in the collimated beam path. Generally scanner based cutting heads are composed of a series of optical components. A conceptual overview of such a scanner system can be seen from figure 3.9. From this it is seen that it consists of the traditional optical components such as the collimating lens. Furthermore it is seen that the DOE is inserted in the collimated section of the beam. Furthermore, a mirror system, which is here depicted by a static mirror and a scanner mirror system,

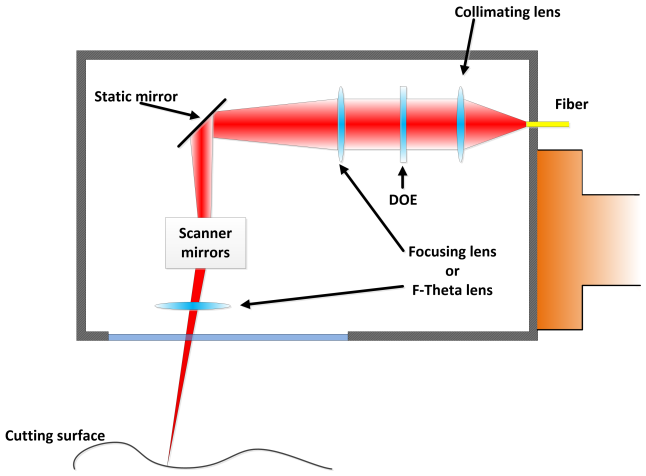


**Fig. 3.9:** Shows a conceptual overview of the configuration of a remote scanner cutting head. Notice that often two scanner mirrors are used and that the focusing optics is either a traditional focusing lens or an F-theta lens.

is inserted in the beam path. Often there are 2 scanner mirrors configured in such a way that they scan in directions perpendicular to each other (X and Y direction). The main difference for such a scanner system, when compared to the traditional laser cutting head depicted in figure 3.3, is however that the focusing can be conducted by a traditional focusing lens inserted before the scanner mirrors or an F-theta lens inserted after the mirrors. An F-theta lens is a specific type of lens often used in laser scanning applications. It ensures that a flat image plane is obtained when using the scanner mirrors. When conventional optics are used this is not the case as the resulting image plane will be curved. This can be seen from figure 3.10. One of the main concerns of using F-theta lenses is however that the lens will affect the intensity pattern generated by the DOE as the F-theta lens relies on a distortion of the image field. This effectively rules out the use of scanner optics based on F-theta lenses for the ROBOCUT project. Instead a scanner system based on conventional optics can be used. The use of conventional optics does however require that focus adjustments can be made in such a way that a flat image field can be generated. This can be achieved in several ways. The first option is to move the collimating lens in the direction of beam propagation. This ensures that the collimated beam width changes and thus the focus position. This is however not a viable option as the DOEs are designed for a specific collimated beam width. Many 3D scanning systems from e.g. Scanlab and Cambridge technology [107, 119] are in fact based on this type of focus adjustment. Another option is to move the focusing lens by means of a linear actuator. This would ensure that the focus adjustment could be done without changing the collimated beam width.

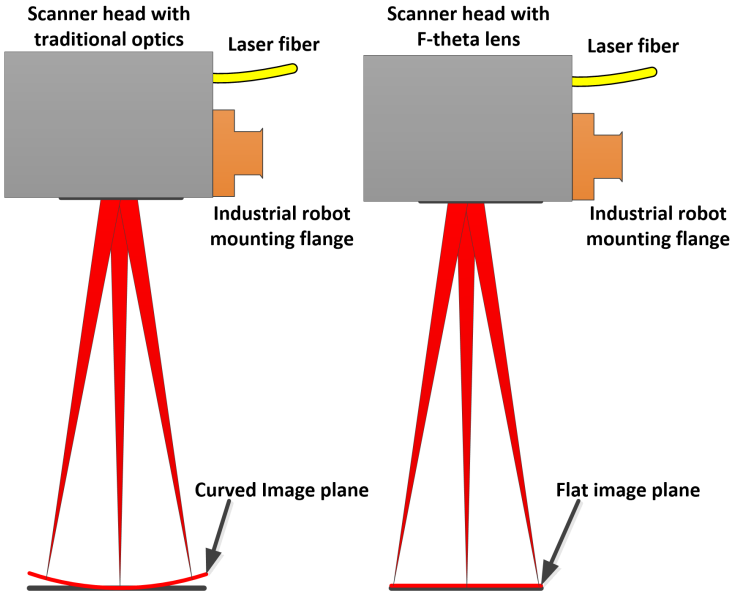


**Fig. 3.10:** The resulting image planes from conventional optics and F-theta lenses. Notice the flat image plane when using F-theta lenses. Furthermore the lenses can ensure that a linear relationship exists between deflection angle and resulting position.

Finally the third option would be to move the scanner mirrors on a linear actuator in such a way that the final mirror remains stationary. Several designs have been investigated during the course of this Ph.D. some of which can be found in Appendix II. No commercial systems have however been identified which are based on these focus adjustment designs. This has entails that it has proven to be difficult to find a suitable 3D scanner systems where the DOE can be inserted. The individual components are however available for purchase so a customized cutting head can be produced.

Furthermore, it has been a concern that the long kinematic chain of the complete mechanical system could pose a problem when considering the accuracy of the beam positioning. This has entailed that a paper has been made which assesses the theoretical accuracy of the mechanical system based on an analysis of joint uncertainties. A summary of this paper will in the following be presented. In this paper the derivations are based on a scanning system from Cambridge technology [119]. It should however be noted that the nomenclature used in the paper differs from the one that is used in this dissertation.

### 3.3.4 Summary of paper B: Theoretical Limits of Accuracy of Industrial Robots with Scanner Heads for Remote Laser Cutting

The following section contains a summary of the obtained results from the paper "Theoretical Limits of Accuracy of Industrial Robots with Scanner Heads for Remote Laser Cutting".

#### Objectives

1. To analyze the potential drawback of the redundancy of scanner head mounted industrial robots with respect to theoretical accuracy.
2. To develop the kinematic descriptions used in the remaining work of this dissertation.
3. To present a conceptual overview of the Remote laser cutting head used for ROBOCUT cutting.

#### Summary

In the last decade remote laser processes have received much attention from the research community as their ability to cut and weld from distances $> 1000$mm has the possibility to greatly increase the productivity of modern production lines. Furthermore the remote position of the cutting head reduces the risk of cutting head collisions with the work piece. These benefits does however come at a cost as the requirements, when it comes to beam quality of the laser and the accuracy of scanner and robot systems, are high. The mechanical systems are also very complex as they are often composed of both a scanner processing head and an industrial robot. For remote ablation cutting as much as 9 DOF are necessary. As the ROBOCUT technology alters the round symmetrical pattern of standard laser beams it is necessary to include a rotational axis for rotation of the diffractive optical element. The resulting 10 DOF's can be seen as one long kinematic chain, which, due to the many DOFs, can be seen as being redundant in terms of the cutting or welding task. These kinematic system can be seen as two chains F and K, where K describes the kinematics link between the robot base and the robot tool flange and F describes the kinematic link between the robot tool flange and the focus point of the laser beam. This is illustrated in figure 3.11. This redundancy is beneficial as it increases the flexibility of the system and offers the possibility of solving other tasks such as collision avoidance. The many degrees of freedom can however also be seen as a disadvantage as every joint introduces inaccuracies that propagate throughout the system.

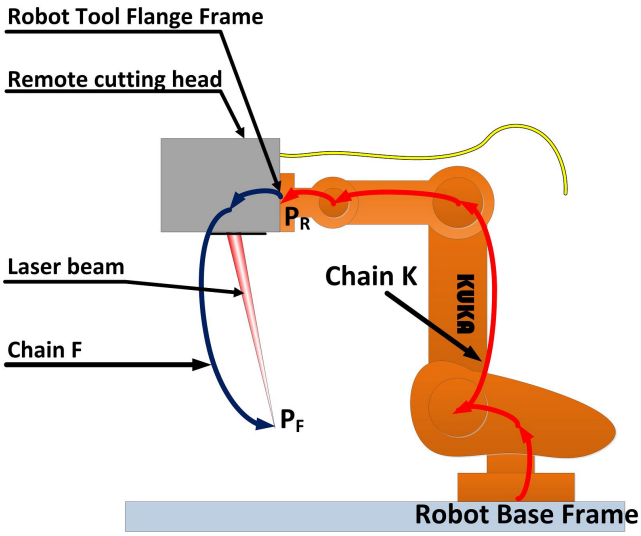


**Fig. 3.11:** The two kinematic chains describing the robot mounted with scanner mirrors [124].

By using the kinematics of the robot and the scanner mirrors it is possible to derive expressions describing the link from robot base frame to the robot tool flange frame. And the position of the laser beam focus point $P_f$ in the tool flange frame. If $P_F$ is decomposed into its X Y and Z components in robot base frame coordinates then its position can be defined by the forward kinematics F of the entire chain. If the joint variables are put into a vector v;

$$v = \begin{bmatrix} R_X & R_Y & R_Z & R_\alpha & R_\beta & R_\gamma & \phi & \theta_1 & \theta_2 & d \end{bmatrix}^T \tag{3.6}$$

Where $R_X, R_Y, R_Z$ are the positional coordinates of the tool flange frame, $R_\alpha, R_\beta, R_\gamma$ are the orientation components of the tool flange frame in xyz Euler angles. $\phi$ is the variable associated with the beam rotator,$\theta_1$ is the variable associated with the first mirror in the beam path and $\theta_2$ is the second mirror in the beam path, and finally $d$ is the distance of the linear actuator controlling the focus. Then $P_F$ can be written as:

$$P_F = \begin{bmatrix} X_{P_F} \\ Y_{P_F} \\ Z_{P_F} \end{bmatrix} = F(v) \tag{3.7}$$

A conceptual overview of the configuration of the cutting head can be seen on figure 3.12. The kinematic equations for the the cutting head seen in this image is described in appendix II.1. By using the forward kinematics it is possible to calculate how variances in the input variables effects the variance of the output

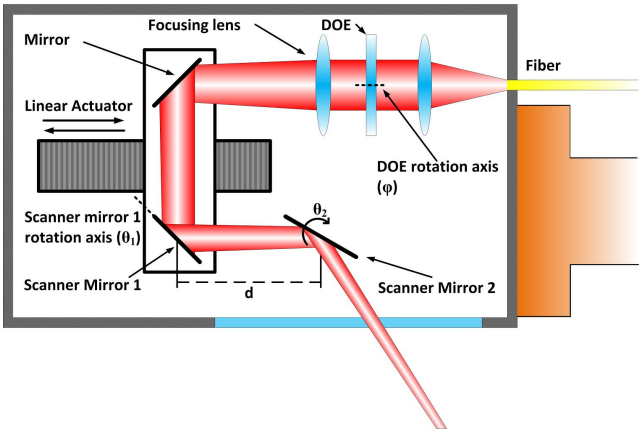


**Fig. 3.12:** A conceptual image of the components in a laser cutting head used for the derivation of the inverse kinematics [124].

variables. By using the derived kinematic definitions it is possible to determine how variances in $v$ are mapped to $P_F$. This is given in the form of a covariance matrix $C_{P_f}$, which is shown in 3.8.

$$C_{P_f} = \begin{matrix} \\ \\ \\ \end{matrix} \begin{matrix} X_{P_F} \\ \\ \\ \end{matrix} \begin{matrix} Y_{P_F} \\ \\ \\ \end{matrix} \begin{matrix} Z_{P_F} \\ \\ \\ \end{matrix} \begin{bmatrix} 0.0186 & 0.0051 & 0.0234 \\ 0.0051 & 0.0442 & -0.0143 \\ 0.0234 & -0.0143 & 0.0456 \end{bmatrix} \tag{3.8}$$

This can, in terms of positional inaccuracy, be interpreted by realizing that the eigen values of this a matrix is equal to the variance of the focus position along the axes spanned by the eigen vectors of the matrix. By finding the eigen values and converting it to the $3\sigma$ notation defined by [54] the following variances along the eigen vectors are found:

$$d_f = \begin{bmatrix} 0.1265 \\ 0.6162 \\ 0.7617 \end{bmatrix} \tag{3.9}$$

As we are looking for the maximum variance this can be seen to be 0.76 mm.

### Results

By performing the above calculations a theoretical 3 $\sigma$ repeatability value of 0.76 mm has been found. This deviates from the results shown by e.g. [133] where it is shown that they have measured inaccuracies for the robot alone with an amplitude of approximately $\pm 60 \mu m$. With these accuracies RFC can

still be conducted with limited speeds of the robot (10mm/s). The results presented in [133] are however not obtained in an identical setup and furthermore their experiments are not based on a worst-case configuration of the robot as the results presented in this paper. Finally their results are not based on a statistical evaluation such as the $3\sigma$ estimations used herein.

### 3.3.5 Variable name assignments

As discussed in the previous section, the variable names for the mechanical actuators used in the paper differs from the definitions used in the remaining of this dissertation. If a 10 DOF system is envisioned (6 from the robot +3 from the cutting head +1 from beam rotation) the mechanical joint variables of the system will be named based on the following convention:

- $\psi$ -The DOE rotation angle
- $\theta_i$ - The joint angle associated with joint i of the industrial robot
- $\phi_k$ - The deflection angle from the deflection mirrors, where k is the scanner mirror number
- $\delta$ - Focus adjustment distance

The variables associated with the XY table, and the Z-axis will generally be named X, Y and Z. It should however be noted that when discussing 3D cutting systems these variables will often refer to the traditional positions of the robot end effector as seen from the robot base coordinate frame. Which definition is used should be apparent from the context as the XY table and Z axis will not be used when conducting 3D cutting.

#### Further work with remote cutting head

The results presented in the previous section were based on a cutting head design developed during the early stages of this Ph.D. Since then other designs have been developed and their kinematics have been derived based on equations for ray tracing. In appendix II a more detailed description of three designs with their kinematic equations are presented. Figure 3.13 shows the design of the cutting head currently used for simulation purposes. Here it should be noted that the design relies on a change in the distance $\delta$ for focus adjustment.
Generally speaking the kinematic equations yield a homogeneous transform from the cutting head focusing lens to the coordinate frame located on the deflection point on the final mirror with the Z axis pointing in the inverse

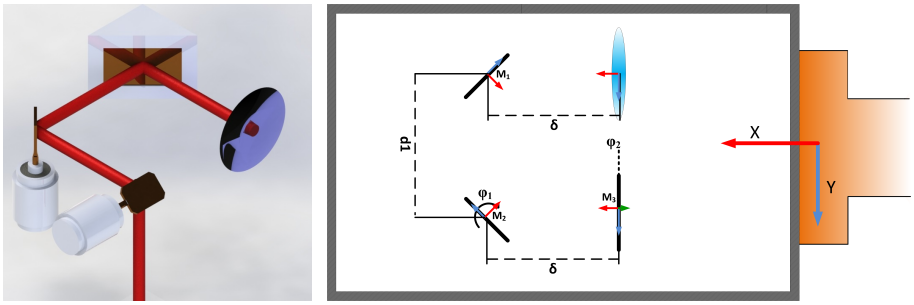


(a) Shows the conceptual beam path when the beam is deflected by three mirrors, of which two can be rotated.

(b) Shows a diagram of the cutting head configuration seen from figure 3.13(a).

**Fig. 3.13:** A conceptual image of the beam path of a scanner based cutting head.

direction of the beam. The found transform can be seen from equation 3.10.

$$T = \begin{bmatrix} -\left(c\left(2\,\phi_1\right)\right)^2 \left(s\left(2\,\phi_2\right)\right)^2 + 1 & 0 & -c\left(2\,\phi_1\right) s\left(2\,\phi_2\right) & 0 \\ -1/2\, s\left(4\,\phi_1\right) s\left(2\,\phi_2\right) & c\left(2\,\phi_1\right) c\left(2\,\phi_2\right) & -s\left(2\,\phi_1\right) & \frac{\delta s(2\,\phi_1)}{c(2\,\phi_1)} + d_1 \\ 1/2\, \left(c\left(2\,\phi_1\right)\right)^2 s\left(4\,\phi_2\right) & s\left(2\,\phi_1\right) & c\left(2\,\phi_1\right) c\left(2\,\phi_2\right) & 0 \\ 0 & 0 & 0 & 1 \end{bmatrix} \tag{3.10}$$

To find the beam waist location a translation along the negative Z axis is required by an amount equal to:

$$d_c = \delta + d_1 + \frac{\delta}{c\left(2\,\phi_1\right)} \tag{3.11}$$

For more information, the derivation of the cutting head transformation matrices can be found in appendix II.

This concludes the work conducted on the mechanical system. In the following the software platform will be described in detail.

## 3.4 Software platform

Now that the mechanical aspects of the ROBOCUT laboratory has been described the software platform will be discussed. In section 3.1.4 several requirements for the software system was described.

- **Software and hardware interfaces :** It is a requirement that the system can interface to the acquired hardware components used on the system.

- **Real time system**
- **CAM interpreter :**The system is required to be capable of interpreting G-codes.
- **Options for programming :** high-level programming required.
- **Upgradeable**

Based on these requirements it has been chosen to develop software for the laboratory on an industrial PLC system from BECKHOFF gmbh. These systems are soft PLC's based on a windows operating system. However, the windows kernel has been modified to yield real-time performance. As the IPC itself is windows based it has all the flexibility that comes with an operating system. This entails that software development can be conducted directly on the unit in e.g. visual studio. Due to the inherent support of the .net framework on the windows platform it has been chosen to program high-level functionality, such as user interfaces in C# and PLC related functionality in structured text. The architecture of the PLC can be seen from figure 3.14 [9]. Here it can be seen that the system is divided into two parts connected by a TCP/IP connection. The first part is a real-time module with a PLC server and IO mapping and the second part is a non-real-time module which offers a multitude of programming approached and interfaces. The TCP/IP connection that enables the communication internally also entails that the same system architecture can be applied to systems where the real-time part running on a different piece of hardware. On top of the TCP/IP protocol the ADS interface yields a standardized way of transmitting various signals. It has however been chosen to use a BECKHOFF IPC C6920, which integrates the windows platform with the PLC to reduce the number of components in the setup. This entails that on the same unit a PLC interface can be used to program real-time control structures for the mechanical system while high level control algorithms can be developed directly via the interface.

### 3.4.1 Actuation and laser control

It has been chosen to develop a custom user interface for controlling the laser and the actuating parts of the system. The user interface can be seen from figure 3.15. The current implementation supports 2D cutting by using G-codes combined with system specific M-functions for e.g. turning on the laser and gas pressure. From this figure it is seen that the interface be divided into four main areas.

1. Table Control
2. Real time position monitoring

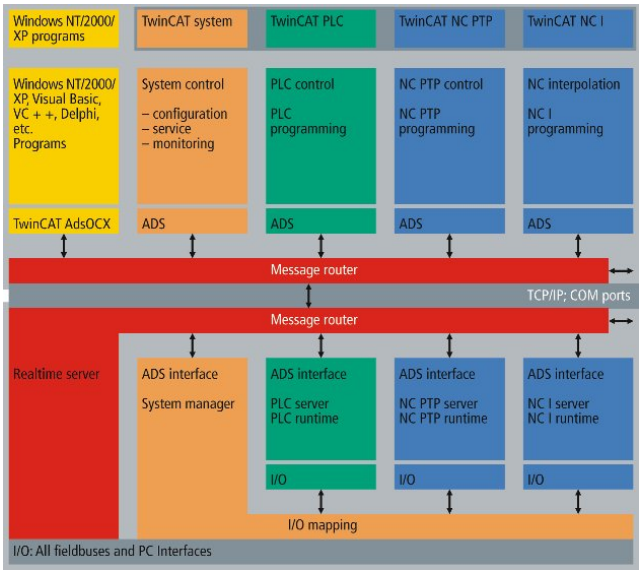


**Fig. 3.14:** Shows the architecture of the messages in the BECKHOFF PLC system [9]

3. Laser control
4. PLC connection control

The first area concerns the position and execution of programs on the XY table. The second area shows real-time plots of X and Y position and speeds. The third area is used for controlling the attached lasers and the fourth area controls the PLC connection to the ADS interface shown on figure 3.14. Interfaces to the Industrial robot is conducted by using a set of inputs and outputs which are connected by the Ethercat communications protocol supported both by the Beckhoff PLC and the industrial robot.

### 3.4.2 Interfaces for advanced control

As described in the previous sections, the development of a flexible laser processing laboratory has been a main priority of this project to accommodate the possible need for more advanced control algorithms. By selecting a software platform which is flexible in terms of programming options, upgradeability and communications interfaces this has been ensured. In section 3.5.2 this statement is investigated in further detail as an iterative learning algorithm is implemented on the system.

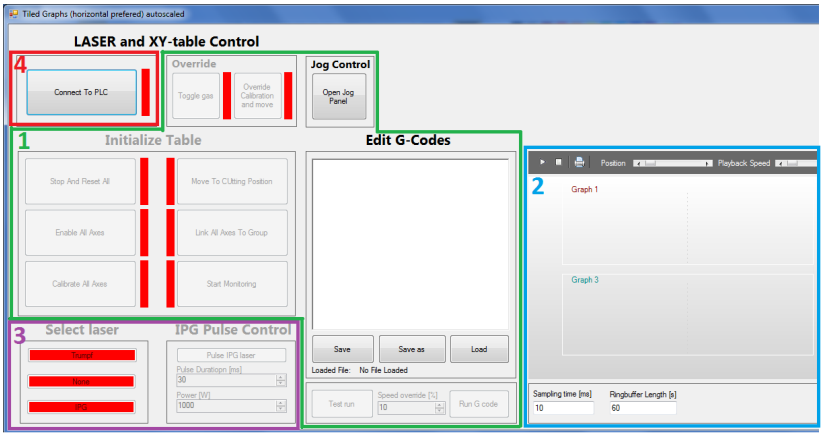


**Fig. 3.15:** The user interface used to control various parts of the system

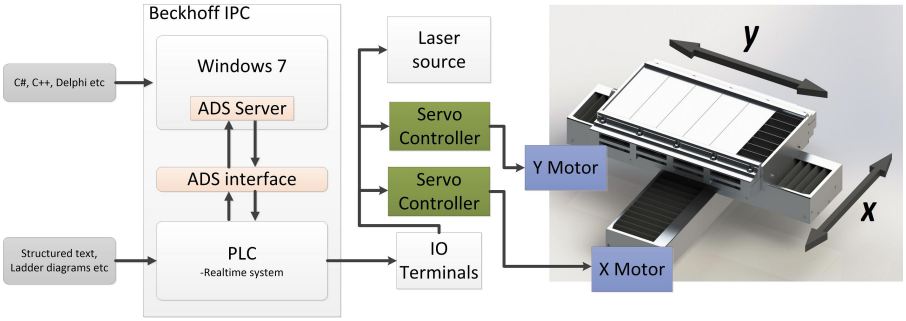


**Fig. 3.16:** The programming structure

## 3.5 Evaluation of the research objectives for the first area of focus

In the following section an evaluation of the flexible laser processing laboratory will be presented. The evaluations will be based on the research objectives presented in section 2.5:

- Develop a flexible laser processing laboratory for laser processing with DOE patterns.
- Develop a control architecture for the mechanical actuators with a flexible interface to allow for advanced control structures to allow for e.g. controlling beam orientation and further more advanced control algorithms.
- Investigate the applicability of using scanner mirrors for remote cutting

. To keep it short only a selected set of summarizing topics will be presented.

### 3.5.1 Evaluation of research objective: Develop a flexible laser processing laboratory for laser processing with DOE patterns

The first research objective, the development of a flexible laser processing laboratory for laser processing with DOE patterns, has over the course of this Ph.D. been tested and validate in several ways. As the key element of DOE cutting is the produced intensity pattern an intensity profile of one of these patterns will in the following be shown. To analyze the intensity pattern of a beam a caustic needs to be made. A caustic is a series of measurements of the intensity profile, conducted in different focus levels, to produce a depth map of the produced pattern. To verify the optical setup the laser beam has been measured multiple times, both for unmodified laser beams and for the obtained beam shapes with the use of DOEs. All measurements have been done with the equipment described in [41]. A program for generating automated caustics has been created by communicating with the industrial robot. Figure 3.17 shows a caustic of the unmodified beam with a focal length of 780mm. It is seen that in the focus area the spot size is approximately 100 $\mu m$. Through this caustic the $M^2$ value has been estimated to be approximately 1.2, which is in the range of $M^2$ described in table 3.1. Figure 3.18 shows the beam caustic of the initial DOE design presented in [123] and summarized in section 2.3.1.

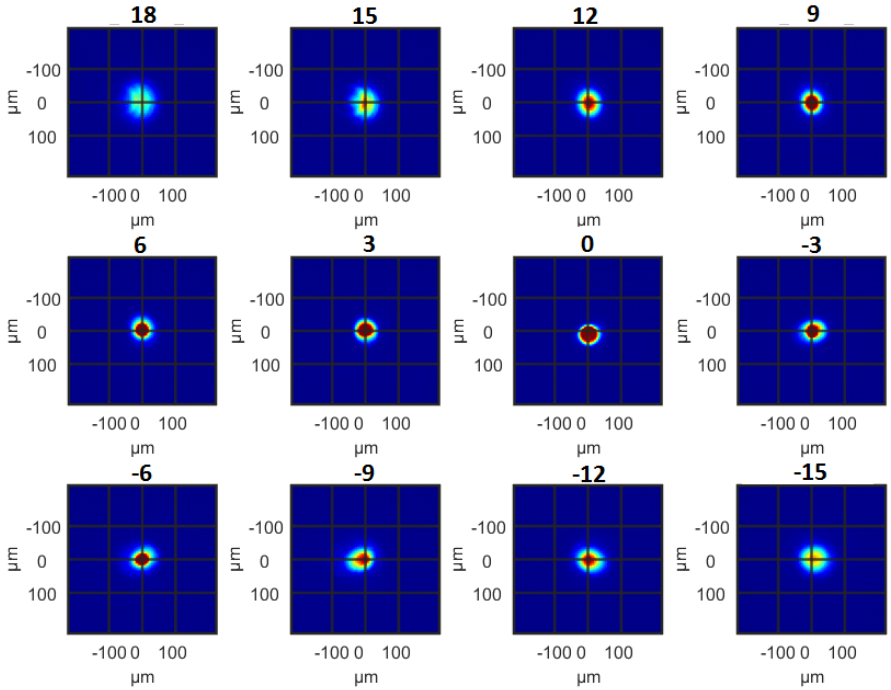


**Fig. 3.17:** A series of plots showing how the beam intensity changes with various focal depths. The images are taken 3 mm apart and the focus is indicated by the 0.

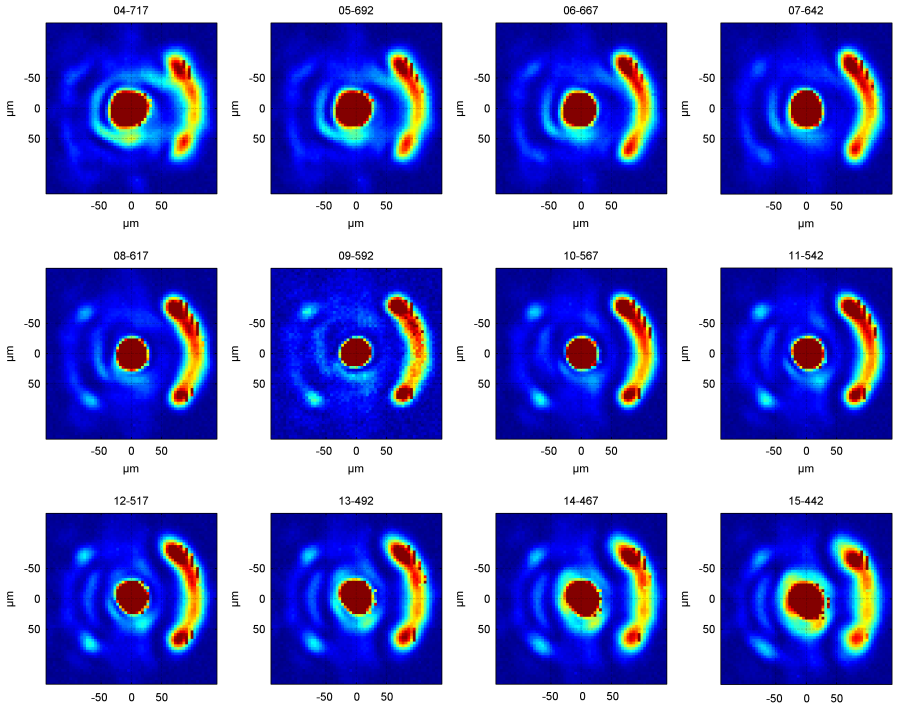


**Fig. 3.18:** A caustic showing the beam propagation of the initial DOE design described in 2.3.1

From this it can be seen that the beam pattern design of the first DOE is quite wide when compared to the unmodified beam. As a wider beam will interact with a larger amount of material this will generally result in slower cutting speeds. Since the laboratory was commissioned in 2013 it has been used for a wide range of experiments ranging from laser induced bending, engraving, welding, cutting, remote fusion cutting, DOE cutting and DOE welding. Many of the obtained results have furthermore been published see e.g. [28,39,65,125]. The sheer number of cutting experiments can be seen from figure 3.19. From

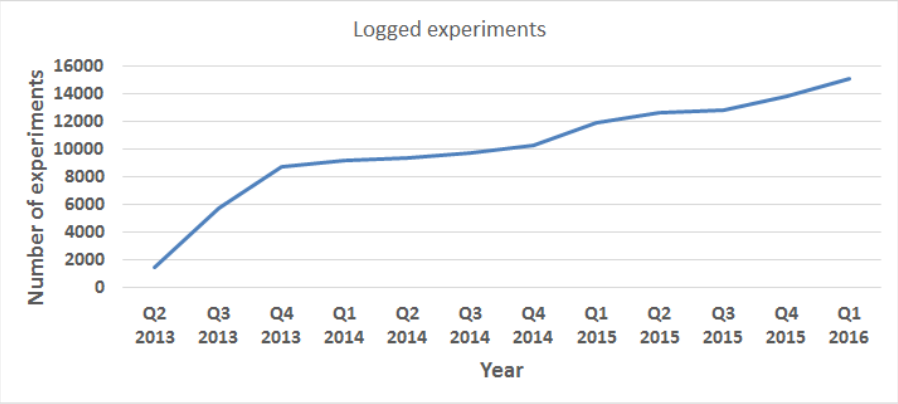


**Fig. 3.19:** A figure showing an accumulated view of the number of experiments conducted on the experimental setup

this figure it is seen that more than 15000 experiments have been conducted on the developed system. Out of these 15000 experiments approximately 2800 have been conducted with the use of a DOE.

### 3.5.2 Evaluation of research objective: Develop a control architecture for the mechanical actuators with a flexible interface that allows for the implementation of advanced control algorithms.l

To illustrate the power of the combined high-level interface programming in c# and the real-time PLC server an implementation of a machine learning algorithm has been created by using a server client structure between a PC running MATLAB and the BECKHOFF software platform. The results from this paper will be summarized in the following section.

### Summary of paper A: Optimizing Tracking Performance of XY Repositioning System with ILC

The following section contains a summary of the obtained results from the paper "Optimizing Tracking Performance of XY Repositioning System with ILC".

#### Objectives

1. Optimize tracking performance of the XY table used for laser cutting in the laser cutting laboratory, based on a non-mathematical approach.
2. Verify that a master controller architecture can compensate for poor subsystem performance for systems containing locally controlled subsystems.
3. Implement server/client control structure for further laser research.
4. Verify software and hardware interfaces to the laser cutting system.
5. Verify the flexibility of the developed software and the chosen hardware for the laboratory.

**Summary** When conducting laser cutting of parts, the accuracy of the mechanical system moving the cutting head is essential as any deviation of the movements of the cutting head will be mapped to the accuracy of the resulting processed work piece. Due to this it is of high importance to develop robust and efficient control algorithms for the mechanical actuators. Highly efficient and complex control algorithms have over the years been developed see e.g. [8, 12, 135] . This has entailed that in many cases the limiting factor of the performance of the control algorithm is not limited by the availability of control algorithms but instead on the skill of the developer doing the implementation. Furthermore, developing control algorithms for machinery which contains several subsystems can be challenging as each subsystem is often programmed in a proprietary program provided by the subsystem supplier. This often leads to the use of more general rules that are not based on mathematical formulations such as the Ziegler–Nichols method [136]. In mass production environments laser cutters are often responsible for producing large quantities of products over the course of several hours or days. This entails that they are executing a given trajectory multiple times. The aim of this paper is to show that increased performance on system level, for systems composed of many subsystems, can be obtained by using iterative learning control (ILC) [7] to refine the reference trajectory of a given part by feeding back the measured trajectory of the executed reference trajectory. By modifying the C# code on the main PLC an execution server was created. By combining this server with a Matlab script

that functioned as a client it was possible to create a framework for sending trajectories from the client to the server. The execution of these trajectories were conducted by modifying the existing laser processing software. This structure can be seen from figure 3.20 By sending reference trajectories from the client

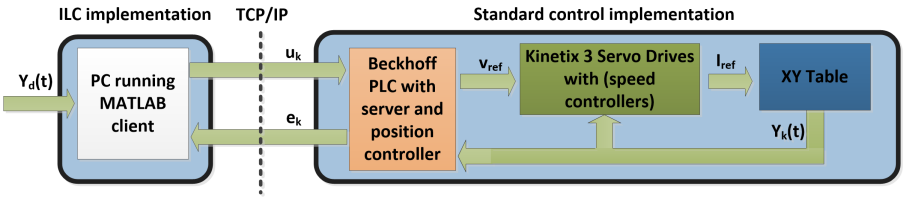


**Fig. 3.20:** The structure of the implementation of the ILC algorithm [129].

to the server and by returning executed trajectories to the client an ILC algorithm was implemented client side. Several learning gain values were tried and a learning gain of 0.1 proved to be robust for all executed trajectories. Two tests were conducted, one on a square with a side length of 100 mm and one on a circle with a diameter of 100 mm.

**Results** In the paper results from two reference trajectories were provided. In the following only the square reference results will be provided. The reference trajectory provided in this case should yield a 100 x 100 mm square with origin in x=200 mm y=200 mm cut in the counter clockwise direction. Cutting square contours with a constant edge speed is challenging due to the limited acceleration capabilities of the system as described in 4. By utilizing the implemented ILC algorithm a series of 20 ILC iterations were conducted. The obtained results can be seen from figure 3.21(a) and 3.21(b) where it is seen that the trajectory moves closer to the real reference with more iterations. The final executed trajectory lies close to the reference trajectory, but with the corners somewhat cut off.
This enables the system to conserve the system velocity and change direction more gradually. From figure 3.22 the summed positional error can be seen.
The error, with regards to the X direction, is reduced from approximately 160 to 80 and the Y error drops from approximately 80 to 35.

**Future research** The presented results indicate that increased performance can be obtained by utilizing various learning algorithms in the laser cutting process. Further research should be conducted to expand the applicability to the enhancement of robot and scanning mirror reference trajectories.

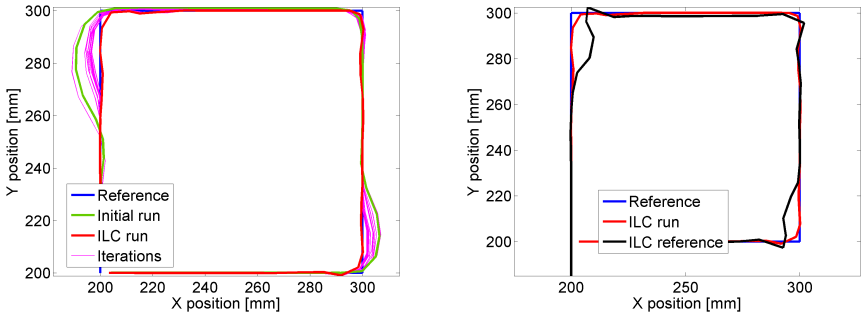


(a) The convergence of the executed trajectory when conducting 20 iterations of ILC. The purple lines show the iterations, the green the initial run and the red the final iteration.

(b) The final executed trajectory marked by red and the associated reference trajectory marked by black.

**Fig. 3.21:** The results from an ILC run with 20 iterations on a 100mm square at 25000 mm/min. It is seen that the tracking performance is significantly improved by the altered trajectory reference [129].

### 3.5.3 Evaluation of research objective: Investigate the applicability of using scanner mirrors for remote cutting

In 3.3.3 it was determined that due to the potential cutting speed of the ROBOCUT cutting technology a scanner cutting head would be necessary when considering the repositioning rate of the system, especially when considering the cutting of detailed contours. As the ROBOCUT laser process should be robot based it would result in a system similar to what is often discussed for remote laser welding and cutting as described in section 2.4. The accuracy of such a combined system might however be affected due to the long kinematic chain. In [124] it was assessed that the total accuracy of the system would be affected by the long kinematic chain resulting in an accuracy of 0.76 mm. The calculations were however based on several assumptions with regards to the robot pose as the necessary parameters for the calculations are the intellectual property rights of KUKA. Furthermore the introduction of the DOE in the beam path has the drawback that it makes it difficult to find a scanner system that does not interfere with the generated intensity profile. Based on these arguments it has been chosen to postpone the acquirement of a scanner cutting head as it is not strictly necessary to prove the capabilities of the ROBOCUT process. A scanner cutting head will however be included in the kinematic chain when considering the development of the task sequencing algorithms described in chapter 5.

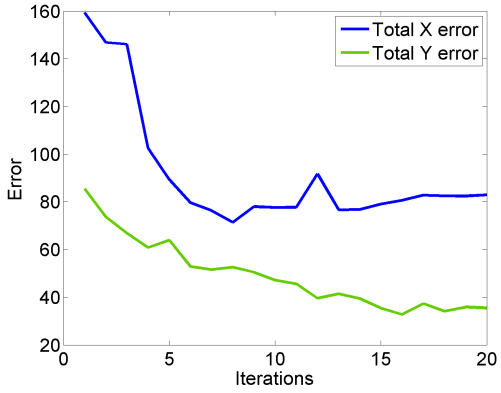


**Fig. 3.22:** The summed error in the X and Y direction for the 20 ILC iterations. It can be seen that the error falls in the beginning and starts to stagnate after 8 iterations in the X direction and 16 in the Y direction [129].

### 3.5.4 Conclusion

From the presented results it is seen that the designed laboratory is capable of producing beam patterns by inserting DOEs in the beam path of the single mode fiber laser. Furthermore several cuts and welds have been conducted with DOE's on the system. Also, the choice of control architecture made it possible to develop a machine learning algorithm and implement it on the system without writing PLC specific code. As more than 15000 cuts have been made since the laser laboratory was commissioned, out of which 2800 have been conducted with DOE, it is concluded that the research objectives regarding the flexible laser cutting laboratory have been fulfilled.

# Chapter 4

# The ROBOCUT process benchmarked against remote fusion cutting

As discussed in section 1.3 this dissertation is composed of three areas of focus. This chapter covers the second focus area, the evaluation of the current capabilities of the ROBOCUT remote laser cutting technology. In section 2.5, three research objectives with regards to this focus area were described:

- Develop a method and metric for fast evaluation of the stability of conducted laser cutting experiments.
- Determine the process windows within which RFC can be conducted with respect to parameters such as focus region, processing speed and incident angle.
- Evaluate the potential of ROBOCUT remote cutting by comparing experimental results to the RFC experiments.

This can generally be seen as a three step process which needs to be conducted in order to be able to evaluate the capabilities of the current DOE design for the ROBOCUT technology.

The first of these three steps concerns the development of a semi-automated laser process stability measurement system. As the performance of the ROBOCUT technology will be determined experimentally a large parameter space needs to be searched for optimum parameter combinations. As laser processing is notoriously nonlinear it is however difficult to reduce the number of experiments. This again means that many experiments are necessary if a large

parameter space should be searched. This entails that due to the sheer amount of experiments a computer vision based algorithm has been implemented to aid in the evaluation of cut stability. This, combined with images acquired by a programmable microscope with a mounted XY table, can analyze the obtained cuts.

The second of the three steps involves the establishment of a benchmark with which it is possible to evaluate the performance of the ROBOCUT process. As the main focus of this dissertation is the ROBOCUT remote cutting (RRC), this benchmarks needs to be based on a similar remote process conducted on equipment which is similar to the equipment described in chapter 3. The only remote cutting process that can be seen as similar to the RRC process is remote fusion cutting (RFC), as remote ablation cutting (RAC) relies on melt ejection generated by scanning the laser beam over the surface (see 2.1.2 for more information). As RFC with a single mode fiber laser is not described in the scientific literature and as the laser power generally used for RFC is above the 3 kW which is available in the ROBOCUT test laboratory it is necessary to create an experimental series showing the stability of the process with respect to this laser power.

The third step concerns the evaluation of the performance of the RRC process. By repeating the benchmark experiments, described in step two, with the insertion of a DOE in the beam path, a set of results can be obtained. These can then in turn be compared to the benchmark results and an evaluation of the performance can be conducted.

In the following sections these three steps will be discussed in further detail. The chapter will be composed in the following way: In section 4.1 a description of the automatic cut stability measurement system is presented. In section 4.2 the establishment of the RFC benchmark is described in further detail. The results found through the experiments conducted herein are presented in a summary of a paper in section 4.2.1. In section 4.3 a set of RRC results will be presented and compared to the established RFC benchmark. Finally, in section 4.4 an evaluation of the research objectives will be presented.

## 4.1 Development of an automated stability evaluation system

As described in the introduction to this chapter an automated measurement system needs to be created. In the following a more detailed description of the automated system will be given. A summarized version of what will be explained here has been included in the paper [125].

### 4.1.1 Definition of stability

Before a system for automatic stability assessment can be developed it is necessary to define what is meant by stability and how it should be measured. It has been chosen to evaluate the stability of a cutting process based on the resulting cutting kerf of the process and not by monitoring the process itself. This entails that the stability assessment can be done offline at a later time than the actual cutting. As the RRC process potentially can improve the ejection of molten material from the cutting kerf this will be the main parameter of interest. The definition will be based on the assumption that when conducting a cutting process, the current state of the process is either stable or unstable. This means that a resulting cutting kerf can be divided into sections of stability and sections of instability. Stable sections are characterized by a free cutting kerf and unstable ones by a blocked. To ensure that spurious holes originating from e.g. turbulent melt flow, a stable region should have a minimum length of $l_{min}$. If $l_C$ denotes the total length of the cutting kerf and $l_S$ the total length of the stable regions, then the total stability S of a cut can be evaluated as the fraction of the kerf that is unblocked 4.1.

$$S = \frac{l_S}{l_C} \tag{4.1}$$

By tuning the minimum distance $l_{min}$ it is possible to remove small section of unblocked kerf from the stability measure. One of the main benefits of this definition of stability is that all evaluations can be conducted without monitoring the process itself and that it can be evaluated by visual inspection of the top of the cutting kerf. The use of a percentage ensures that the stability is measured as a quantity that can be used as a baseline for comparing different cuts. The main drawback of this approach is however that it doesn't take quality aspects into account such as kerf perpendicularity, straightness and heat affected zone.

### 4.1.2 Experimental and measurement setup

When conducting laser cutting experiments such as the ones presented in section 4.2.1 it is often practical to conduct several cuts on a single plate with different parameters for each cut. However, many remote processes such as RFC are quite inefficient, this entails that the heat input of the cuts causes the plate to warp. To reduce the warping a fixture has been made that allows for creating 6 cuts with a length of 60mm on a 100x120mm work piece. The work piece and fixture can be seen from figure 4.1.
For measuring a corresponding measurement fixture has been created, which can be seen from figure 4.2. The measurement fixture is mounted on an XY table on a Carl Zeiss programmable microscope and the processing fixture is mounted in the laser cell.

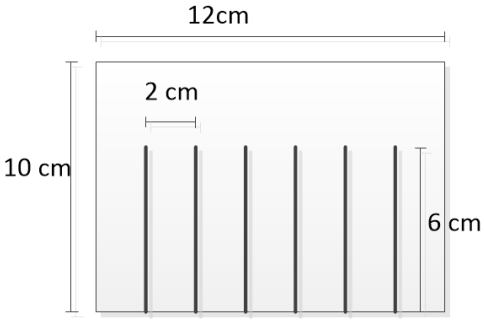


(a) The used workpiece for remote fusion cutting. 6 cuts with a length of 60 mm are made into a workpiece.

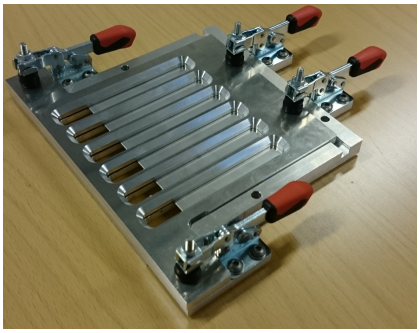

(b) The used fixture used for cutting the workpiece seen on figure 4.1(a). The clamps are used to ensure that warping does not happen.

**Fig. 4.1:** The workpiece and fixture used to conduct the benchmark cuts presented in 4.1(a). Notice the 2cm gap between cuts to reduce the amount of warping.

The work piece that has been cut in the cutting fixture seen from figure 4.1(a)

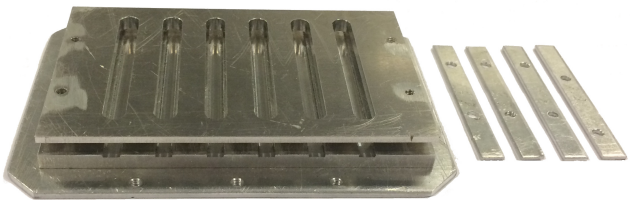

(a) The measurement fixture used for the measurements. The four rectangular pieces of metal on the right are spacers used for adapting the fixture to various sheet thicknesses.

(b) The axio imager microscope on which the measurement fixture is mounted

**Fig. 4.2:** The measurement setup used for the imaging process involved in generating data for the obtained cuts

can then inserted into the measurement fixture and be measured by the programmable microscope. This entails that if any warping has taken place it is reduced due to the pressure applied to the plate by the fixture. This is of high importance as the depth focus for the microscope is very small. By utilizing the software suite "Axio vision" with the additional library "Mark & Find 2" it is possible to define a set of positions from which a series of images can be created. By specifying 6 positions, one for each cut, a series of images can be taken of all cutting kerfs automatically. This results in a set of images that

needs to be analyzed to obtain a measure of the stability of the process. The images will however have to be combined into one large image before the stability analysis is conducted. This is done by a simple image stitching algorithm which will be presented in the following section.[1]

### 4.1.3 Image stitching

In the previous section it was described that a programmable microscope was used to generate a series of images of each of the 6 cutting kerfs on each of the test work pieces. To obtain an image of the entire cutting kerf these images need to be stitched together into one large image. This is done by a simple image stitching algorithm implemented in Matlab. The image stitching process is depicted on figure 4.3. The stitching has been conducted by taking all images

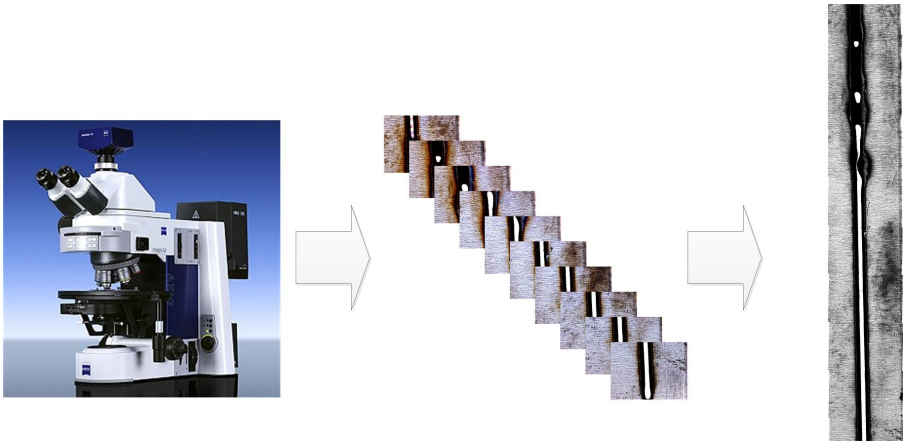

**Fig. 4.3:** The image stitching process: A programmable microscope takes a series of images of the cutting kerf. As the images are taken with an overlap of 10% it is possible to determine how two consecutive can be combined. By applying this to all images a complete image of the cutting kerf can be constructed.

with an overlap of 10%. This overlap entails that the last part of the previous image will display the same region on the cutting kerf as the first part of the current image. An image stitching algorithm can utilize such overlaps to create a complete image of the cutting kerf. A simple algorithm has been developed for this based on finding the maximum correlation between the overlapping areas of two images. The procedure is seen on figure 4.4. From this figure it is seen that the overlapping parts of two images are extracted from the images. This first image part is treated as a reference and the other as a mask. The mask is then moved over the reference and the difference between the two

[1] The axio imager suite has the possibility to create stitched images, however it only works for a proprietary Carl Zeiss image format that cannot be interpreted in e.g. Matlab.

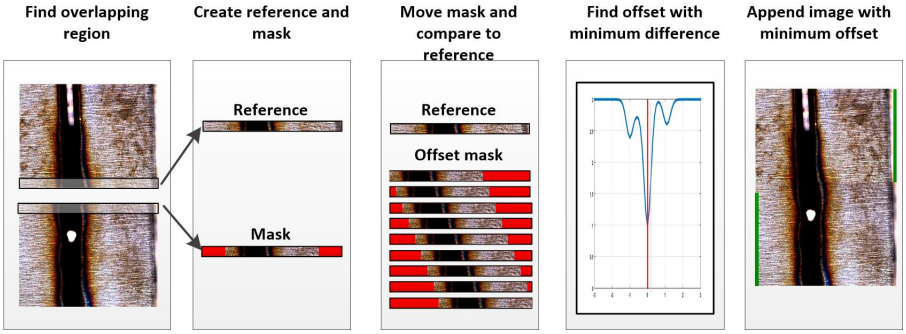


**Fig. 4.4:** The image stitching process in detail.

images is calculated. The offset with the minimum difference is found and the reference image and the second image without the mask area are concatenated into one, with the last image shifted by the offset that gives the minimum difference. It should here be noted that the offset of the stitching is only done in the horizontal plane. It could be expanded to the vertical plane as well, but as the 10 % overlap is ensured by the position control of the XY-table of the microscope this has been omitted. Often, when conducting image stitching a perspective transformation and other transformations are needed [79]. This can however be omitted as all images are taken of a flat surface from the same angle and as the camera has been calibrated to remove warping of the image field due to lens imperfections. In the following section the image processing algorithm will be explained in more detail.

### 4.1.4 Image processing algorithm

Now, that a complete cutting kerf image has been acquired, it will be analyzed and a measure of the stability will be obtained. The algorithm works in several steps which will be described in the following.

#### Transform to grayscale

As the edges of the cuts are black (burned) and the cutting kerf is white (over exposed) the additional information that color can provide is unnecessary. This has entailed that it has been chosen to transform the image to a gray scale image to reduce the computational load of the image processing algorithm. In a later implementation this is done already before the image stitching process. As the cut image sections generally appear as being white and as the HAZ generally appears black, this transformation does not remove the basis for an accurate detection. The original image can be seen from figure 4.5 which shows the result of cut #17793 which was remote cut at a speed of 7000 mm/min with a

beam diameter of 0.475 mm and with a work angle equal to +6° and a travel angle equal to -6°. The stitching process generates images that are 1410 by

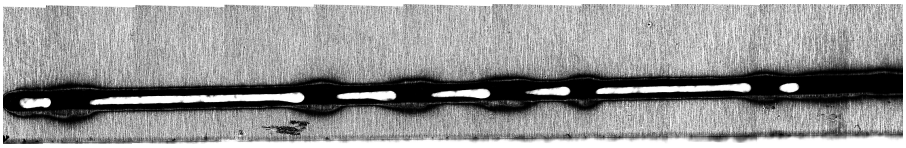

**Fig. 4.5:** The original stitched image. Notice that the end of the cut is furthest to the left.

9100 pixels. After the stitching process the start and end pixels are removed to ensure that areas outside of the cut are not included in the image processing. This is done as the kerf detection algorithm is based on the existence of a pronounced HAZ. The cropping removes 400 pixels from the start and the end

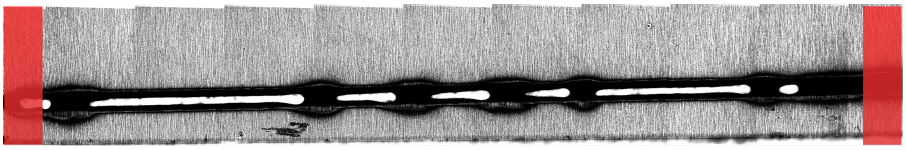

**Fig. 4.6:** The start and end part of the image is cropped out of the picture to ensure that unprocessed areas are not a part of the image for the further analysis.

of the image. This entails that the resulting image is reduced to a size of 1410x8300. From the figure it is seen that the cropping only removes a small part of the image, which leaves more for the remaining analysis. To increase the processing speed, the image has furthermore been down sampled by a factor of 2 to a size of 705x4150. The next step involved in finding the stability measure is to find the location of the cutting kerf.

### Finding the cutting kerf center

To find the location of the cutting kerf the image is divided into several segments and the cutting kerf is found in each of these. Several experiments were carried out to determine an appropriate number of segments and the process is generally not very sensitive to the exact number as all cuts are straight. In the end 20 segments were chosen as an appropriate value as it proved to be robust when the algorithm found a misplaced kerf center point, while still keeping the computational time low. To find the position of the kerf on these segments a column vector is created containing the sums of all the columns of the image segment[2]. The resulting column vector can then be seen as the amount of white

[2]Images can be considered as matrices. In our case each segment can be considered to be a 1410x455 matrix with values describing the whiteness of each pixel. 0 means completely black 255 means completely white

of the segment as one moves from left to right over the cutting kerf. As the kerf is generally black this gives a way to identify its position. Figure 4.7, 4.8 and 4.9 show the results of the segmentation and summation procedure described above.

From these figures it can be seen that the resulting

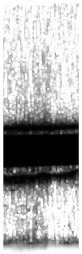

(a) A segment from the image of the cutting kerf. The kerf is completely blocked.

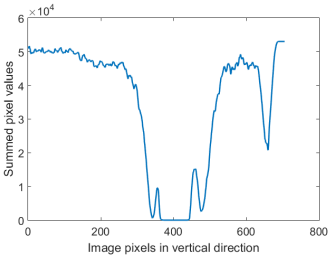


(b) A summarized plot of the pixel values for the segment. Notice the two "dips" The first comes from the uncut cutting kerf and the other comes from a shadow from the fixture.

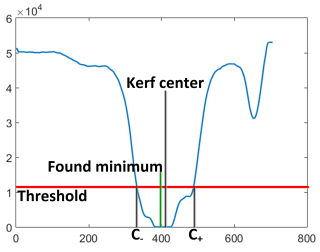


(c) After a smoothing has been applied the shadow is partially removed and only a few minima remain.

**Fig. 4.7:** Summarized plots of the pixel values for an uncut segment of the cutting kerf.

graphs vary depending on the amount of cleared material in the center of the cutting kerf. To remove the fluctuations coming from the specular reflections from the metal surface, the values of the column vector are smoothed and all minima between 10% and 90% of the image length are found. The reason that the minima needs to lie within 10 and 90 percent is that the field of view of the microscope is larger than the milled tracks in the measurement fixture. This entails that the fixture becomes visible and casts a shadow on the workpiece. This can be seen as a dip in the vector containing the summarized values on either the right or left side. This is clearly seen on the right side of figure 4.7(b),4.8(b) and 4.9(b). From these graphs it can generally be seen that if only one minima is found, then there is no cut, if two minima are found with a small peak between them then there is a partial cut and if two minima with a large peak between are found then the kerf is completely unblocked. The center point of the cutting kerf is found by using a threshold analysis. First a dynamic threshold T is found. It has been chosen to set the threshold 30% of the value range above the minimum value.

$$T = MaxVal + 0.3 \cdot (MaxVal - MinVal); \tag{4.2}$$

Where MaxVal and MinVal is the maximum and minimum value of the column vector respectively. Two crossing points are then found $C_-$ and $C_+$. These

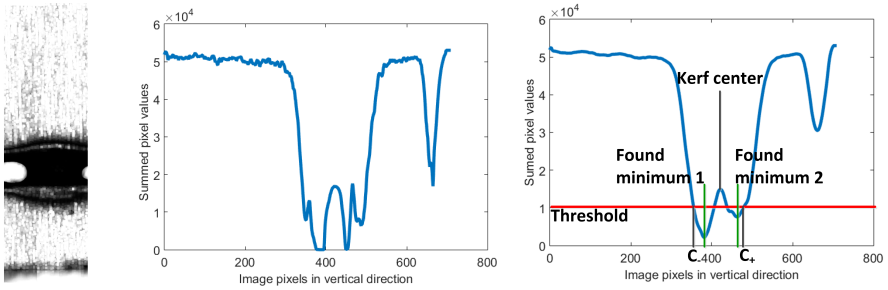


(a) A segment from the full cutting kerf. The kerf is partially blocked.

(b) A summarized plot of the pixel values for the segment. Notice the three "dips" The first two comes from the partially cut cutting kerf and the remaining comes from a shadow from the fixture.

(c) After a smoothing the two dips from the cutting kerf is still visible.

**Fig. 4.8:** Summarized plots of the pixel values for a partial cut segment of the cutting kerf.

points can be seen from figure 4.9. $C_-$ is the column vector index that first exceeds the threshold when moving in the negative direction from the found minima. In a similar way $C_+$ denotes the column vector index that first exceeds the threshold when moving in the positive direction from the found minima. If two minima are found, then $C_-$ moves in the negative direction from the minima furthest to the left on the graph. In a similar fashion $C_+$ starts from the minima furthest to the right. The center of the cutting kerf can then be said to lie in the center point between $C_-$ and $C_+$. When these steps are repeated for all 20 segments, the cutting kerf position can be found for the entire image. Figure 4.10 shows a plot of the found kerf positions plotted in the center of each of the 20 segments. The found kerf position can then be used for cropping the image to reduce the workload even further. This is discussed in the following section.

### Image cropping

Based on the found kerf centers a straight line fit is then found through these points. Based on this line a section 30 pixels wide are taken from the image on either side of the line going through the center points. This crops the image to a section around the cutting kerf which can be seen from figure 4.11. From this figure it is seen that the cropped image only contains the unblocked kerf and the HAZ. However reflections and small holes caused by e.g. turbulence still needs to be filtered out. This will be done in the following section.

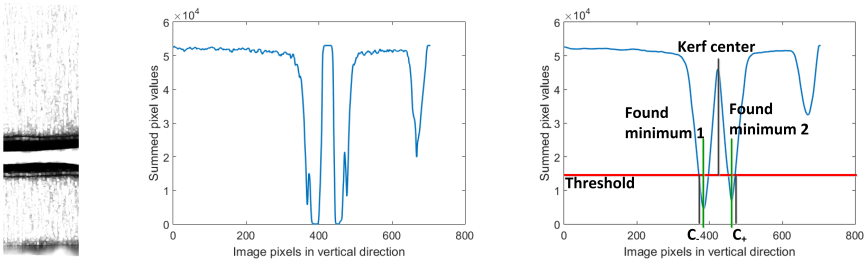


(a) A segment of the cut that is completely cut through.

(b) The summarised plot shows that the dips are very significant which makes them easy to detect.

(c) A smoothed summarized plot of the figure seen in 4.9(b)

**Fig. 4.9:** A series of summarized plots of the pixel values for a completely cut segment of the cutting kerf.

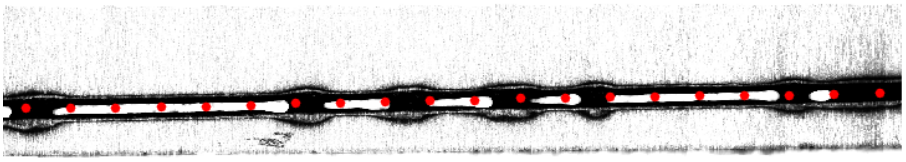

**Fig. 4.10:** A kerf image with red dots marking the position of the found position of the cutting kerf.

### 4.1.5 Thresholding and blob filtering

If the grayscale image shown in figure 4.11 is converted to a binary black/white image, it is seen that it is quite noisy. This can be seen from figure 4.12. To remove the noise the MATLAB operation bwareaopen is used to remove clusters of points with a pixel area less than 4000 pixels. In the paper summarized in section 4.2.1 a slightly different approach was used. Here it was done with the regionprops command which can remove areas based on a set of statistics such as length. A more thorough description of the used commands can be found in the MATLAB documentation [77]. This has however been changed for a simpler length filtering step which will be presented in the following section. When the area filtering has been applied, the result can be seen on figure 4.13. From this it is seen that most of the noise has been removed. One could argue that if the cutting kerf is very narrow, the area filtering might have to be reduced. This is however a step that will be considered if the need arises. In the following section the length filtering step will be presented.

**Fig. 4.11:** A cropped section of figure 4.10 taken around a straight line going through the red dots.

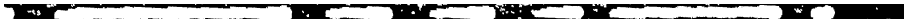

**Fig. 4.12:** The image from figure 4.11 shown as a binary image to increase contrast.

### 4.1.6 Cut length filtering

The remaining white parts of the image are now only originating from the sections in the cutting kerf in which the molten material has been removed. A row vector is now created containing the summarized values of the image shown in figure 4.13. The resulting graph from this can be seen from figure 4.14. From this figure two things can be seen. When the cutting kerf is blocked the graph drops to a value of 0. When the kerf has become unblocked the value in the graph represents the width of the cutting kerf in pixels. An unblocked kerf is then detected in all cases where the graph has a non-zero value. Figure 4.15 shows a binary version of figure 4.14. By determining the length of the high areas it is easy to filter out areas with a length less than a given threshold as described in section 4.2.1. As discussed there a length of 10 mm was chosen, the length value in pixels can be calculated based on the fact that the entire length of the cutting kerf is 60 mm. If the image is 705x4150 then the pixel distance must equal 691 pixels. In figure 4.15 the red color shows the high regions that are too short to be treated as a cut. In the following section the final step will be presented where the stability is measured and an image overlay is added to indicate cut regions.

### 4.1.7 Image color overlay and result

The final step of the algorithm is to convert the graph from figure 4.15 to a number. This is quite simple as the percentage of stable cuts can simply be derived by summing the binary graph containing the valid cut positions and dividing it by the image length. For this image this yields:

$$\text{Stability} = 45.5531\% \tag{4.3}$$

Furthermore a green and red layer is added to the image depending on the values of figure 4.15. This can be seen from figure 4.16. This is done to ensure that a fast manual inspection can be made of the image folder in such a way that it can easily be detected if the algorithm performs as expected. This is the final step involved in the automatic analysis of the cuts conducted in this dissertation. In the following sections this algorithm will be used for evaluating the stability of the RFC cutting process and thereafter the ROBOCUT remote cutting process.

**Fig. 4.13:** The image from figure 4.12 with removed noise by blob filtering.

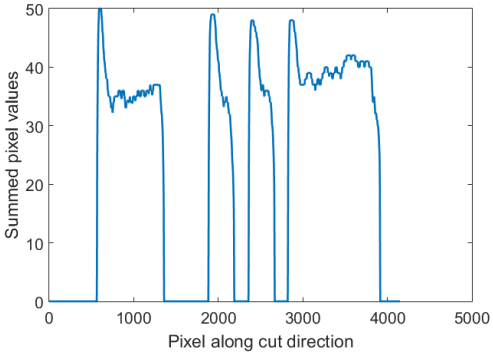


**Fig. 4.14:** Shows the graph produced when a row vector containing summarized column values is plotted.

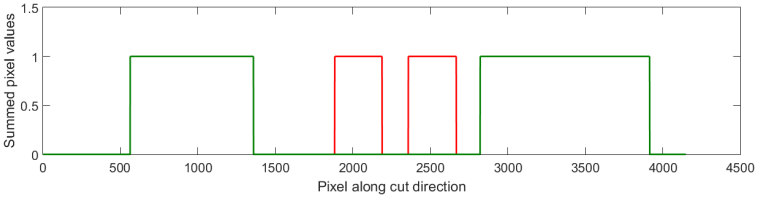


**Fig. 4.15:** The regions of the cutting kerf that are cut/not cut. The red color indicates cuts that are too short and blue indicate valid ones.

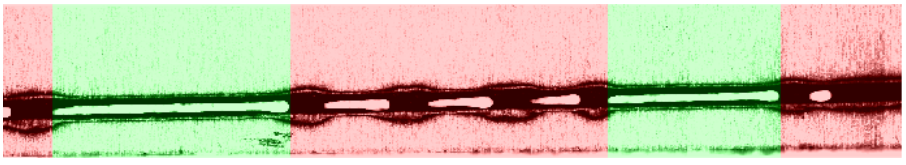

**Fig. 4.16:** The original image with a color overlay showing the result of the evaluation. Green indicates a valid cut section and red an invalid one.

## 4.2 Establishing a RFC benchmark

As discussed in the introduction to this chapter the second step involved in evaluating the current performance of the ROBOCUT remote cutting (RRC) technology is to create a benchmark. With this benchmark it will be possible to determine how well the RRC process performs. As laser cutting, and especially remote laser cutting is quite sensitive to its operating parameters it has been chosen to establish this benchmark by performing an experimental study which evaluates several parameter combinations.

When considering remote laser processing the main variables that should be taken into consideration will in the following be listed. It will generally be divided into two groups, one regarding beam delivery and generation and one regarding the work piece and the positioning of the work piece:

**Beam delivery and generation**

- Laser power
- Pulse frequency
- Beam quality (in the $M^2$ sense)
- Focal length
- Focal position
- Angle of incidence

**Workpiece and workpiece positioning**

- Travel speed
- Work piece material
- Work piece thickness
- Work piece surface

It should however be noticed that the above list is not exhaustive as many parameters influence the laser cutting process. Compiling a list of all variables would be a study in itself. These extra parameters could e.g. include the composition of the surrounding air, the degree of contamination of cover slides and focusing lenses, changes in the metal surface (e.g. scratches and residual oil) and many other disturbances. As these parameters are difficult to directly control they will in the following be assumed to be constant. For this benchmark it has been chosen to focus on stainless steel sheets (thickness >0.15mm [131]).

We have chosen to vary the focus, the cutting speed and the angle of incidence. The chosen values of the benchmark tests can be seen from table 4.1. From this table it is seen that three parameters are treated as variables - the

**Beam delivery and generation**

| Parameter | Value |
|---|---|
| Laser power | 3kW |
| Pulse frequency | CW (Not pulsed) |
| Beam quality (in the $M^2$ sense) | 1.2 |
| Focal length | 470mm |
| Focal position | Variable |
| Angle of incidence | Variable |

**Workpiece and workpiece positioning**

| Parameter | Value |
|---|---|
| Travel speed | Variable |
| Work piece material | SST EN Type:X2CrNi19-11 No. 1.4307 |
| Work piece thickness | 0.5mm |
| Work piece surface | non-coated |

**Table 4.1:** A table showing the values of the variables used in the study

cutting speed, the beam diameter/focal position and the incident beam angle. By choosing these as variables it is possible to determine an appropriate beam diameter when conducting RFC. This is of importance when creating the DOE patterns. It is furthermore possible to determine a maximum cutting speed at this optimal focus and finally it is possible to determine the stability of the process when changing the incident angle of the beam. This is in many ways important as the maximum allowable incident angle directly determines to what extent the beam can be moved over a work piece by means of tilting the cutting head instead of translating it. The results from this benchmark has been published [125]. A summary of the results are presented in the following section.

### 4.2.1 Summary of paper D: Angular Stability Margins for the Remote Fusion Cutting Process

The following section contains a summary of the obtained results from the paper "Angular Stability Margins for the Remote Fusion Cutting Process".

#### Objectives

1. To identify to what extent the incident angle effects the cutting quality of remote fusion cutting.

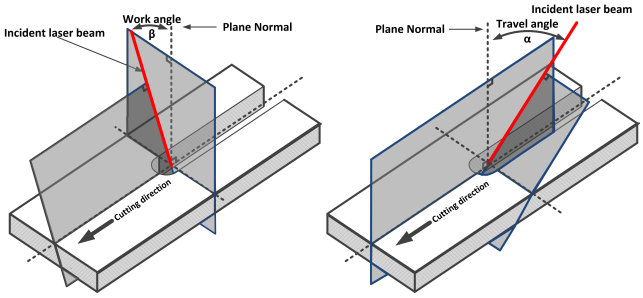


**Fig. 4.17:** The decomposition of the incident angle into a work and travel angle [125].

2. To create baseline results for the remote fusion cutting process which can be used as benchmarks when evaluating the performance of the ROBOCUT technology.

3. To identify a measure of stability that can be used for evaluating the cutting performance of ROBOCUT beam patterns.

**Summary**

Remote fusion cutting (RFC) and remote ablation cutting (RAC) are currently the most known remote cutting technologies. As the ROBOCUT technology relies on melt ejection principles that resemble the principles of remote fusion cutting it is of great interest to investigate the performance of this technology so that benchmark results for remote cuts without DOE exist.
This has entailed that it has been chosen to conduct a series of experiments which can indicate an appropriate process window for RFC cutting with regards to speed, focus and incident angle. It has been chosen to decompose the incident angle into a work and travel angle. This decomposition can be seen from figure 4.17. Here the travel angle is denoted $\alpha$ and the work angle $\beta$. From this figure it is seen that both angles are defined as the angular deviation from a work piece normal, and thus a perpendicular beam will have a travel and work angle equal to 0°. Four sets of experiments were conducted, based on the design shown in figure 4.18, to analyze the effect of the speed, the focus and the incident angle. From this figure it is seen that in the first set of experiments a suitable range of traveling speeds and focus positions are found. In the three subsequent experiments (2-4) the work and travel angle is varied and the cut stability is measured to yield an area within which stable cuts can be obtained. Due to the large number of conducted cuts, the definition of cut stability described in section 4.1.1 is used along with the automatic measurement system described in section 4.1.

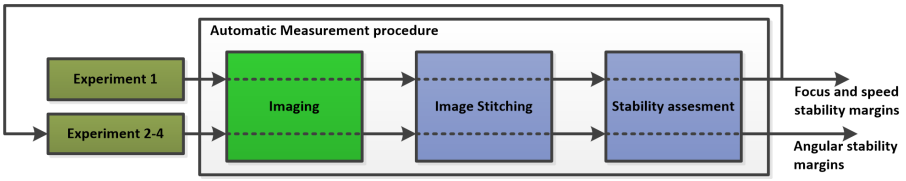


**Fig. 4.18:** The experimental design used to uncover the effect of work and travel angles on the cutting quality of RFC [125].

### 4.2.2 Results

As seen on figure 4.18 four sets of experiments were conducted labeled experiment 1-4. In the following the obtained results from these experiments will be presented.

#### Experiment 1

The results from the first set of experiments yielded an area of stability of the RFC process with regards to speed and focus position to be used in the subsequent experiments. The results were obtained by varying the speed and beam diameter and repeating the experiments three times. The obtained results of these experiments can be seen from figure 4.19(a) where the cut stability is plotted in color as a function of beam diameter and processing speed. From this figure it is seen that a semi coherent area of beam diameters and processing speeds is found between speeds of 5000-11000 mm/min and beam diameters between 0.35.0.65mm. There are however areas with low stability in this semi coherent region. As an example one could use the point 7000 mm/min with beam diameter 0.475 where the stability was found to be 0% for all three repetitions. Based on this, the working point of the angle experiments was chosen to be 7000 mm/min with a beam diameter of 0.55 mm. This point was chosen as it provided tolerance with regards to beam diameter and as it offered the largest region of stability.
Figure 4.19(b) shows the obtained minimum cut stability of the three repetitions. It is seen that the coherence seen in 4.19(a) is greatly reduced and that the stability region becomes separated into two regions. The chosen working point is however still the one providing the best stability in the region.

#### Experiment 2-3

In the second set of experiments the effect of variation of the work and travel angle individually was investigated. The two variables were varied one at a time and 6 repetitions were recorded for each operating point.
Figure 4.20(a) and 4.20(b) show the results from the second and third experiment where the work and travel angle is changed one at a time. Here it is seen

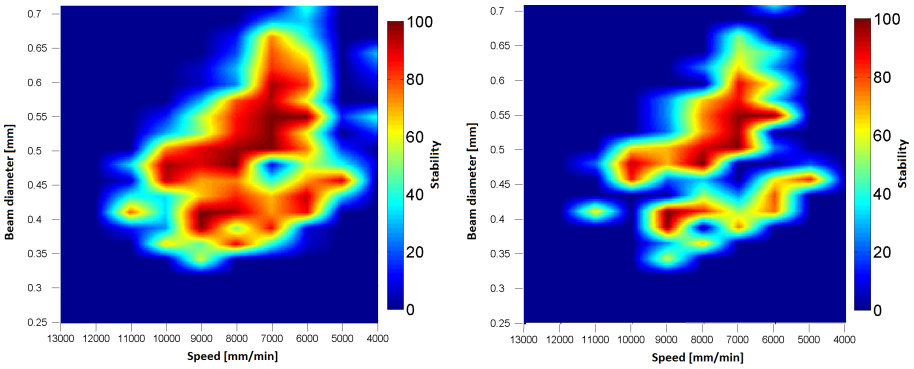


(a) The average stability of three repetitions when varying speed and focus position.

(b) The minimum stability of three repetitions when varying speed and focus position.

**Fig. 4.19:** A plot of the obtained results from experiment 1. The minimum and average stability scores for the remote fusion cutting process when the travelling speed and the focus position is changed [125].

that the average stability decreases significantly as the angles increase (in the positive and negative direction). For the work angle the stability plot seems to be centered around 0°. Furthermore the results seems to have a level of symmetry which will be utilized to reduce the number of cuts for experiment 4. This is however not the case for the travel angle which seems to centered around +4°. The figures also indicates that there is a large span between the stability measures of cuts made with the same parameters. In all experiments, except two, at least one repetition yielded a stability measure of 0%.

### Experiment 4

Figure 4.21(a) and 4.21(b) shows the results from the final experiment where the travel and work angle is changed simultaneously. Again 6 repetitions were made and the stability was recorded.
As it was concluded from experiment 2-3, that the work angle has stability measures centered around 0°, and that symmetry can be assumed, it has been chosen to only carry out experiments in the positive range of work angles and mirror them around the travel angle axis except for the results obtained from experiment 2-3. These results have been included in the dataset. This entails that the work angle results where the travel angle equals 0°, and the travel angle results, where the work angle equals 0°, are the results from experiment 2 and 3. From figure 4.21(a) and 4.21(b) it is seen that the stable region is coherent and bound by work and travel angles within ±6°. The large spans between maximum and minimum stability discussed for experiment 2 and 3 can also be found here. This can be seen by comparing figure 4.20(a) and 4.20(b).

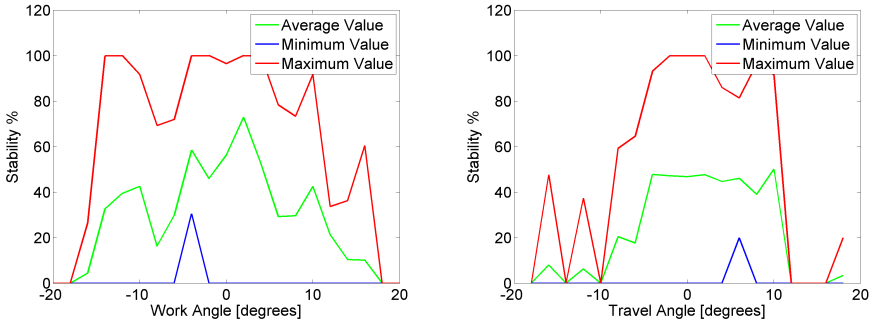


(a) Plots of the stability score as a function of the work angle of the laser beam.

(b) Plots of the stability score as a function of the travel angle of the laser beam.

**Fig. 4.20:** Plots of stability for experiment 2-3 where the work and travel angle are changed one at a time [125].

From these two figures it is seen that the area of stability is greatly increased when using the maximum measure. A plot of the minimum quality has not been included as almost all points have a repetition with a stability score of 0° just as in experiment 2 and 3.
Generally it was concluded, based on the conducted experiments, that the RFC process is quite unstable and has a low repetition rate. This could make it difficult to integrate in a production environment. It should however be noted that other parameters, such as higher laser power, potentially could stabilize the process.

### Future research

Future research into the RFC process should indicate if the found stability margins are expanded when using laser power above 3kW. Furthermore, the obtained stability margins for the RFC process should be used in task sequencing and path planning as maximum bounds on the incident angle of the laser beam.

## 4.3 ROBOCUT results

Now that an automatic measurement system has been developed in section 4.1 and a benchmark has been established in section 4.2 the performance of the current ROBOCUT DOE can be evaluated. The results presented in the following have been scheduled to be published at the 9th international conference on Photonic Technologies 2016 (LANE 2016) [71]. The submitted abstract can be seen in appendix H. This entails that only selected parts of the obtained

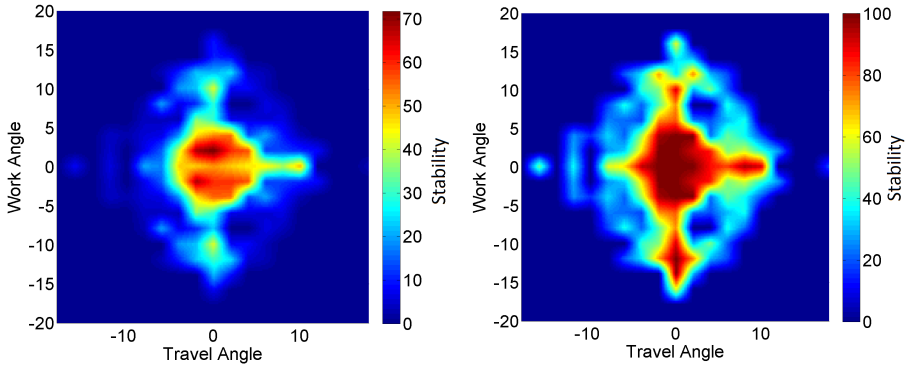


(a) The average stability score of 6 repetitions of remote fusion cutting with varying incident angles.

(b) The maximum stability score of 6 repetitions with varying inceident angle.

**Fig. 4.21:** A plot of the obtained results from experiment 4. The maximum and average stability scores for the remote fusion cutting process [125].

results will be presented in the following. This paper will treat three areas - the chosen DOE pattern, results obtained through varying the speed and focus and results obtained by varying the incident angle.

### 4.3.1 DOE pattern and cutting parameters

In this section a series of results obtained with the currently used DOE design will be presented. As discussed in section 2.3.1 the initial DOE(N100) produced a pattern that was too wide for cutting. This pattern can be seen on figure 4.22(a).
This has entailed that currently another beam shape is being investigated (N101). This new beam design has some interesting properties when compared to the results obtained in [125]. As the beam design itself is considered to be the intellectual property rights (IPR) of IPU a full caustic of the beam cannot be presented here. Instead a single image of the beam in focus +7 can be seen from figure 4.22(b). It should be noted that even though the new ROBOCUT intensity profile is measured out of focus, the pattern diameter is considerably smaller than for the original ROBOCUT pattern. The smaller pattern diameter should ensure that less material is melted by the beam and thus a better performance, with regards to cutting speed, is expected. As the initial DOE was not tested for its applicability with regards to remote processing the following sections will only consider RFC against ROBOCUT remote cutting (RRC) with DOE N101. The parameters for the conducted tests with RRC can be seen from table 4.2 which is a modification of table 4.1. The main difference being that it has been chosen to use a pulsed laser beam for RRC.

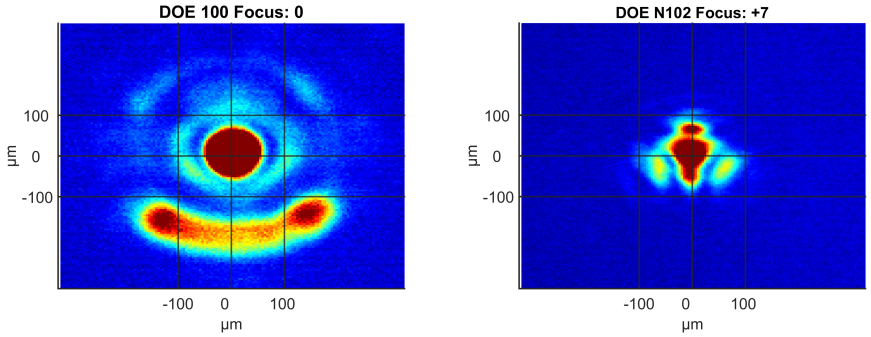


(a) The beam intensity profile of the initial ROBOCUT DOE design. Notice the barrier and melt beam from figure 2.14(b). This beam has throughout the project been denoted N100. The lid beam is somewhat hidden in the background noise due to intensity truncation in the measurement system [123].

(b) The beam intensity profile of the new ROBOCUT DOE design N101. Notice that the pattern has changed considerably when compared to the beam in figure 4.22(a). The shown profile originates from a measurement which is out of focus by 7mm.

**Fig. 4.22:** The two ROBOCUT beams used throughout this project. Notice that for the new DOE design shown on figure 4.22(b) the concept of lid, barrier and melt beam has not been preserved on this out of focus measurement.

The specific pulse parameters are not published as they are also considered the IPR of IPU. From this table it is seen that the three variables used in the above table are the focus offset, the travel speed and the incident angle. To reduce the number of experiments it has been chosen to organize them as described in 4.2.1. This entails that a series of experiments will be conducted to find an appropriate region of stability with regards to focus and cutting speed. This set of experiments is then used for determining the values for cutting speed and focus offset that yields the highest stability. These stable values can then be used in the second set of experiments where the incident angle is changed. The results from these two experimental series will in the following be presented.

### 4.3.2 Speed and focus experiments

To find an appropriate area with regards to focus and cutting speed several initial experiments have been conducted showing that good results could be obtained with speeds in from approximately 800 mm/min to 1600 mm/min and with focus ranging from 0 to +10 mm. This has entailed that this area was investigated in higher detail. By varying the focus in steps of 1 mm and the speed in steps of 200 mm/min and by applying the automatic stability measurement system figure 4.23(a) was created.
From this figure it is seen that the stability of the cuts reaches 100% for a large

| **Beam delivery and generation** | |
|---|---|
| Parameter | Value |
| Laser power | 3kW |
| Pulse frequency | **Pulsed (21% duty cycle)** |
| Beam quality (in the $M^2$ sense) | 1.2 |
| Focal length | 470mm |
| Focal position | Variable |
| Angle of incidence | Variable |
| **Workpiece and workpiece positioning** | |
| Parameter | Value |
| Travel speed | Variable |
| Work piece material | SST EN Type:X2CrNi19-11 No. 1.4307 |
| Work piece thickness | 0.5mm |
| Work piece surface | Non coated |

**Table 4.2:** A table showing the values of the variables used when evaluating ROBOCUT remote cutting (RRC).

section of the parameter window. The quality only drops around the edges of the process window. In [125] it was noted repeatedly that the repeatability of the conducted RFC experiments were very low with the chosen equipment. From figure 4.23(a) it can be seen that the repeatability of the DOE cutting process is much higher than for RFC. This does however come at the cost of processing speed as it is approximately 1/5 of the RFC cuts. If the obtained results are plotted with the results obtained through RFC the graph seen on figure 4.23(b) is obtained. On this figure the obtained RFC results can be seen as the semi coherent blob in the upper right corner and the DOE cut results are seen in the left bottom corner. From this figure the large difference between the two processes, when considering both speed and quality, can be seen. On one hand the obtained DOE cutting results are conducted at approximately 1/5 of the speed of the RFC process, on the other hand a much more stable process is achieved. Furthermore, as the cuts were obtained with a duty cycle of 21 %, the available laser power to do the processing is approximately 1/5 of the power used for RFC. Further research should be conducted to come up with other DOE designs capable of obtaining the same speed as RFC, but with the reliability of the current process. As discussed in the previous section it is necessary to determine a set of speed and focus position parameters with which the subsequent series of experiments can be conducted. Based on figure 4.23(a) it has been chosen to use a speed value of 1200 mm/min and a focus position of +5 mm.

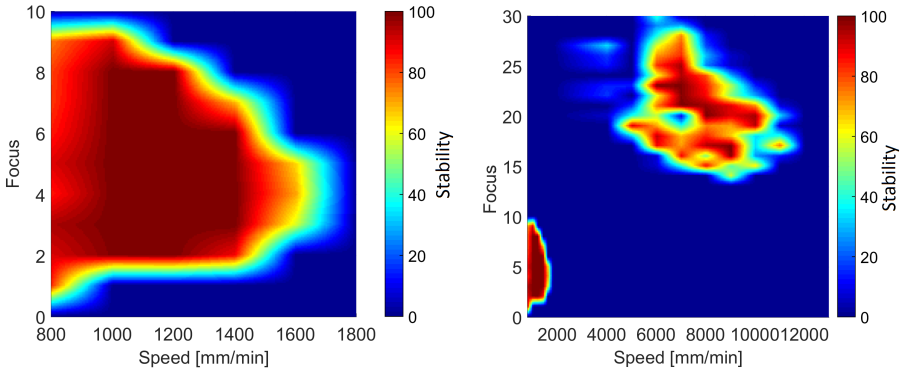


(a) Stability of the DOE cuts when cutting while pulsing the laser.

(b) A plot of RFC and RRC cutting when conducting cuts on 0.5 mm stainless steel.

**Fig. 4.23:** The stability area searched for the current iteration of the RRC process. On figure 4.23(a) the searched area is plotted on its own. On figure 4.23(b) it is plotted in the same plot as for RFC.

### 4.3.3 Angular experiments

When considering the angular stability of the process a series of cuts have been made with different angles of the cutting head. As in the experiments regarding RFC described in section 4.2.1 it has been chosen to decompose the angle into a travel and work angle as described in appendix III. In the following the results which concerns both positive work and travel angles will be presented. Results with regards to negative angles will be published in LANE as described in the introduction.

From this figure it is seen that with regards to travel angle the stability quickly decreases when passing 4-5 degrees. For remote fusion cutting (RFC) a limit was in [125] determined to be $\pm 6°$ for the same laser power. For RFC, the general stability level was however much lower and the $\pm 6°$ can be seen as a limit to where cuts were achievable. From figure 4.24(a) it is seen that cuts are generally still obtained with travel angles in the range of $8°$. The difference between the RFC and the RRC cutting strategy is however much more pronounced when considering the work angle. In [125] it was determined that the work angle limit was identical to the travel angle limit (approximately $\pm 6°$ ). From figure 4.24(a) it is seen that RRC cuts have been obtained with a travel angle of as much as $32°$. The general stability level is also much higher, when compared to RFC. An interesting outlier is seen from the figure close to the work angle cutting limit. It is seen that for a work angle equal to $32°$ several 100% cuts are obtained. As this 100 % stability values are experienced for 8 travel angle measurements ($0° - 14°$) with 6 repetitions it's quite unlikely that this is simply a statistical fluctuation.

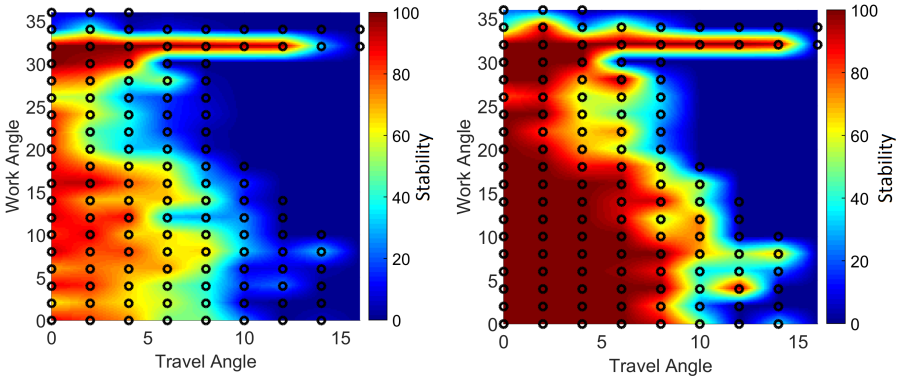


(a) Mean stability of the DOE cuts when cutting at an angle. The results are obtained by taking the average of 6 repetitions.

(b) A plot of the maximum quality of the DOE cuts. The results are obtained by taking the maximum stability value of 6 repetitions.

**Fig. 4.24:** The mean and maximum stability of DOE cuts while varying the incident angle of the beam. On the figure the color indicates the level of stability and the black rings denote measurements. The in-between values are obtained by means of linear interpolation between data points.

Figure 4.24(b) shows the maximum quality obtained through the 6 repetitions. If the process should be implemented in the industry it is necessary to ensure that the variance of the process is kept at a minimum which again indicates that the difference in mean stability and maximum stability should essentially be zero. When figure 4.24(b) and 4.24(a) are compared it is seen that there still is a difference, even for travel angles below 8° .
As discussed in section 2.3 one of the drawbacks of using diffractive optical elements is however that it adds an extra optical component in the beam path which might suffer from thermal lensing. While conducting the described set of experiments it was noticed that often the first cut on a plate had a lower stability compared to the remaining cuts. To investigate this notion further it has been chosen to remove the initial cut from the calculations of mean stability. The results from this can be seen from figure 4.25(a) and 4.25(b).
From this it is seen that by removing the first experiment, an increase in stability is obtained for low angle values. It is however difficult to determine if the observed changes are due to thermal lensing, statistic fluctuations or other differences between the cuts. As the laser power is the same in all experiments the focus offset obtained by thermal lensing should be identical for all operating points. This does however not imply that the change in stability should be identical in all experiments as the shifted focus might increase the stability for small incident angles and reduce it when they are large. To investigate this further the standard deviation has been calculated based on the set of repeti-

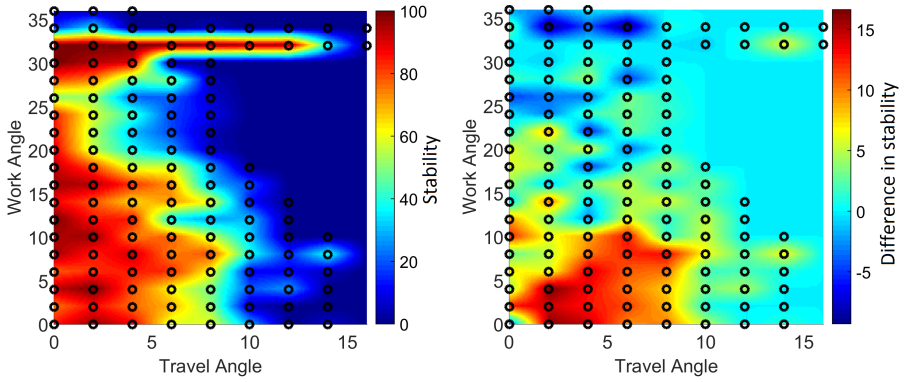


(a) Mean stability of the DOE cuts when cutting at an angle when the first cut on each workpiece has been removed. The results are obtained by taking the average of the remaining 5 repetitions.

(b) A plot of the difference in quality between the mean quality shown in figure 4.24(a) and the results obtained when removing the first sample 4.25(a).

**Fig. 4.25:** The figure shows two plots, one showing the mean stability of DOE cuts when removing the first cut on each plate from the data and one showing the difference in mean value that this causes. On the figures the color indicates the level of stability and the black rings denote measurements. The in-between values are obtained by means of linear interpolation between data points.

tions. This can be seen from figure 4.26.
From this figure it is seen that by removing the first cut on all plates the magnitude of the standard deviation has been reduced, especially for small angles. For larger angles the effect is less pronounced. It is however difficult to conclude if the described effect is actually caused by thermal lensing or if it is due to other influences. Further experiments should determine if this is indeed the case.

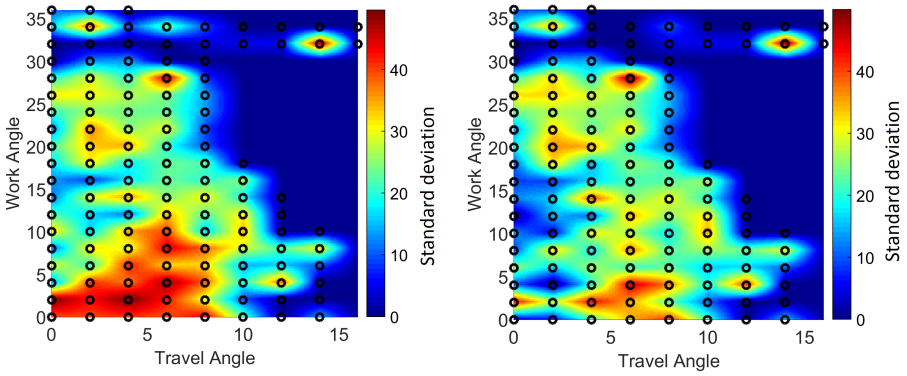


(a) A plot of the standard deviation for the conducted experiments based on all six repetitions.

(b) A plot of the standard deviation for the conducted experiments based on the five last repetitions.

**Fig. 4.26:** The standard deviation of the conducted experiments. To investigate if the first cut on a plate suffers from thermal lensing it has been chosen to calculate it in twice where the first calculation takes all 6 repetitions into account and the second only the last 5.

## 4.4 Evaluation of the research objectives for the second area of focus

In the following section an evaluation of the research objectives for the second area of focus will be presented. The evaluations will be based on the research objectives presented in section 2.5 and the results obtained in the previous sections. The research objectives were:

- Develop a method and metric for fast evaluation of the stability of conducted laser cutting experiments.
- Determine the process windows within which RFC can be conducted with respect to parameters such focus region, processing speed and incident angle.
- Evaluate the potential of DOE beam patterns by comparing experimental results to the baseline experiments.

### 4.4.1 Evaluation of research objective: Develop a method and metric for fast evaluation of the stability of conducted laser cutting experiments

It was chosen to define the cut stability based on an evaluation of the cutting process' ability to eject melt from the cutting kerf. This was chosen to allow

for an image processing based evaluation of the cut stability. The percentage of unblocked cutting kerf was chosen as a metric to assess the stability. The designed algorithm was developed to work on images from a Carl Zeiss axioimager microscope. It was implemented in MATLAB and has during the course of this Ph.D. been used to evaluate more than 3300 cuts. Figure 4.27 shows the result from an analysis of several cuts. As discussed in 4.1.7 the green overlay denotes stable sections of a cut and the red overlay denotes unstable ones. The effect of the length threshold of 10 mm can be seen in in e.g. cut #16727 where short stable sections are still marked as stable and in cut #16705 where small unstable occurring holes are rejected. The algorithm has proven to provide a

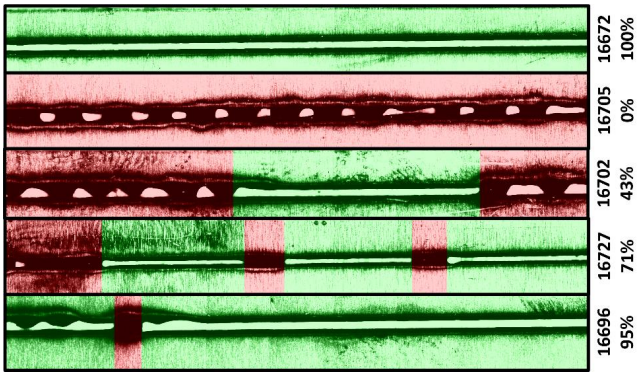


**Fig. 4.27:** An analysis of 5 different cuts by the developed algorithm. All cuts were done with work and travel angle =0° (#16672 velocity = 6000mm/min, beam diameter = 0.592mm) (#16705 velocity = 9000mm/min, beam diameter = 0.71mm) (#16702 velocity = 6000mm/min, beam diameter = 0.71mm)(#16727 velocity =7000 mm/min , beam diameter = 0.36 mm)( #16696 velocity =6000 mm/min , beam diameter =0.685mm) [125].

robust way of measuring the cut stability rapidly. It is furthermore possible to improve the algorithm to extract further parameters such as the kerf width and kerf variance.

### 4.4.2 Evaluation of research objective: Determine the process windows within which RFC can be conducted with respect to parameters such as focus region, processing speed and incident angle

The stability of the remote fusion cutting process was determined within two main parameter windows. The first with respect to beam diameter and traveling speed and the second with respect to work and travel angle (see appendix III). During the course of these experiments it was determined that a semi coherent area of stability was found for speeds between 5000 mm/min and 10000 mm/min with a beam diameter between 0.35 - 0.65 mm. Based on this a set of

angular experiments were conducted with a speed of 7000 mm/min and a beam diameter of 0.475 mm. It was found that stable cuts could be obtained within a window of ±6° with regards to both travel and work angle. It was however also noted that the RFC cutting process generally had a low stability and a very low repeatability with the test setup. In section 4.2.1 it was speculated that an increase in laser power could stabilize the process.

### 4.4.3 Evaluation of research objective: Evaluate the potential of ROBOCUT remote cutting by comparing experimental results to the RFC experiments

In the following section an evaluation of the current DOE used for ROBOCUT remote cutting (RRC) will be presented. It will be summarized from the results presented in 4.3. A general overview of the obtained results can be seen from table 4.3. From this it is seen that generally the obtained cutting speeds

| **Stability Parameter** | **RFC** | **RRC** |
|---|---|---|
| Velocity | 5000-10000mm/min | 800-1600mm/min |
| Focus interval | 25 mm | 10mm |
| Work angle | ±6° | 32° |
| Travel angle | ±6° | 8° |

**Table 4.3:** A table showing the values of the variables used when evaluating the remote ROBOCUT DOE cutting.

while conducting RRC are much slower than for RFC. However the allowable angle of incidence with regards to both travel and work angle is much greater. The main difference is however the general level of stability. With the RRC technology a stability of approximately 100 % were obtained within the entire parameter space when the incident angle was equal to 0°. For RFC the region of stability was only somewhat coherent and it was determined that a 1 mm offset of the cutting head could entail decline from 100% stability to 0% stability. When considering the stability with respect to the incident angle, the average stability of the RRC technology was generally much higher when compared to RFC within the incident angle parameter window. For RFC the stable region contained values ranging from 40-70 % while for the RRC technology the stable regions contained average stability values between 80-100%. Also, as discussed in section 4.3.1, the results were obtained with a pulsed laser with a duty cycle of 21%. This again entails that the results were obtained with an average laser power of approximately 600 Watts, which is much less than what is required by RFC.

To obtain the processing time optimization that is proposed in the title of

this dissertation, it is however necessary to develop beam patterns which are capable of utilizing the full power of the laser and still obtain stable cuts.

# Chapter 5

# Algorithms for joint space task scheduling

As discussed in section 1.3 this dissertation is composed of three main areas of focus. This chapter covers the third and final area - the development of a framework for joint space task scheduling. Two research objectives were presented in section 2.5.

- Develop an algorithm for generating paths for the remote laser cutting system that allows it to reconfigure itself while still cutting the specified contour.
- Investigate and develop algorithms for path sequencing for workpieces that requires multiple cuts, which takes the robot redundancy into account

In the following sections these research objectives will be investigated by conducting a more thorough analysis of the task sequencing problem.

This chapter will be organized in the following way: In section 5.1 a set of definitions and a preliminary point task sequencing analysis will be presented. This view on sequencing will in section 5.2 be expanded with a set of parameters related to remote laser processing. This leads to a presentation of the chosen solution strategy in section 5.3. In this section two unpublished papers will be presented as the foundation of the proposed approach. In section 5.4 the task of including the beam rotator for the DOE will be discussed. Finally in section 5.5 an evaluation of the research objectives will be presented.

## 5.1 Definitions and preliminary analysis

In this section a set of definitions related to the task of scheduling will be presented. This will generally be done by using the preliminary interpreting that the tasks can be considered to be points in space requiring processing for a fixed duration.

### 5.1.1 Definition of task and task sequence

When doing remote laser cutting or welding one has a work piece that needs to be processed. It might be a piece of sheet metal that needs to be cut into hundreds of identical pieces for use in a mass production environment or it might be more complex parts that needs to be cut in several places. In the following it is not important if the process itself is welding, cutting or even engraving, the matter of importance is that the laser needs to traverse several contours on the work piece. A cutting scenario can be seen from FIG. 5.1. It is seen that

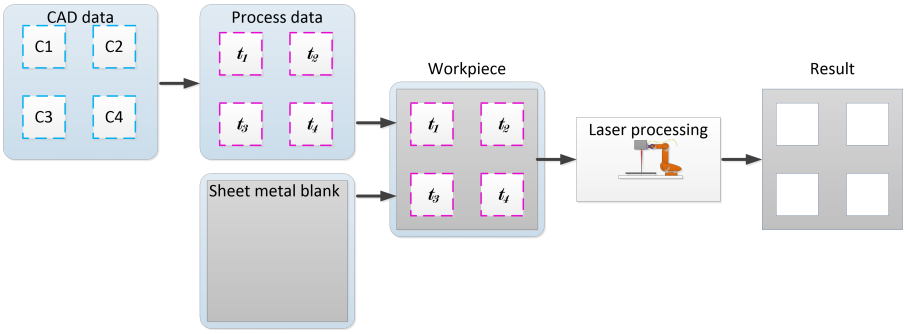


**Fig. 5.1:** Shows how a sheet metal blank is combined with process data to yield a work piece. This is then fed into a laser cutting station which carries out the cutting to produce the finished part.

the input to the system is in the form of a set of four contours C1-C4 which are derived from a CAD program. The source could potentially be anything such as manual input contours or even contours derived by argumented reality as in [101]. As the contours does not convey any process information themselves a CAM program adds the necessary process parameters to obtain a satisfactory process. By specifying process parameters these contours are transformed into processes e.g. cutting or welding. In the following a contour combined with processing parameters will be grouped under a common term - task or $\boldsymbol{t}$. The task information can then directly be used as input to the laser processing station and the processes can be executed. This transforms the work piece into a part that reflects the design made in the CAD program. If each task $\boldsymbol{t}$ on a

work piece is labeled $\boldsymbol{t}_1$-$\boldsymbol{t}_N$ then the set of tasks that needs to be completed on a work piece is denoted $\mathbb{T}$. When a robotic laser processing system needs to perform such a set of tasks on a work piece, a task sequence S is determined which complies with all constraints imposed on the problem while still optimizing a goal e.g. the processing time of the part. The task sequence S can be seen as a permutation of the numbers from 1 to N. This permutation denotes the sequence in which the given tasks are processed. If the vector S contains such a permutation it can be used to generate a vector of tasks that needs to be executed in sequence.

$$[\boldsymbol{t}_{S(1)} \ldots \boldsymbol{t}_{S(N)}] \tag{5.1}$$

Such a sequence is depicted on Fig. 5.2 which shows the sequence ($\boldsymbol{t}_0$,$\boldsymbol{t}_1$,$\boldsymbol{t}_2$,$\boldsymbol{t}_4$,$\boldsymbol{t}_3$ $\boldsymbol{t}_0$). Note that $\boldsymbol{t}_0$ denotes the initial and final position of the robot. From

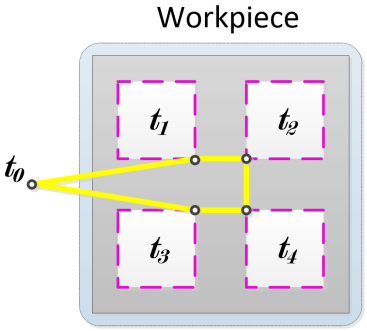


**Fig. 5.2:** Shows a task sequence for a set of points on a workpiece. Notice that the colors indicate two types of movements. Purple indicates task movements - movements of the system when the laser is on and processing. Yellow indicates intertask movements - movements between tasks.

this figure it is seen that robot movements can generally be divided into two categories.

- Movements between tasks. (Inter task movements)
- The actual execution of the contour (Task movements)

When executing a sequence the type of movements will alternate between intertask movements and task movements. In the following section these movement types will be used when considering the task of scheduling point tasks.

### 5.1.2 Sequenceing of point tasks

In this section the problem of determining an appropriate sequence of a set of tasks $\boldsymbol{t}_1 - \boldsymbol{t}_N$ will be described briefly. It will preliminarily be assumed that these tasks can be considered to be points in space that a mechanical

actuator needs to visit, and "process" for a given time $d_{\boldsymbol{t}_n}$. This assumption will be expanded to include the processing contours of e.g. laser cutting in section 5.2. As the main concern of this dissertation is to investigate how a cycle time optimization for a given part can be achieved, the cycle time will in the following be used as a cost function for evaluating sequences. If the total cycle time of a workpiece for a given sequence S is denoted $d_{\mathbb{T}}(S)$, then it can be expressed by the summation of two parameters. The total processing time of the individual tasks $dP_{\boldsymbol{t}}$ (task movements) and the total time spent on movements between the tasks $dI_{\boldsymbol{t}}(S)$ (inter task movements).

$$d_{\mathbb{T}}(S) = dP_{\boldsymbol{t}} + dI_{\boldsymbol{t}}(S) \tag{5.2}$$

The two parameters $dP_{\boldsymbol{t}}$ and $dI_{\boldsymbol{t}}$ can furthermore be broken down into sums.

$$dP_{\boldsymbol{t}}(S) = \sum_{i=1}^{N} \left(d_{\boldsymbol{t}_i}\right) \tag{5.3}$$

$$dI_{\boldsymbol{t}}(S) = \sum_{i=S(1)}^{S(N-1)} \left(d_{\boldsymbol{t}_i}^{\boldsymbol{t}_{i+1}}\right) + d_{\boldsymbol{t}_{S(N)}}^{\boldsymbol{t}_{S(1)}} \tag{5.4}$$

where $d_{\boldsymbol{t}_i}$ is the duration of a task i and $d_{\boldsymbol{t}_a}^{\boldsymbol{t}_b}$ is the intertask time between two tasks a and b. If a sequence S yields the lowest cycle time it will in the following be denoted as the optimum sequence $S^*$.

$$S^* = \arg\min_{S} d_{\mathbb{T}}(S) \tag{5.5}$$

Here it should however be remembered that minimizing $d_{\mathbb{T}}$ is equivalent to minimizing $dI_{\boldsymbol{t}}(S)$ as $dP_{\boldsymbol{t}}(S)$ is determined by the geometry of the contour and the cutting parameters of the process. This entails that it is invariant to changes in the sequence.

$$S^* = \arg\min_{S} dI_{\boldsymbol{t}}(S) \tag{5.6}$$

If all tasks are considered to be nodes in a fully connected graph with edge costs equal to $d_{\boldsymbol{t}_a}^{\boldsymbol{t}_b}$ then the graph from figure 5.3 can be created. The minimization problem can be interpreted as finding the path that visits each node in the graph with the lowest total cost $dI_{\boldsymbol{t}}(S)$. This can be seen as the definition of a traditional traveling salesman problem which has been studied extensively for several decades. However, the traveling salesman problem is NP-hard and solutions are, for large problems, generally found by means of various heuristic approaches [80]. This is necessary as the number of possible circuits expands rapidly with the number of nodes. For nodes in a directed graph the exact number can be calculated by:

$$R_u(N) = (N-1)! \tag{5.7}$$

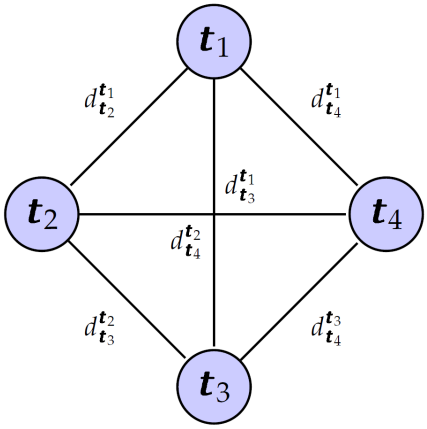


**Fig. 5.3:** Shows a 4 node graph where the inter task movement times $d^{t_b}_{t_a}$ are used as edge weights.

If the graph is undirected the number of solutions are halved and equation 5.8 is obtained.

$$R_d(N) = \frac{(N-1)!}{2} \tag{5.8}$$

This again entails that a system with 20 nodes will have $10^{18}$ different circuits. The developed heuristic approaches have however evolved to be very powerful and implementations have been proved to find optimal solutions for large datasets [94, 104]. In fact, good solutions to problems in the range of more than 80.000 points have been published [6, 45]. These algorithms are often compared by utilizing various benchmark libraries such as TSPLIB [100]. The TSP representation is however only valid when it is assumed that the tasks can be considered to be points in space. In the following section this view will be expanded to include the specific requirements and constraints for remote laser processing.

## 5.2 Sequencing of remote laser processing

In the previous section it was discussed that a series of point tasks on a workpiece can be sequenced by representing the problem as a traveling salesman problem. The problem of sequencing remote laser processing tasks is however much more complicated as the problem differs in some key areas. In the following section these key areas will be investigated in further detail. This investigation will cover several areas that needs to be taken into account:

1. The laser process.
2. The robotic positioning system.

3. Other .

In the following these three categories will be discussed in further detail.

### 5.2.1 Considerations related to remote laser processing

When moving from the point tasks discussed in section 5.1 to the full contours that needs to be cut or welded when considering remote laser processing three things needs to be considered.

1. A laser processing task is defined as a contour in space that the laser beam needs to traverse
2. The point where the laser processing starts on a given contour can vary
3. Remote laser processes remain stable within a range of incident angles and focus

These three considerations will in the following be addressed more throughly.

#### Definition of processing contour

In section 5.1 it was shown how a set of contours $C1$-$C4$ were designed in a CAD program. Such a contour, $C$, can be defined as a curve in Cartesian space $p(\sigma)$.

$$C = p(\sigma), \forall \sigma \in [0, 1] \tag{5.9}$$

The variable $\sigma$ is a path variable that is normalized such that $\sigma \in [0, 1]$ and the point $p$ is given in homogeneous coordinates such that it can be specified by a transformation matrix $T(\sigma)$. Generally the task space is represented in $SE(3)$, which can be seen as a representation of the end-effector position $\mathbb{R}^3$ and orientation $SO(3)$ i.e., SE(3) = $\mathbb{R}^3 \times SO(3)$.

$$T = \begin{bmatrix} R_{3\times3} & T_{R_{3\times1}} \\ 0_{R_{1\times3}} & 1 \end{bmatrix} \tag{5.10}$$

Where: the $3 \times 3$ rotation matrix $R_{3\times3}$ represents the orientation and $T_{R_{3\times1}}$ is a $3 \times 1$ vector representing the position. Generally the path variable $\sigma$ can be seen as a normalized time variable.

$$\sigma_n = \frac{t_n}{d_t} \tag{5.11}$$

where $t_n$ is the time it takes to reach processing sample point n for a task and $d_t$ is the total duration of the task. In the following the terms entry point and exit point will be used on a regular basis. They are defined as the points in Cartesian space where the laser beam enters and exits the contour and starts

/ ends the processing. The entry point is defined as $p_E = p(\sigma_0)$ and the exit point as $p_X = p(\sigma_s)$. By sampling the contour in the interval of the path variable, the contour can be represented in a discretized manner as a sequence of points.

$$C_d = \{p(\sigma_0)\ p(\sigma_1)\ \ \ldots\ \ p(\sigma_{s-1})\ p(\sigma_s)\} \tag{5.12}$$

To specify the orientation and position of these points around the contour it is necessary to define a frame attachment procedure. The direction of the X axis points in the cutting direction, the Z axis points in the direction of the plane normal and finally the Y axis is assigned to ensure that a right hand coordinate system is obtained. Such a frame assignment can be seen from figure 5.16 The contours will in the following generally be divided into

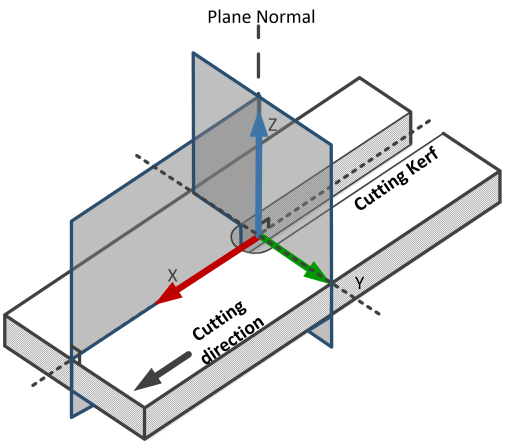


(a) A figure showing the frame assignment for the cutting kerf. The direction of the X axis points in the cutting direction, the Z axis points in the direction of the plane normal and finally the Y axis is assigned to ensure that a right hand coordinate system is obtained.

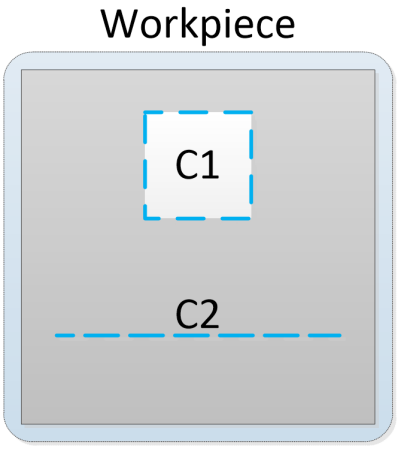


(b) Shows two different types of processing contours - open and closed. It is seen that C1 is closed and C2 open

**Fig. 5.4:** A figure showing the chosen frame assignment in the cutting kerf (5.4(a)) and the definition of open and closed contours (5.4(b))

two categories depending on its geometry. If the contour can be seen as a fully closed loop the contours will in the following be considered to be closed. If it is not a loop it is an open contour. This can be seen from figure 5.4(b). From this figure it is seen that C1 is closed and C2 is open. If a task set $\mathbb{T}$ contains open contours the assumption that all tasks are point tasks is no longer valid as the entry point is not coincident with the exit point. For closed contours the assumption can still be seen as valid, when the mechanical system is not taken

into account, as the entry point is coincident with the exit point. It should however be noted that the location of this common point can be put anywhere on the contour. In the following section this will be discussed in further detail.

### Task entry and exit points

As discussed in the previous section a tasks processing contour $C_n$ has an entry point $p_{E_n}$ and an exit point $p_{X_n}$ from which the laser processing starts and ends. The position of these entry/exit points are however not necessarily fixed for a given contour. For closed contours such as circles the entry and exit point are considered to be coincident [1], but can be located anywhere on the contour, for open contours such as lines the entry point and exit point are not located at the same position. Instead they are located at opposite sides of the contour line. The processing can generally be started from either side which entails that either line extreme can be considered as the entry point, forcing the exit point to the opposite side. This can be seen from figure 5.5. From this figure

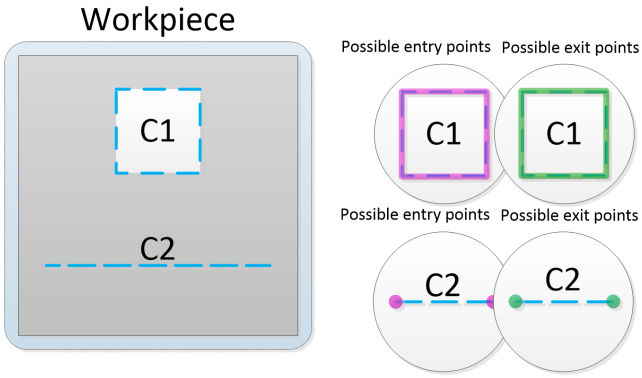


**Fig. 5.5:** The position of possible entry points on the two types of contours. On this figure the blue dashed line is the contour that needs to be processed. The purple areas denotes the possible entry positions and the green areas denotes the possible exit points

two contours are seen, a closed contour and an open contour. Possible entry points are marked by purple and possible exit points are marked by green. Notice that in both cases the regions are identical, but that they are mutually dependent. If an entry point is chosen for any contour the exit point will be fixed accordingly.

[1] This is not necessarily the case when cutting a contour out of a work piece as piercing often leaves stains around the initial point. This entails that piercing is sometimes done in the part of the plate that is discarded afterwards, the a smooth curve is traversed which links the piercing point to the contour. In such a case the exit point will be at the position where the smooth initial cut blends with the original contour This entails that the two points will not be on the same position

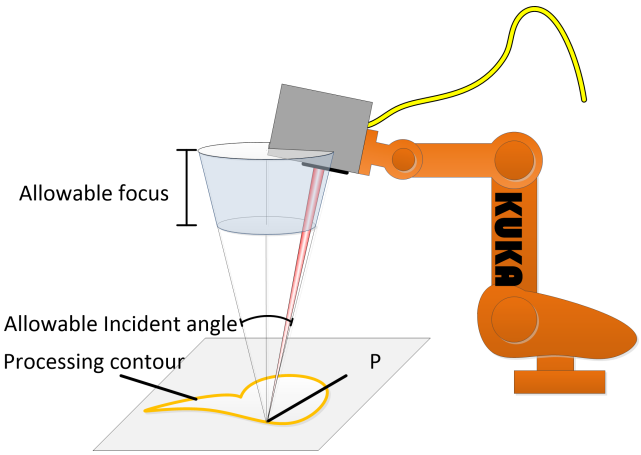


**Fig. 5.6:** A region in Cartesian space depicting a region within which stable cuts can be obtained. Notice that the region has the shape of a cone and is bounded by the maximum allowable change of focus and the maximum allowable incident angle for a given processing point P.

### Process Stability

When considering remote laser cutting it has been shown in this dissertation that both RFC and ROBOCUT cutting remain stable within a parameter window with regards to incident angle and focus (see table 4.3). This can generally be depicted as a cone from within which the beam can be directed at the point and still obtain a stable process. Such a cone is depicted in figure 5.6 along with an industrial robot mounted with a remote cutting head. If it is furthermore assumed that the laser beam is round symmetrical then it is clear that a stable process can be obtained with a beam rotated about its propagation axis (the Z axis as defined in III). This essentially entails that the three rotational variables related to the frame assignment described in section 5.2.1 are not fixed. The only fixed parameters related to the contour is the three positional variables X, Y and Z. This notion will become important when discussing the redundant nature of the robotic positioning system described in section 5.2.2.

## 5.2.2 Considerations related to the robotic positioning system

Now that a series of definitions and considerations have been presented with regards to remote laser processing this section will describe some similar thoughts with regards to the robotic repositioning system. In section 2.4 it was discussed that remote laser processing often involves mechanical systems with more degrees of freedom than 6. For scanner head based systems as much as 9 DOF

have been presented in the scientific literature due to the use of standard components [42]. This entails that it has been chosen to base the following analysis on a mechanical system composed of the KUKA KR120 which was specified in section 3.3 with 6 DOF mounted with a 3 DOF scanner head as described in appendix II. A total of four considerations have been identified which the sequencing algorithm needs to take into account.

1. Frame assignment on robotic positioning system
2. Redundancy and joint space of the positioning system
3. Connectivity of entry and exit points
4. Collision avoidance

These considerations will in the following be addressed more thoroughly.

### Frame assignment on robotic positioning system

In section 5.2.1 a frame assignment procedure was described for the cutting kerf. A similar frame assignment procedure needs to be defined for the robotic positioning system. A total of four frames have been defined. The robot base frame **B**, the robot tool flange frame **F**, a processing frame **P** and the final mirror frame $M_3$. These can be seen from figure 5.7(a)

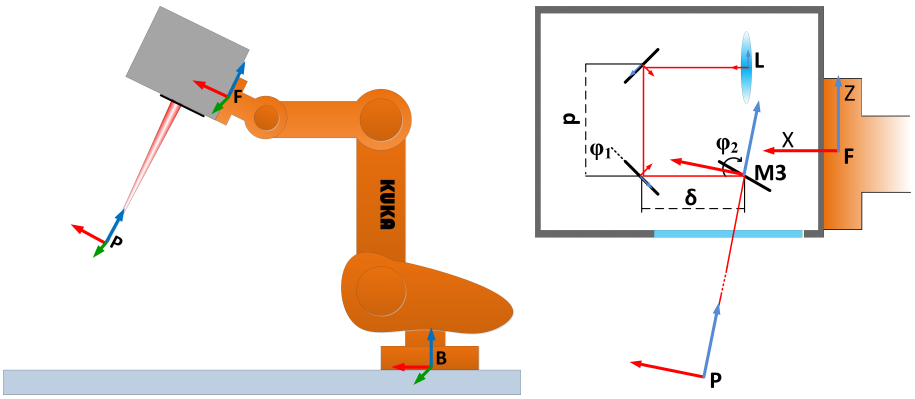


(a) A figure showing the frame assignment for the robot system. Notice the three frames the robot base frame **B**, the robot tool flange frame **F** and the processing frame **P**

(b) Shows the frame assignment inside the robot cutting head. Notice that the processing frame **P** is a translation of the third mirror frame **M3** inside the cutting head along the direction of the beam propagation.

**Fig. 5.7:** A view of a selected set of frames for the robot and for the remote cutting head.

The orientation of **B** and **F** are predefined by the robot but the Mirror frame $M_3$ and the processing frame **P** needs to be assigned. This will for $M_3$ be done based on the following procedure. The Z axis of the frame should be pointing in the inverse direction of the beam propagation. To keep the orientation it is furthermore specified that the X axis should lie in the XZ plane of the focusing lens frame **L** seen from figure 5.7(b). By taking the cross product between the direction of the Z axis and any vector in the XZ plane (e.g. [1,0,0]) the direction of the Y axis can be found. Finally by taking the cross product between the newly found Y axis vector and the original Z axis vector an orthogonal X axis can be found to complete the frame. It should be noted that the resulting vectors needs to be normalized as the use of cross products for non-orthogonal vectors will be scaled. The position of **P** is derived by translating $M_3$ in the direction of beam propagation by an amount equal to the distance from $M_3$ to the beam waist. A more thorough description of the derivation of the mirror kinematics and the frame assignment procedure can be found in appendix II.

**Redundancy and joint space of the positioning system**

In the previous sections the notion of tasks $\boldsymbol{t}$ were introduced as a processing contour $C$ on a work piece with appended processing data. As the contour is defined on the work piece it is defined in Cartesian space. The motions of the laser beam over the contour is however determined by the joint actuators of the laser processing machinery. This essentially entails that it is necessary to define the contour as a contour in the joint space of the manipulator. As discussed in section 3.3.5 the variables associated with the robotic positioning system are the following:

- $\psi$ -The DOE rotation angle
- $\theta_i$ - The joint angle associated with joint i of the industrial robot
- $\phi_k$ - The deflection angle of the scanner mirrors, where k is the mirror number
- $\delta$ - focus adjustment distance

With the 6 DOF robot and the 3DOF cutting heads specified in section 5.2.2 this entails that a joint vector can be created.

$$q = [\theta_1, \theta_2, \theta_3, \theta_4, \theta_5, \theta_6, \phi_1, \phi_2, \delta] \tag{5.13}$$

If the laser processing machinery is considered a fixed base manipulator with n joints whose end effector task can be represented by m variables, then the forward kinematics can be expressed as the mapping from configuration space to task space.

$$p = f(q) \tag{5.14}$$

where $p \in \mathcal{R}^m$ is the end effector pose and $q \in \mathcal{R}^n$ is the joint vector. As the number of joints n has been found to be 9 it generally entails that the resulting system can be considered to be redundant for tasks specified in Cartesian space as it has a dimensionality of 6. The contour $C$ can then be defined by using the forward kinematics of the positioning system into a contour defined by values of the joint vector q indexed by the same path variable $\sigma$ which was used for defining the contour in 5.2.1.

$$C = p(\sigma) = f(q(\sigma)), \forall \sigma \in [0, 1] \tag{5.15}$$

If the focus point of the laser beam is considered as being the robot end effector the contour can furthermore be seen being the desired path $p(\sigma)$. It is furthermore assumed that the path lies within the dexterous task space $\mathcal{T}$ which is defined as the set of end effector poses that can be obtained with $\infty^{n-m}$ joint configurations:

$$p(\sigma) \in \mathcal{T}, \forall \sigma \in [0, 1] \tag{5.16}$$

From this it is clear that every point $p(\sigma)$ can be realized with $\infty^{n-m}$ number of configurations. This is also the case when concerning the entry points and exit points $p_E = p(\sigma_0)$ and $p_X = p(\sigma_s)$. This again means that in joint space the entry points and exit points for a closed contour can no longer be assumed to be coincident. This essentially entails that the point task assumption from 5.1.2 is neither valid for open contours nor for closed contours (In joint space). This leaves room for optimizing the configuration of the robot to achieve faster movements between tasks. In fact, as it is assumed that the system contains a scanner head the repositioning could be made much faster if a scanner system was used for repositioning the beam between tasks instead of using the robot. The presence of redundancy in such a system is often seen as a benefit as it allows for optimization with regards to tasks such as collision avoidance [32], or singularity avoidance [112]. In [84] a general approach is presented where several prioritized tasks are optimized by the use of redundancy. The main task here is however to generate a set of sample configurations that can be evaluated by a sequencing algorithm. To generate a single solution one could sample (generate random values for) n-m axes of the manipulator and use the inverse kinematics to solve for the remaining axes giving a wanted position on e.g. a contour. In [92, 93] such a strategy is developed to generate samples around a contour that needs to be tracked by a robot end effector. In this dissertation a very similar approach will be used for generating configuration samples. However, instead of fixing axes directly it has been chosen define a sample vector $q_S$ composed of the following variables:

$$q_S = [\sigma, \beta, \alpha, Z_R, \phi_1, \phi_2, \delta] \tag{5.17}$$

By utilizing the work, travel and Z axis rotation angle from appendix III it is possible to generate samples anywhere on a given contour that are still within

the constraints of the process, with regards to the incident angle. This approach is presented in further detail in [126, 127].

### Connectivity of entry and exit points

In the previous section it was discussed that the redundancy of the robotic positioning system entails that the entry and exit points $p_E$ and $p_X$ of a contour can be realized in an infinity of ways. The robot configurations that positions the laser beam at the entry and exit points $p_E$ and $p_X$ will be denoted $q_E$ and $q_X$. If such a pair of configurations are given for a contour C which needs to be processed with a given speed and with a given process then it is necessary to use robotic path planning algorithms to connect the two robot configurations $q_E$ and $q_X$ while traversing the Cartesian contour. It cannot however be guaranteed that such a connection exists as it might require the robot to move faster than it is capable of. Furthermore collisions might make certain configurations impossible to achieve. This dissertation proposes a solution strategy to this problem by utilizing the sampling strategy described in the previous section. By evaluating the sample vector $q_S$ at several locations on a contour paths can be generated in the redundancy space of the manipulator. By utilizing traditional path planning algorithms for generating these paths directly in the redundancy space of the manipulator it is possible to generate a matrix that indicates to what extent the manipulator can reconfigure itself while still tracking the contour. The approach is not limited to a single approach, so algorithms such as rapidly exploring random trees (RRT) [67], probabilistic roadmaps (PRM) [74] or even their optimal counterpart $RRT^*$ or $PRM^*$ [58]. As the problem inherently is a multi-query problem PRM might however be an interesting choice. One might consider using the constraint motion planning framework CbiRRT [10, 11], but as it is based on the single query RRT connect algorithm this has not been done. Also as a method for generating samples directly on the constraint manifold has been employed it is seen as a more efficient strategy instead of e.g. rejection sampling or various projection methods.

### Robot collision avoidance

The final element that should be taken into account is the avoidance of collisions, both when considering collisions between the individual links of the robot with the mounted cutting head, and collisions between the robot and environment, including the work piece. This is of great importance as it prevents the algorithm from finding paths where the robot collides with its surroundings. Several available collision detection algorithms exist such as the I-COLLIDE library [15] / SWIFT [24]. It has however been chosen to use the built in obstacle collision detection algorithms in the simulation tool V-rep [21].

### 5.2.3 Other considerations

Now that several aspects of the robotic positioning system have been described a set of other considerations can be investigated in more detail. In this section two considerations will be discussed

1. Evaluation of cost functions
2. Other sequencing constraints

The first of these investigates the difference between using Cartesian distance as a metric for the duration of a robot reconfiguration between two points. The second of these discusses the inclusion of other constraints that could be imposed on the sequencing problem.

#### Cost evaluation

It was in section 5.1.2 presented that the reconfiguration time $d_{\boldsymbol{t}_i}^{\boldsymbol{t}_{i+1}}$ is a measure of the duration of a given intertask move. It was furthermore discussed that the goal of the sequencing algorithm is to minimize the reconfiguration time. If joint interpolated movements are assumed, the time it takes for a robot to move from one configuration to another is not necessarily correlated to the Cartesian length of the movement of the end effector [97]. It will however be correlated to the distance the individual joints needs to travel. To illustrate this a series of experiments were performed on the KUKA kr120. Several positions were defined within its workspace and the reconfiguration time between them were noted. Figure 5.8(a) shows the reconfiguration time when plotted against the Cartesian distance. From this figure this non correlation can be seen. If the reconfiguration between two points a and b is denoted $d_a^b$, and the Cartesian length between the two points is denoted $l_a^b$ this can more formally be expressed.

$$d_a^b \not\propto l_a^b \tag{5.18}$$

Instead of using the Cartesian distance another measure is needed. When considering a robot moving from one position to another, this should be considered as a joint space trajectory. The reconfiguration time will obviously depend on the taken joint path. If collisions needs to be avoided a longer and thus more time consuming path is taken. However, if a straight path in joint space is taken, it can be assumed that each joint moves from its initial configuration in a monotonic way. If it is furthermore assumed that the joint moves at the maximum velocity in the entire interval, then the time it takes for a joint to go from one configuration to another can be expressed as the joint value difference divided by the joint maximum velocity. The reconfiguration time of the robot can then be assessed by finding the joint that uses the most time on this reconfiguration.

$$d_a^b \quad \propto \quad max((c-p) \odot P_{I_{MAX}}) \tag{5.19}$$

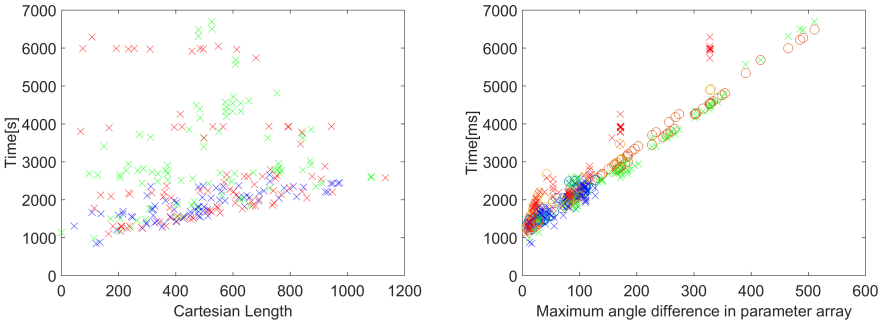


(a) A plot of a set of measurement the reconfiguration time of the KUKA kr 120 when moved between random configurations

(b) The predicted reconfiguring time when plotted against the maximum joint angle weighted by the speed of the joint

**Fig. 5.8:** Figure showing the reconfiguration time as a function of the Cartesian distance and the maximum joint angle weighted by the maximum joint speed

where $\odot$ denotes element wise multiplication of each array element and $P_{I_{MAX}}$ denotes a vector containing the 1/max speeds. By modifying this with a weight vector to adjust for robot load and deviations from the data sheet and by adding a constant $t_C$ to allow for any static delays the following reconfiguration time prediction $t_a^b$ is proposed

$$t_{P_a}^b = max((c-p) \odot P_{I_{MAX}} \cdot W_S) + t_C \tag{5.20}$$

Where $t_P$ is the time prediction vector and $W_S$ is a weight array calibrated to the robotic system. By using this as a measure it is possible to predict the reconfiguration time between two configurations. This has been done with the dataset shown in figure 5.8(b). For this evaluation the maximum joint values for the KUKA kr120 robot found in appendix IV were used. By using the MATLAB global optimization toolbox with the "GlobalSearch option" the following weights were found for the prediction:

$$W_S = \begin{bmatrix} 0.636 & 0.844 & 1.08 & 1.07 & 0.91 & 0.99 \end{bmatrix}^T \tag{5.21}$$

Furthermore a value of 831 ms was found for the constant $t_C$. It is however important to note that this constant delay should be seen as a representation of the time it takes for the robot to conduct the task of trajectory planning and to initialize the movement. As the robot program that produced the data has been designed to block the controllers ability to plan trajectories ahead[2]

[2]This was necessary as the timers used for measuring the reconfiguration time were being reset by the controllers ability to plan ahead. By disabling this feature readings could be obtained, but they will include the time utilized for trajectory planning and movement initialization. It is however assumed that this time is constant.

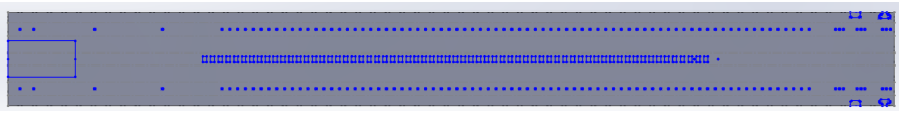

**Fig. 5.9:** The test work piece that was sampled. The work piece is a steel profile from one of our industrial partners [51]. It has a length of 2250 mm and a width of approximately 250 mm when flattened.

this delay will not be present in a real production set-up. This entails that it in the following will be omitted. By utilizing the found formula it is possible to determine a warping of the Cartesian space based on optimal joint configurations. The reason for this investigation is that it is expected that the presence of scanner mirrors has a great influence on the reconfiguration time when dealing with short repositions. The characteristic is found by means of sampling the positions of a work piece seen from figure 5.9. The workpiece contains 252 contours that needs to be laser cut with given entry and exit points. By selecting two entry points points e.g. a and b, it is possible to generate two robot configurations $q_a$ and $q_b$ that forces the beam waist of the laser beam to be in a and b. Due to the redundant nature of the mechanical positioning system the sampling strategy, that was discussed in in section 5.2.2, was used. The configurations $q_a$ and $q_b$ are found by specifying a set of sampled variables $q_{PS_a}$ and $q_{PS_b}$. By selecting the sample variables in an appropriate manner one can ensure that the beam waist can be made to lie in the correct position while still complying with requirements concerning e.g. maximum incident angle. If two such sample vectors are defined $q_{PS_a}$ and $q_{PS_b}$ it is possible to construct a combined sampling vector $q_{PS_C}$.

$$q_{PS_C} = [q_{PS_a}\ q_{PS_b}]^T \tag{5.22}$$

This sample vector, in combination with the resulting robot configurations and in combination with equation 5.20 can be used to derive the reconfiguration time between two robot configurations. By treating this as an optimization problem where the input vector is $q_{PS_C}$ and the cost function is the reconfiguration time defined in equation 5.20 a minimum reconfiguration time can be found by using numerical optimization methods. By using the numerical optimization toolbox in MATLAB optimal poses for all combinations of the 252 points were found. The resulting reconfiguration times are shown in figure 5.10 where they are plotted against the Cartesian distance. It should be noticed that to keep similar scales all values have been normalized according to the maximum values. From this figure it is seen the main difference can be seen to be the area where the Cartesian distance is close to 0. Here the reconfiguration time is approximately truncated to zero. This is due to the high speed of the scanner mirrors. When the distances are small they can be used for all repositioning, but as the distance increases the robot system takes over. From

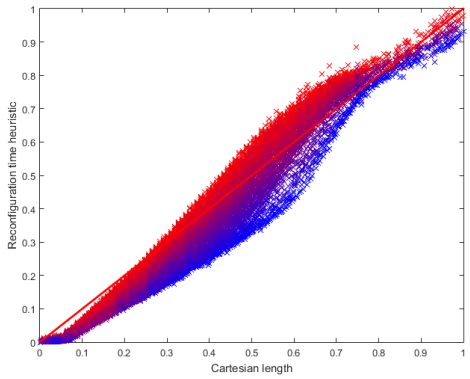


**Fig. 5.10:** The reconfiguration time plotted against the Cartesian distance of the cutting head. It is seen that a small truncated region exists to the far left. This region can be seen as the region where the reconfiguration time is governed by the scanner mirrors of the cutting head. As this depiction is again in Cartesian space it has been chosen color the data points by a factor that indicates the movement of the slowest joint (Joint 1). The more joint 1 is moved compared the more red the data point becomes. From this it is seen that generally the slowest reconfiguration times are obtained when the ROBOT needs to reposition itself by using its slowest axis.

this figure it is seen that there is a zone between 0 and 80 mm which provides a very low repositioning time. The 80mm limit is due to the limited allowable angle of incidence as described in 4.2. The above graph is created with an allowable incident angle of 5 degrees and a focal length of 780 and with the maximum joint values indicated in I. Furthermore a cutting head design as the one described in II.2 was used with $\delta = 100mm$ and $d_1$=50mm. This yields a cutting head configuration similar to what can be seen from figure 5.11. If it is assumed that $\delta = 100mm$ is static and that mirror $M_2$ remains fixed then a theoretical value of 92mm can be found for the truncated zone where the mirrors are allowed to reach ( $2 \cdot \sin(5°) \cdot 530 = 92mm$). The difference between the 80mm from the simulation and the 92 mm from the calculation originates not only from the assumption that $M_2$ is static, but also from the optimization algorithm itself. To reduce the running time 1000 iterations have been made for each combination resulting in difficulties with finding optimal solutions as the search space where only the mirrors are moved decreases as the distance approaches the limit of 92mm.

The main conclusion from the above simulation is that it is problematic to assume that the reconfiguration time of the robot can be predicted based on the Cartesian distance. This again entails that when considering task sequencing it can result in sub optimal sequences if Cartesian distance is used purely as the cost function.

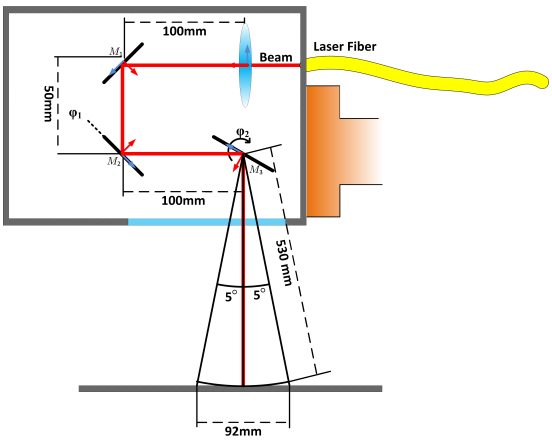


**Fig. 5.11:** A figure showing the resulting low reconfiguration time distance that results from the determination of the maximum allowable angle of incidence

### Other sequencing constraints

When considering the problem of sequencing tasks one often meets many different constraints that are more or less process specific. When considering 2D cutting a common consideration is the presence of precedence constraints, these define if one task should be conducted before another. This is often the case when considering the cutting of nested contours. Furthermore, it might be allowed to divide a contour into sub contours and process them at different times. It might also be necessary to include the piercing time or to include deadline constraints if e.g. the work pieces are moving on a conveyor. For further considerations see e.g. [18], which treats the case of 2D laser cutting.

## 5.3 Solution strategy for sequencing of remote laser processes

A complete task sequencing framework would have to take all the considerations listed in the previous sections into consideration when finding the optimum sequence $S^*$ described in section 5.1.2. It was in the previous section found that the scheduling of remote laser processes differs from the case of point tasks in the following areas:

1. Tasks are represented by processing contours which can be either open of closed and not by a single coordinate frame.

2. The laser processing can begin and end at either extreme of an open contour and essentially anywhere on a closed contour.
3. The laser process remains stable for a range of incident angles and focus
4. The mechanical position system is redundant in terms of the task which means that all entry and exit points can be reached by an infinite number of configurations
5. The connectivity of entry / exit point configurations is not guaranteed and must be determined by path planning.
6. Robot collisions should be taken into consideration.
7. Cost evaluations should be conducted by evaluating the configurations of the robot and not the Cartesian distance.

In equation 5.6 it was described that the optimum sequence $S^*$ is the one that can minimize the summed intertask times $dI_t(S)$. If the reconfiguration time between two contours is evaluated by equation 5.20 then it is seen that the reconfiguration time depends on the robot configuration in the exit point of the first contour and the entry configuration of the next. This again entails that the sequencing task is composed of finding both a task sequence and a set of associated entry and endpoint configurations that minimizes the cycle time. The task sequencing framework presented in this section will find this sequence along with a set of entry / exit point configurations by using a sample based approach. This sample based approach considers robot redundancy, process constraints and entry / exit point positions on closed and open contours. The evaluation is done by using the heuristic for reconfiguration time seen in equation 5.20. Furthermore collision avoidance is taken into account when considering the connectivity of entry point / exit point combinations. It is presented in the two papers [127] and [126] which can be found in appendix F and G. These will in the following be summarized. [127] describes an algorithm that generates a map of robot entry poses that can reach a set of exit poses while the contour is traversed at a given speed, while still ensuring that robot joints are not saturated speed wise. Based on these maps [126] describes a task sequencing framework based on traditional solvers for the generalized traveling salesman problem. The two papers will use the variable names which were presented in section 3.3.5.

- $\psi$ -The DOE rotation angle
- $\theta_i$ - The joint angle associated with joint i of the industrial robot
- $\phi_k$ - The deflection angle from the deflection mirrors, where k is the scanner mirror number

- $\delta$ - focus adjustment distance

To ensure that the task sequencing framework can be applied to other laser cutting or welding processes it has in the papers been chosen to remove the DOE rotation device and to assume that processing is conducted with a round beam. This is done to ensure that the framework treats a more traditional mechanical set-up which is generally used for both remote laser cutting and welding. In section 5.4 it will however be discussed that these two choices are of little consequence when considering the task of scheduling ROBOCUT cutting and that they can be included in a trivial manner.

### 5.3.1 Summary of paper E: PRM based path planning along end effector path for redundant robotic laser processing machinery with scanner mirrors

The following section contains a summary of the obtained results from the paper "PRM based path planning along exit effector path for redundant robotic laser processing machinery with scanner mirrors".

#### Objectives

1. To derive an algorithm yielding the connectivity between entry and exit poses
2. To develop a methods for randomly drawing sample configurations where the end effector remains on the contour and complies with process constraints.
3. To lay the foundation for further sequencing studies.

#### Summary

When considering robot mounted remote laser processing equipment they can generally be said to be redundant in terms of the processing task. This is due to the fact that when conducting remote laser cutting an industrial robot with 5-6DOF is mounted with a scanner cutting head with 3 DOF [42]. The task of laser processing is generally only specified by a curve in space given by a sequence of XYZ positions. The rotations are not specified, but rather given as an interval within which a stable process is achieved [125]. This entails that generally the robot can reach any point on the contour with an unlimited number of configurations. Essentially this is also true for a given entry and exit point on the contour and in essence this entails that the robot can reconfigure itself while processing the contour. This can be utilized when sequencing multiple tasks as it is possible to bring the robot closer to the next entry point by reconfiguring the robot while processing the current contour. In this paper an

algorithm is presented that uses probabilistic roadmaps [74] to identify possible connections between a sampled set of entry point configurations and a sampled set of exit point configurations while still traversing the contour within the given process constraints. A conceptual overview of this algorithm can be seen from figure 5.12.

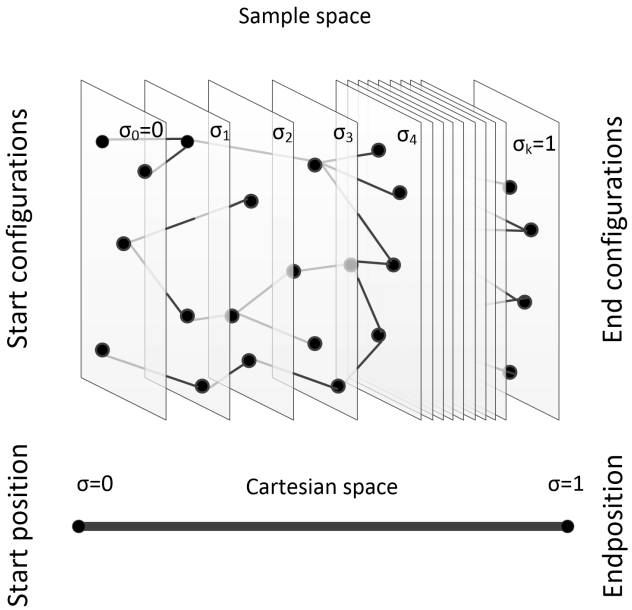


**Fig. 5.12:** A conceptual overview of the implemented algorithm. Notice that the PRM path planning takes place in the sampled redundancy space while the end effector is still ensured to comply with process constraints in Cartesian space

Notice that the PRM path planning takes place in the sampled redundancy space while the end effector is still ensured to comply with process constraints in Cartesian space. An approach similar to [92,93] is applied to ensure that all robot configurations are in compliance with these constraints the sampling of points on the contour is done by defining a sample vector that can be used to generate a pose directly on the end effector path.

$$q_S = \begin{bmatrix} \sigma & \beta & \alpha & Z_R & \phi_1 & \phi_2 & \delta \end{bmatrix}^T \tag{5.23}$$

By using the inverse kinematics this can be converted to poses that are ensured to comply with process constraints with regards to the incident angle. If a set of entry poses are labeled $q_{S_1} - q_{S_L}$ and a set of exit poses are labeled $q_{E_1} - q_{E_I}$ then this paper derives a connectivity matrix determining which entry configurations can reach which exit configurations. Such a matrix can be

| Type | Iterations | # Edges | # Connections | Avg. cost | Time[s] |
|---|---|---|---|---|---|
| PRM$d_s$ | 100 | 350 | 215 | 2,06 | 236,350 |
| | 500 | 3033 | 1217 | 1,58 | 1287,43 |
| | 1000 | 5618 | 1216 | 1,89 | 2397,03 |
| | 2000 | 11195 | 1277 | 1,38 | 4731,03 |
| | 5000 | 27145 | 1264 | 1,37 | 12900,83 |
| PRM$d_q$ | 100 | 395 | 323 | 1,80 | 202,090 |
| | 500 | 2865 | 1038 | 2,55 | 1739,82 |
| | 1000 | 5458 | 1158 | 2,16 | 3263,11 |
| | 2000 | 11069 | 1275 | 1,42 | 6097,64 |
| | 5000 | 27613 | 1261 | 1,47 | 14181,42 |

**Table 5.1:** A summary of the results when using the proposed algorithm for following a straight line in cartesian space.

seen below

$$\begin{array}{c} \\ q_{S_1} \\ q_{S_2} \\ q_{S_3} \\ \vdots \\ q_{S_L} \end{array} \begin{array}{c} \begin{array}{ccccc} q_{E_1} & q_{E_2} & q_{E_3} & \cdots & q_{E_I} \end{array} \\ \begin{pmatrix} c_(1,1) & c_(1,2) & c_(1,3) & \dots & c_(1,I) \\ c_(2,1) & c_(2,2) & c_(2,3) & \dots & c_(2,I) \\ c_(3,1) & c_(3,2) & c_(3,3) & \dots & c_(3,I) \\ \vdots & \vdots & \vdots & \ddots & \vdots \\ c_(L,1) & c_(L,2) & c_(L,3) & \dots & c_(L,I) \end{pmatrix} \end{array}$$

It is seen that each row represents an entry pose and each column represents an exit pose. Each entry contains the cost from moving from the given entry pose to the exit pose. A large integer (999999) indicates that no connection is found between two configurations.
A test was conducted on a line and a set of 40 entry points and 40 exit points were sampled. 8 of the sampled exit points entailed a self-collision which entailed that only 32 exit points were used. The proposed algorithm was run for 100, 500, 1000, 2000, 5000 and 10000 iterations with four different distance metrics. The obtained results by using a sample vector distance metric $d_s$ and a joint vector distance $d_q$ can be seen from table 5.1. From this it was seen that after approximately 2000 iterations more than 1250 paths out of the 1280 possibilities were found. The effect of using the different distance measures were however less conclusive. Generally the sample space metric $d_s$ obtained the largest amount of connections in the shortest amount of time. It might however be a consequence of the chosen processing contour (A straight line). To visually see this a plot was conducted in V-rep where the corners of the robot cutting head were plotted. The color assignment can be seen from figure 5.13 As the 1277 connections indicates that 1277 paths between the entry point

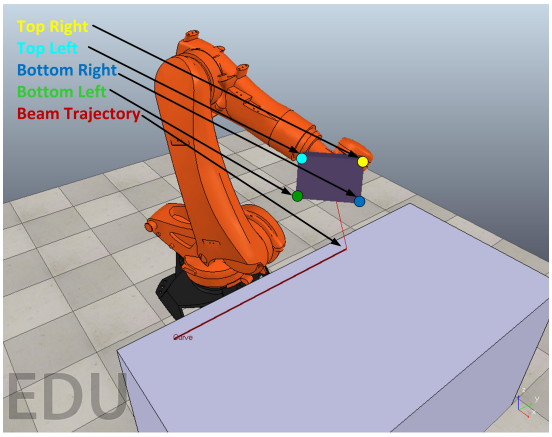


**Fig. 5.13:** Shows the color assignement of the corners of the robot cutting head.

and exit point have been found in cartesian space all paths can obviously not be plotted. To illustrate the generated paths three are plotted with the color assignment seen on figure 5.13. These three paths can be seen from figure 5.14 It should however be noted that a run covering 2000 iterations takes approxi-

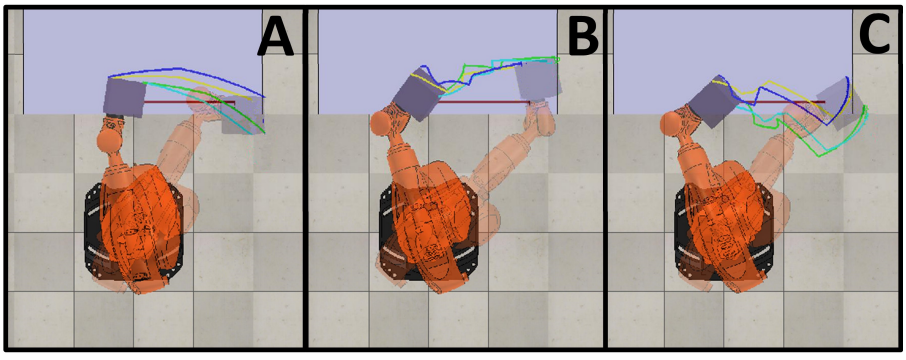


**Fig. 5.14:** Shows three paths A,B and C between the same entry and endpoints. By using the algorithm a total of 1275 paths were found between them

mately 5000-8000 seconds to complete which is generally more than an hour of processing. This slow processing speed originates from the collision detection algorithm which runs in the simulation software V-rep. As the communication between MATLAB and V-rep suffers from a substantial overhead this is quite a drawback of the chosen implementation.

**Future research**

As discussed in the conclusion, one of the drawbacks of the chosen implementation, is the use of MATLAB scripts as the main tool for programming in combination with V-rep for collision detection. This implementation strategy results in the slow speed of the algorithm. As the focus of the implementation has not been on increasing speed, but rather on flexibility it is assessed that the speed can be increased significantly.

### 5.3.2 Summary of paper F: A framework for task sequencing for redundant robotic remote laser processing equipment based on redundancy space sampling'

The following section contains a summary of the obtained results from the paper "A framework for task sequencing for redundant robotic remote laser processing equipment based on redundancy space sampling".

**Objectives**

1. To develop and implement an algorithm for laser process sequencing in robot redundancy space based on solving the generalized traveling salesman problem (GTSP).
2. To develop an algorithm which is based on parts that can be replaced in a modular fashion
3. To develop a heuristic for path start point sequencing.
4. To apply the path sampling developed in section 5.3.1 to a broader range of problems

**Summary**

Sequencing remote laser processing tasks on a work piece is a challenging problem as many factors needs to be taken into account. First of all, the robot can be considered as redundant with regards to the processing task [44, 83]. This entails that all entry / exit points can be achieved by an infinity of robot poses [14]. Furthermore, cutting often involves closed contours where the contour entry point is not given beforehand as the process potentially can be started and stopped at any position around the contour [18]. Finally the laser processes in question requires that certain constraints with regards to e.g. incident angle is taken into account when planning paths [125]. In this paper a scheduling algorithm is presented which takes the described factors into account. Figure 5.15 shows the structure of the proposed algorithm which has

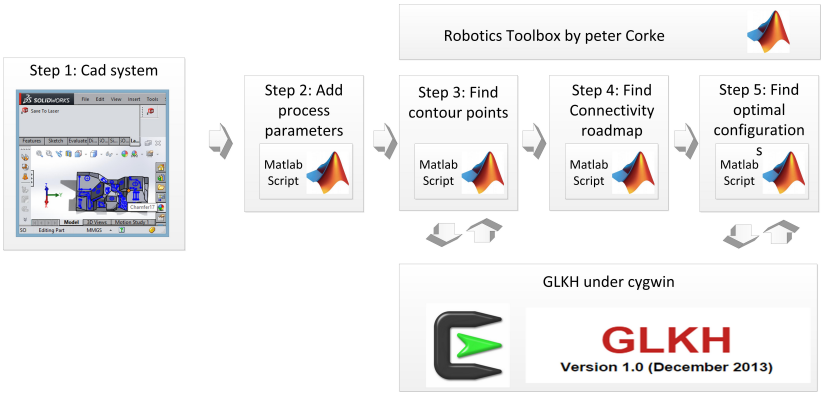


**Fig. 5.15:** The proposed overview of the task sequencing algorithm. It is composed of 5 steps which are run sequentially

been implemented in MATLAB and C#. From this figure it is seen that the presented framework consists of a series of 5 steps.

1. In the first step a CAD system supplies a set of contours that needs to be processed.

2. Then in step 2 process specific parameters such as cutting speed and maximum allowable incident angle is added to the contour description. Depending on these process parameters the contours are transformed into cuts, welds or even engravings

3. In step 3 a set of entry points are sampled over all contours and optimal entry / exit points are found by using a solver for the generalized traveling salesman problem (GTSP). A modified Cartesian distance is used for calculating the cost to for a given entry and exit point combination.

4. In step 4 pose connecting maps are found for each contour describing the link between a set of sampled entry and exit configurations.

5. Finally in step 5 these pose connecting maps are used to formulate another generalized traveling salesman problem which again can be solved by a GTSP solver. The results from this is a pair of entry and exit configurations for each contour that that minimizes the processing time and that is connectible while processing the contour.

It should be noted that the algorithm described in section 5.3.1 is used in step 3 for finding pose connected maps. Furthermore it is seen that it has been chosen to to solve the GTSP problem twice in the above enumeration. Once for finding optimal entry/exit points and once for finding optimal robot poses. From figure 5.15 it can be seen that the GTSP solver GLKH [46] has

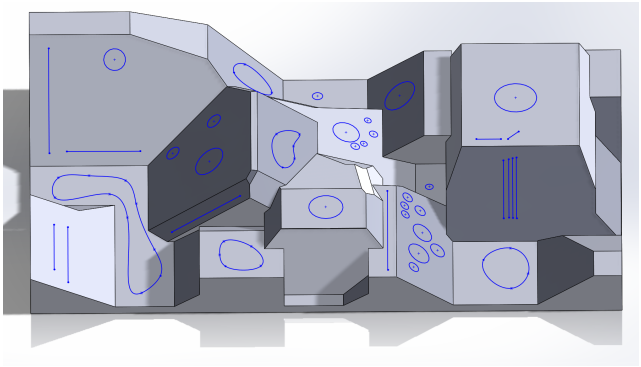

**Fig. 5.16:** The chosen test case. Notice the 38 contours laid out on the various surfaces of the workpiece.

been used. This solver works by converting the GTSP problem into a TSP problem [85] and solving it by using the Lin-Kernighan-Helsgaun algorithm [45]. This algorithm is currently the most efficient solver for the traveling salesman problem. One of the main forces of the above structure is that the interface to the sequencing framework and the GTSP solver is the use of the file format specified by TSPLIB [100]. By supplying a GTSP solver with a file in the TSPLIB format the sequencing problem can be solved. In this implementation this is done by calling the compiled GLKH binaries under CYGWIN and the resulting scheduling is returned to the MATLAB scripts. By doing this it ensures that if more powerful GTSP solvers are developed they can replace GLKH as long as they support the TSPLIB format which is a widely accepted format.
As a test case it has been chosen to use a part with 38 contours laid out on in a series of angles as seen from figure 5.16. The base dimensions of the test case is 800 mm x 1400 mm with the highest plateau being approximately 300 mm above base. By running the start point sequencing algorithm on these 38 contours the following is obtained. Based on the generated entry points connectivity maps were created for each entry point/exit point configuration by using the algorithm presented in [127]. Table 5.2 lists the number of generated paths per node from the 2000 iterations. It is seen that the number of paths range from 86 to 9771 found paths. To increase this number more iterations are necessary. The combined path planning count is however close to 10 hours for 2000 iterations. Finally, when these possible entry /exit point paths are taken into account for the sequencing as described in step 5 of the algorithm the the following path is obtained: From this figure it is seen that much of the repositioning has been conducted while traversing the contour.

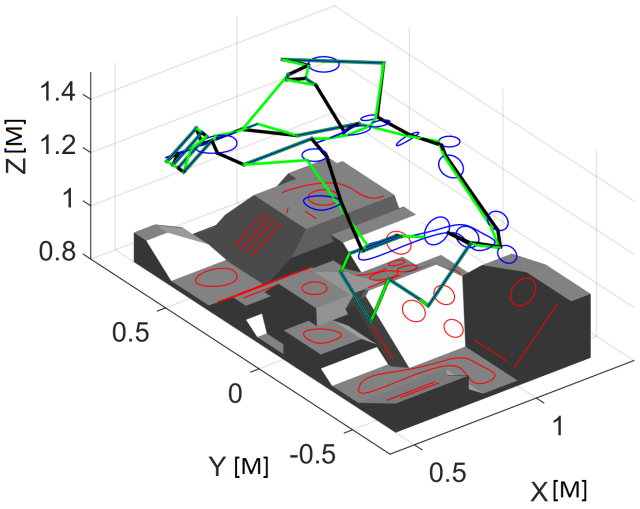


**Fig. 5.17:** The results from the entry point sequencing algorithm.

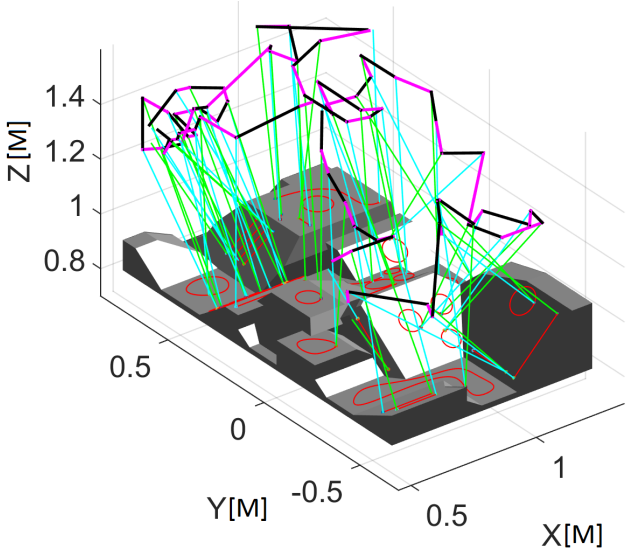


**Fig. 5.18:** The sequence obtained by the scheduling algorithm. On the figure, cyan markings relate the robot end effector position to an entry point on a contour, a green line links an exit point to its corresponding robot end effector position. The magenta lines indicate a robot intertask reposition and a black line entails a repositioning that is conducted while traversing the contour

| # | Paths | # | Paths | # | Paths | # | Paths |
|---|---|---|---|---|---|---|---|
| 1 | 3237 | 11 | 8509 | 21 | 8206 | 31 | 8051 |
| 2 | 433 | 12 | 7302 | 22 | 9272 | 32 | 311 |
| 3 | 7212 | 13 | 9771 | 23 | 86 | 33 | 955 |
| 4 | 7448 | 14 | 402 | 24 | 3609 | 34 | 2988 |
| 5 | 531 | 15 | 2053 | 25 | 577 | 35 | 7690 |
| 6 | 4453 | 16 | 1547 | 26 | 2517 | 36 | 8058 |
| 7 | 877 | 17 | 4489 | 27 | 7710 | 37 | 4035 |
| 8 | 7789 | 18 | 1344 | 28 | 1365 | 38 | 7440 |
| 9 | 390 | 19 | 943 | 29 | 1241 | | |
| 10 | 7425 | 20 | 1289 | 30 | 1241 | | |

**Table 5.2:** Table showing the number of connected paths when finding connected entry and exit points over the 38 contours on the test case

**Future research**

As discussed in the conclusion and future research section precedence constraints are not taken into account by the chosen implementation of the GTSP solver used in the paper. If a suitable algorithm is developed it should replace the GTSP solver in the implementation. Also, if a more efficient roadmap algorithm is devised it would ensure a much faster processing rate. Currently the computation times used to generate a sequence for the 38 contours mentioned in the paper is approximate 24 hours. Such a time frame is generally quite impractical and should be considered as being feasible only for mass production environments where the same process is conducted repeatedly.

## 5.4 Inclusion of ROBOCUT specific parameters in the task sequencing framework

As described in section 5.3 it has been chosen to omit the beam rotation variable $\psi$ in the two paper describing the framework and to assume that the beam is round symmetrical. These simplifications were conducted to keep them as generic as possible. It is however easy to include them in the framework simply by making modifications to the chosen sample vector. In 5.3.1 a sample vector to generate configurations on a given curve was described by the following equation:

$$q_S = \begin{bmatrix} \sigma & \beta & \alpha & Z_R & \phi_1 & \phi_2 & \delta \end{bmatrix}^T \tag{5.24}$$

To remove the assumption of beam symmetry it is necessary the z rotation can simply be removed from $q_S$, creating a new modified sample vector $q_{S_{NM}}$

$$q_{S_{NM}} = \begin{bmatrix} \sigma & \beta & \alpha & \phi_1 & \phi_2 & \delta \end{bmatrix}^T \tag{5.25}$$

Furthermore, to include the beam rotation parameter this can easily be added by adding the beam rotator variable directly to the sample vector.

$$q_{S_{ROBOCUT}} = \begin{bmatrix} \sigma & \beta & \alpha & \phi_1 & \phi_2 & \delta & \psi \end{bmatrix}^T \tag{5.26}$$

Here it should however be noted that there is only a subtle difference between 5.26 and 5.24. If it is assumed that the laser beam has been improved by means of a DOE pattern, it is clear that this pattern should be aligned with the cutting kerf. If a sample is drawn with equation 5.24 this alignment can also be guaranteed if the beam rotator is used as a way to compensate for the generation an unaligned path. If a compensation function $k_c$ is defined it is clear that it should yield an appropriate beam rotation that compensates for the misalignment of the chosen sampling.

$$\psi = k_c(q_S) \tag{5.27}$$

In other words, it is basically an inverse kinematic mapping between robot joint coordinates and the misalignment. Already a similar mapping is taking place between the sample vector $q_S$ and the robot joint vector. As per the work travel and z rotation definition given in III the only rotation around the cutting kerf is obtained by the rotation $Z_R$. This entails that $\psi$ directly compensates for $Z_R$ in $q_S$. This entails that one or the other sample vector can be used to represent a ROBOCUT sample vector. In the case that $q_S$ is chosen as the sample vector a $Z_R$ rotation is chosen and the beam rotator compensates for the misalignment. If equation 5.26 is used, $\psi$ is chosen and a $Z_R$ is found for compensating. This entails that in fact the difference between a given ROBOCUT sampling vector and a standard sampling vector is minimal.

## 5.5 Evaluation of the research objectives for the third area of focus

Now that the task sequencing framework has been presented a short evaluation of the research objectives presented in section 2.5 will be presented. In that section, two research objectives were presented regarding the development of a task sequencing framework for remote laser processing machinery.

- Develop an algorithm for generating paths for the remote laser cutting system that allows it to reconfigure itself while still cutting the specified contour.
- Investigate and develop algorithms for path sequencing for workpieces that requires multiple cuts, which takes the robot redundancy into account

In the following section the obtained results for these research objectives will be summarized.

### 5.5.1 Develop an algorithm for generating paths for the remote laser cutting system that allows it to reconfigure itself while still cutting the specified contour

An algorithm based on probabilistic roadmaps were developed to identify which entry poses of the robot could be moved to which exit poses of the robot while still traversing the processing contour. A sample vector was defined to sample robot configurations directly on the task manifold with regards to process constraints when concerning traveling speed and incident angle. The algorithm was implemented in MATLAB with the simulation software V-rep functioning as a collision detection library. The implementation was tested on a contour with 40 entry configurations and 32 exit configurations. From the test it was determined that after 2000 iterations 1277/1280 solutions had been found. Several distance heuristics were tested however without conclusive results to their efficiency. The running time of the algorithm was however quite slow due to the communication overhead between MATLAB and V-rep.

### 5.5.2 Evaluation of research objective: Investigate and develop algorithms for path sequencing for work pieces that requires multiple cuts, which takes the robot redundancy into account

A task sequencing framework was in [126] presented. It worked in five steps where of which the first two concerns the task of generating contours and process related data. In the third step a set of optimal entry / exit points are generated by converting it to a generalized traveling salesman problem GTSP. In step four these optimal entry / exit points are used and several robot configurations are sampled by using the sample vector defined in [127] for each of these points. By using the path planning algorithm presented in [127] a set of pose connecting maps were found. In step 5 the pose connecting maps for all contours on a work piece were converted into another GTSP problem. The solution to this problem gives a path between all contours that optimizes the

reconfiguration time. It has been chosen to utilize the GTSP solver GLKH as it is based on one of the most efficient GTSP solvers available [46]. It is however not capable of handling other constraints such as precedence constraints. This has entailed that it has been chosen to create an interface to the GTSP solver based on the TSPLIB [100] file format which entails that if a better solver is found GLKH can easily be replaced.

# Chapter 6

# Concluding remarks

In the following chapter some concluding remarks will be given based on the research presented in this dissertation. This section will contain a review of the obtained results with regards to the proposed research objectives from section 2.5, a conclusion and predictions for future research activities.

## 6.1 Review of research objectives

In chapter 2.5 a set of research objectives were presented which were divided into three areas of focus;

1. Developing and commissioning a flexible laser processing laboratory for the ROBOCUT technology
2. Analyzing the ROBOCUT and the remote fusion cutting process
3. Developing a framework for task sequencing and path planning

Within these three areas of focus several results have been obtained. These have been presented in this dissertation both as individual sections and as summaries of scientific papers. In the following the conclusions presented in section 3.5, 4.4 and 5.5 will be summarized.

**Developing and commissioning a flexible laser processing laboratory for the ROBOCUT technology**

- *Develop a flexible laser processing laboratory for laser processing with DOE patterns.*

  In chapter 3 several requirements with regards to the laser laboratory were derived based on a preliminary analysis of the ROBOCUT process.

It was discussed that the most appropriate laser for the process was a single mode fiber laser with a modified cutting head so that diffractive optical elements could be inserted in the beam path. It was discussed that as remote fusion cutting can be conducted with 4kW of laser power a laser source with at least 3kW should be acquired. To accommodate these requirements two cutting heads were acquired with modifications allowing for DOE insertion. Furthermore a DOE rotating device was constructed for DOE pattern alignment with the cutting direction. A 3kW Single mode fiber laser was purchased and commissioned with the cutting heads and beam rotator. A mechanical positioning system was furthermore acquired composed of several elements. An XY table for conducting 2D cutting and a robot for conducting 3D cutting. Both systems can move at speeds greater than 1m/s to ensure that cuts can be made with speeds that matches industrial laser cutting systems.

- *Develop a control architecture for the mechanical actuators with a flexible interface that allows for the implementation of advanced control algorithms.*

  In section 3.1.4 several requirements were set-up with regards to the software control architecture. As the system is required to control the moving axes of the mechanical system and the laser source it was required that the system has real time capabilities. Furthermore it was required that it contained a CAM interpreter based on G-codes as it is the most common way to program industrial and domestic laser cutters and 3D printers. Also it was discussed that it should be possible to program it by using high level languages such as C#. Based on these requirements it was chosen to base the control system on a BECKHOFF PLC. This was chosen as it provides hardware and software interfaces to all pieces of auxiliary equipment. By utilizing and expanding the server client structure already used in the PLC, for its variable I/O interface, a platform with which advanced control algorithms could be implemented was obtained. A scientific paper was presented which showed how this interface could be used for the implementation of an iterative learning control algorithm on the XY table [129]. By utilizing this machine learning algorithm on the chosen control architecture it was possible to reduce the tracking error by more than 50% without changing the internal controller parameters of the system.

- *Investigate the applicability of using scanner mirrors for remote cutting.*

  In 3.3.3 it was determined that due to the potential cutting speed of the ROBOCUT cutting technology a scanner cutting head would be necessary when considering the repositioning rate of the system, especially

when considering the cutting of detailed contours. As the ROBOCUT laser process should be robot based it would result in a system similar to what is often discussed for remote laser welding and cutting as described in section 2.4. The accuracy of such a combined system might however be affected due to the long kinematic chain. In [124] it was assessed that the total accuracy of the system would be affected by the long kinematic chain resulting in an accuracy of ±0.76 mm. The calculations were however based on several assumptions with regards to the robot pose as the necessary parameters for the calculations are the intellectual property rights of KUKA. It has been chosen to postpone the acquirement of a scanner cutting head as it is not strictly necessary to prove the capabilities of the ROBOCUT process.

**Analyzing the ROBOCUT and the remote fusion cutting process**

- *Develop a method and metric for fast evaluation of the stability of conducted laser cutting experiments.*

  It was chosen to define the cut stability based on an evaluation of the cutting process ability to eject melt from the cutting kerf. This was chosen to allow for an image based evaluation of the cut stability. The percentage of unblocked cutting kerf was chosen as a metric to assess the stability. A computer vision algorithm was developed based on images from a Carl Zeiss axioimager microscope. The algorithm was implemented in MATLAB and has been used to evaluate more than 3300 cuts. The algorithm has proven to provide a robust way of measuring the cut stability rapidly. It is furthermore possible to improve the algorithm to extract further parameters such as the kerf width and kerf variance.

- *Determine a process windows within which RFC can be conducted with respect to parameters such as laser power, focus region and processing speed and incident angle.*

  The stability of the remote fusion cutting process was determined within two parameter windows. The first with respect to beam diameter and travelling speed and the second with respect to Work and travel angle (see appendix III). During the course of these experiments it was determined that a semi coherent area of stability was found for speeds between 5000 mm/min and 10000 mm/min with a beam diameter between 0.35 - 0.65 mm. Based on this a set of angular experiments were conducted with a speed of 7000 mm/min and a beam diameter of 0.475 mm. It was found that stable cuts could be obtained within a window of ±6° with regards to both travel and work angle. It was however also noted that

the RFC cutting process generally had a low stability and a very low repeatability with the test setup.

- *Evaluate the potential of ROBOCUT remote cutting by comparing experimental results to the RFC experiments.*

  In section 4.3 the current ROBOCUT beam design and cutting results were presented. By using the proposed beam pattern it was possible to obtain remote cutting for speeds between 800 mm/min and 1600 mm/min with a focus offset between 0 and 10mm.[1]. Within this region a very coherent stable region was found with a stability of close to 100%. The cuts were, however, obtained by pulsing the laser with a duty cycle of $\approx$ 20% which resulted in speeds that were also approximately 20 % of RFC. Based on this a set of angular experiments were conducted with a speed of 1200 mm/min and focus offset of 5 mm. For positive angles it was found that stable cuts could be obtained within for travel angles between 0° and 6° For work angles it was however found that cuts could be obtained for angles between 0 and 32°. From this it was concluded that the current ROBOCUT beam design can improve the cut stability significantly, however at the cost of speed. It is however expected that an increased speed can be obtained by modifying the beam pattern so that more laser power can be utilized to remove the molten material.

**Developing a framework for task sequencing and path planning**

- *Develop an algorithm for generating paths for the remote laser cutting system that allows it to reconfigure itself while still cutting the specified contour.*

  An algorithm based on probabilistic roadmaps were developed to identify which entry poses of the robot could be moved to which exit poses of the robot while still traversing the processing contour. A sample vector was defined to sample robot configurations directly on the task manifold with regards to process constraints when concerning traveling speed and incident angle. The algorithm was implemented in MATLAB with the simulation software V-rep functioning as a collision detection library. The implementation was tested on a contour with 40 entry configurations and 32 exit configurations. From the test it was determined that after 2000 iterations 1277/1280 solutions had been found. Several distance heuristics were tested however without conclusive results to their efficiency. The running time of the algorithm was however quite slow due to the communication overhead between MATLAB and V-rep.

[1] Notice that the beam diameter in focus is considered the IPR of IPU [53]

- *Investigate and develop algorithms for path sequencing for work pieces that requires multiple cuts, which takes the robot redundancy into account*

  A task sequencing framework was presented in [126]. It worked in five steps out of which the first two concerned the task of generating contours and process related data. In the third step a set of optimal entry / exit points were generated by converting it to a generalized traveling salesman problem GTSP. In step four these optimal entry / exit points were used and several robot configurations were sampled by using the sample vector defined in [127] for each of these points. By using the path planning algorithm presented in [127] a set of pose connecting maps were found. In step 5 the pose connecting maps for all contours on a work piece were converted into another GTSP problem. The solution to this problem gives a path between all contours that optimizes the reconfiguration time. It has been chosen to utilize the GTSP solver GLKH as it is based on one of the most efficient GTSP solvers available [46]. It is however not capable of handling other constraints such as precedence constraints. This has entailed that it has been chosen to create an interface to the GTSP solver based on the TSPLIB [100] file format which entails that if a better solver is found GLKH can easily be replaced.

## 6.2 Conclusion

In the preliminary analysis of this dissertation, in section 2, it was discussed that the processing time optimization of parts should optimize both the cutting process itself and the motions of the mechanical positioning system. In this dissertation, ways of optimizing both of these aspects have been presented. When considering the task of optimizing the cutting process, this dissertation has shown that it is possible to change the characteristics of the remote cutting process (remote fusion cutting) by customizing the shape of the intensity profile of the laser beam. By changing the shape of the beam it is possible to achieve better stability with 20% of the average power needed for remote fusion cutting. The drawback is however, that the current beam design only performs at a slower cutting speed [128]. As stability data for remote fusion cutting, conducted on similar equipment, was not present in the scientific literature, a parameter study was performed [125]. This study was used as a benchmark, with which cutting with customized beam patterns could be evaluated. To be capable of conducting remote laser cutting, with customized beam patterns, a laser processing laboratory was developed and commissioned as a part of the work conducted during the course of this dissertation. To prove the flexibility of the laboratory a control algorithm was implemented based on iterative learning control (ILC). This algorithm was capable of optimizing the performance

of the XY table used for 2D cutting by as much as 50 %. When considering the task of planning the motions of the mechanical positioning system, this dissertation has presented a framework for remote laser task scheduling based on sampling in redundancy space [126, 127]. A sampling vector has been developed which is capable of taking process constraints into account while the laser traverse a contour. By using the probabilistic roadmaps algorithm the mechanical systems ability to reconfigure itself while cutting was investigated. By utilizing this information the task sequencing problem was transformed into a generalized traveling salesman problem which was solved by the open source GTSP solver GLKH [46].

## 6.3 Further work and predictions of future research activities

Based on the described findings in section 6.1 some clear directions for future research can be seen within all three areas of focus.

**Developing test facilities for the ROBOCUT technology**

As discussed in 6.1 the developed testing facilities are working and much research has already been produced. It has however been impossible to evaluate the developed scheduling algorithms based on hardware due to the absence of a scanner cutting head. Future research will help with benchmarking the obtained results against other state-of-the-art technologies. Currently the laser processing group has received funding for such a head, which will be acquired in the spring 2016. Furthermore the process of developing DOEs is a time consuming process, however, spatial light modulating microchips does exist with the possibility of programming DOE's with a frame rate of as much as 60 Hz [37]. Even though their damage threshold is low and even though they are not meant for materials processing preliminary experiments have shown promising results. This entails that such light modulating chips could be developed to become one of the key elements to achieving a faster transition from DOE design to actual DOE evaluation.

**Obtain process knowledge and evaluate ROBOCUT potential**

With regards to obtaining process knowledge and evaluating the effectiveness of produced DOEs it should be considered if it is possible to utilize the power of the programmable DOE as described in the previous section, and the developed automatic measurement system. If these two sub systems are included in the laser processing cell it suddenly becomes possible to conduct automatic evaluation of automatically generated beam patterns. This again entails that the

development of DOEs can be enforced directly based on the obtained results of previous DOEs. If an appropriate parametrization of the DOE pattern can be constructed it will even be possible to use machine learning for optimizing the obtained cuts. Furthermore it should be noted that the implemented automatic stability assessment algorithm can be improved in numerous fashions. First of all it can, with only small changes to the current implementation, be used to generate a width profile of the cut over the entire cutting kerf. This width profile can then be used to generate derived parameters such as kerf width variance which might give further insight into phenomena such as turbulence or melt oscillations. Such parameters could be included in the optimization loop to ensure that the algorithm would converge towards a good beam design.

**Task sequencing**

When considering the task sequencing algorithms proposed in this dissertation it is clear that one of the drawbacks with the implementation is the performance of the path planning algorithm. As the implementation has been conducted as a proof of concept it has not been optimized for speed. By implementing it in a compiled programming language such as C++ and by moving from collision detection via V-rep to a proper library it is expected that a great speed increase will be seen. As discussed in the previous sections it has been chosen to base the sequencing algorithm on the GTSP solver GLKH. It is however incapable of handling sequencing constraints such as precedence constraints which can be of great importance for laser cutting applications. The GTSP community should be searched for GTSP solvers which considers precedence constraints.

# Appendices

# Appendix I

# KUKA kr120

The robot purchased for the laser processing laboratory was a KR 120 R2500 pro (KR QUANTEC pro) from KUKA roboter gmbh. It has a reach of approximately 2500 mm and a rated payload of 120 kg. It has 6 axes and is manufactured for various industrial applications. The robot can be seen from Fig. I.1(a). From the official website [33] it is recommended for 30 different

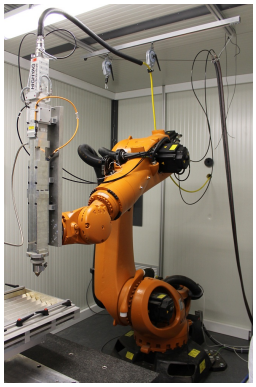

(a) Shows a photo of the laser cutting cell with the KUKA kr120 R2500 pro at Aalborg university. [1]

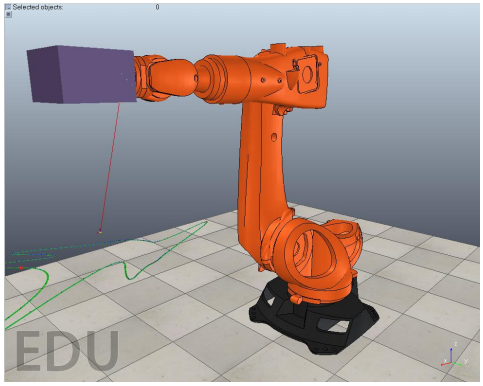


(b) A figure showing the provided 3d model implemented in the simulation software V-rep [21] with a scanner head

**Fig. I.1:** .

applications including laser cutting, laser welding, waterjet cutting, arc welding and machining. It is, with its high accuracy counterpart KUKA KR 120 R2700 extra HA, a common choice in materials processing research [68–70] Kuka has provided a CAD model of the robot online which can be used for evaluating various scenarios. Fig. I.1(b) shows a simulation in V-rep [21] of

the robot mounted with the remote cutting head described in section 3 and II . As it is an industrial robot it is quite difficult to obtain all data necessary for proper simulations as this is considered to be the intellectual property of KUKA. In [33] an image of the robot with joint limitations and link lengths can be found. This is repeated in Fig. I.2. By analysing this and using additional

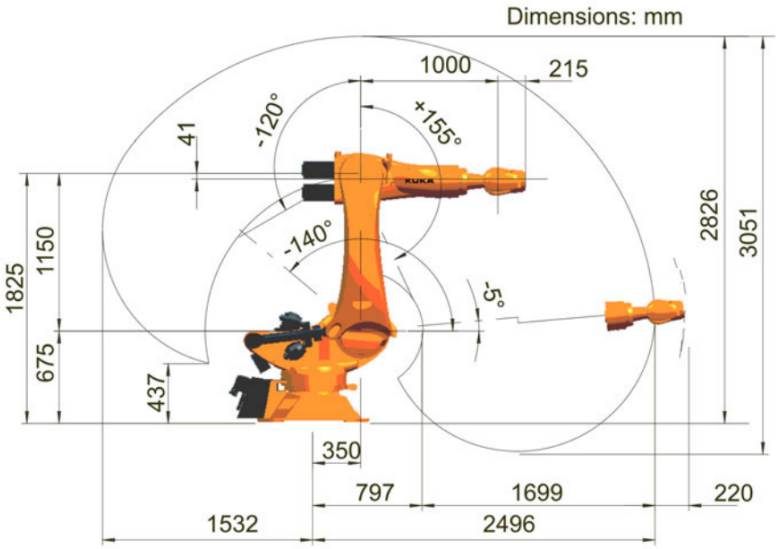


**Fig. I.2:** Shows the KUKA robot with joint limits and link lengths [33]

data from the CAD model it is possible to derive the Denavit–Hartenberg parameters for the robot. These are found to be: It should here be noted that

| Link | $\theta$ | d | a | $\alpha$ |
|---|---|---|---|---|
| 1 | $\theta_1$ | 675 | 0.350 | $\pi/2$ |
| 2 | $\theta_2$ | 0.2 | 1.150 | $\pi$ |
| 3 | $\theta_3$ | 0.2 | -0.041 | $-\pi/2$ |
| 4 | $\theta_4$ | 1.0 | 0 | $\pi/2$ |
| 5 | $\theta_5$ | 0.0 | 0 | $-\pi/2$ |
| 6 | $\theta_6$ | 0.0 | 0 | 0 |

**Table I.1:** A table showing the Denavit–Hartenberg parameters of the Kuka robot

this representation does not include the 215 mm from the spherical wrist to the end effector as the current implementation of the inverse kinematics in the MATLAB robotics toolbox contains several software bugs [17]. Instead this was included as a tool offset in the serial link representation created. The joint limits shown in Fig. I.2 and their maximum angular velocities are summarised

in table I.2. The robot has a pose repeatability (ISO 9283) ±0.06 mm. In

| Axis | Range of motion | Speed with rated payload |
|---|---|---|
| 1 | ±185° | 136°/s |
| 2 | −5° to −140° | 130°/s |
| 3 | +155° to −120° | 120°/s |
| 4 | ±350° | 292°/s |
| 5 | ±125° | 258°/s |
| 6 | ±350° | 284°/s |

**Table I.2:** A table showing the maximum and minimum angles of the robot joints

contrast the high accuracy counterpart which has a repeatability of ±0.05 mm.

# Appendix II

# Derivation of mirror kinematics

In the following section the position of the laser beam focal point will be calculated as a function of the joint parameters of the actuators controlling the deflective optics in the cutting head. As described in section 3 the scanner cutting head has not been constructed which entails that the derivation will be based on designs considered in the ROBOCUT project. A conceptual overview of a cutting head can be seen from figure II.1. From this figure it is seen that the cutting head contains three degrees of freedom, two mirrors for deflection and one linear actuator for focus adjustment. To conduct the kinematic analysis coordinate frames have been attached to the various pieces optics. It is however necessary to keep in mind that the optical path cannot be seen as a serial link manipulator as the link lengths change depending on the deflection angle. Instead, the derivation of the kinematics will be based on optical ray tracing. It is assumed that the mirrors are plane and has 0 % transmission and absorption. This entails that only reflection will be taken into account. The law of reflection states that the angle between the plane normal and the incident beam equals the angle between the plane normal and the reflected beam [111]

$$\phi_{In} = \phi_{Re} \tag{II.1}$$

If the plane normal vector is denoted $\mathbf{n}$ and the incident beam vector is denoted $\mathbf{i}$ then the reflected beam vector $\mathbf{r}$ can be expressed as: [4]:

$$\mathbf{r} = \mathbf{i} - 2 \cdot (\mathbf{i} \cdot \mathbf{n}) \cdot \mathbf{n} \tag{II.2}$$

As all mirrors are assumed to be plane, the intersection point $P_i$ between the beam and the mirror plane can be derived by the following equation (rewritten from [23]).

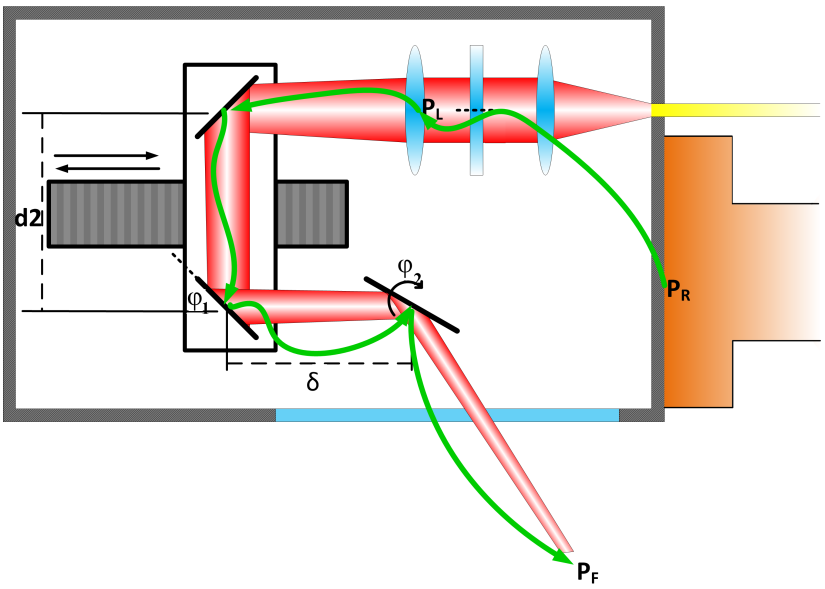


**Fig. II.1:** Shows a conceptual drawing of the modeled scanner cutting head. Notice that it contains three degrees of freedom.

$$P_i = \frac{(p_0 - \mathbf{i}_0) \cdot \mathbf{n}}{\mathbf{i} \cdot \mathbf{n}} \mathbf{i} + \mathbf{i}_0 \tag{II.3}$$

where $p_0$ is a point on the plane, $i_0$ is the origin of the incident beam vector which equals the last mirror reflection point, $\mathbf{n}$ is the normal vector of the plane and $l$ is the equation of the beam vector. By using these equations deriving the governing kinematic equations can be done in an iterative process which includes a series of steps.

1. Select a reference frame e.g. the middle point of the focus lens.
2. Derive expressions for the normal vectors of all mirrors.
3. Calculate all reflection vectors by using equation II.2
4. Iteratively calculate all intersection points by using equation II.3

By following this procedure the final reflection point $P_R$ can be found. From this point the beam extends from the cutting head and down towards the workpiece. The direction of the beam is found by the final reflection vector $\mathbf{r}$. In 5.2.2 it was defined that the Z axis should be pointing towards the cutting head of the robot in the beam direction. This entails that the resulting

beam vector **r** should be treated as the the negative Z axis of the coordinate transformation.

$$Z = -\mathbf{r} \tag{II.4}$$

However, if a coordinate frame should be attached to the beam it is necessary to add some additional steps as the X and Y axis cannot directly be specified. In the following it has been chosen to limit the X axis to be parallel to the XZ plane of the focus lens. This entails that the Y axis can be found by a cross product between any vector in this plane e.g. $[1\ 0\ 0]^T$ and the Z axis. Then the X axis can be found to be perpendicular to the resulting Y and Z axes. It should however be noted that a normalization is required of the resulting vectors as the resulting length is dependent on the angle between the vectors as described by equation II.5.

$$|a \times b| = |a||b|sin(\theta) \tag{II.5}$$

This can also be represented by a series of steps:

5. Select vector V in XZ plane e.g. $[1\ 0\ 0]^T$
6. Calculate New Y vector as $Z \times V$
7. Calculate New X as $Y \times Z$
8. Create transformation matrix $T = \begin{bmatrix} X & Y & Z & P_R \\ 0 & 0 & 0 & 1 \end{bmatrix}$

By following this procedure a transformation matrix can be found. It will however not describe the position of the beam waist of the laser beam as it is dependent on the focal length of the chosen optics. Instead it describes the coordinate frame of the intersection point of the last mirror of the cutting head. Normally a transformation to the focus position is necessary instead. To achieve this the achieved coordinate frame should be translated by $d_f$ in the direction of the negative Z axis. This quantity $d_f$ is equal to the focal length

$$d_{foc}$$

of the focusing lens minus the distance the beam has already traveled inside the cutting head $d_c$.

$$d_f = d_{foc} - d_c \tag{II.6}$$

This can be added as a final step to the step by step procedure described above.

9. Calculate $d_f$
10. Translate T by $d_f$ in the negative Z direction;

As several types of cutting heads are evaluated the following section will be divided in three sections describing each of these designs, The first section describes the derivation of the design described in [124]. The remaining two concerns the derivation of the kinematics based on some more standard designs. All cutting heads will have two rotating mirrors that can move the beam in a plane under the cutting head, and a focus adjustment. The mirror frames will be denoted $M_s$ where s is the mirrors place in the optical path (the first mirror that is struck by the beam is $M_1$). The joint variables for the rotating mirrors are denoted $\phi_k$ where k is the mirrors place in the sequence of rotating mirrors in the optical path. Finally, the joint variable describing the focus offset is denoted $\delta$. The derived expressions are quite cumbersome due to the many dot and cross products. They can however be extensively simplified by using the double angle formula:

$$c(2\theta) = c^2\theta - s^2\theta = 2c^2\theta - 1 = 1 - 2s^2\theta \tag{II.7}$$

To keep the derived expressions as short as possible, it has been chosen to abbreviate the trigonometric functions sine and cosine to 's' and c respectively. Furthermore, standard rotational matrices around the x, y and z axis will be denoted $rotx(\theta)$,$roty(\theta)$ and $rotz(\theta)$ respectively as by [17].

## II.1 Case 1: Inline mirors

The first design to be analyzed is the design used for evaluating the cutting accuracy in [124]. The design is schematically shown in Fig. II.2.
It is clear that in the above schematic there are three mirrors. If these three

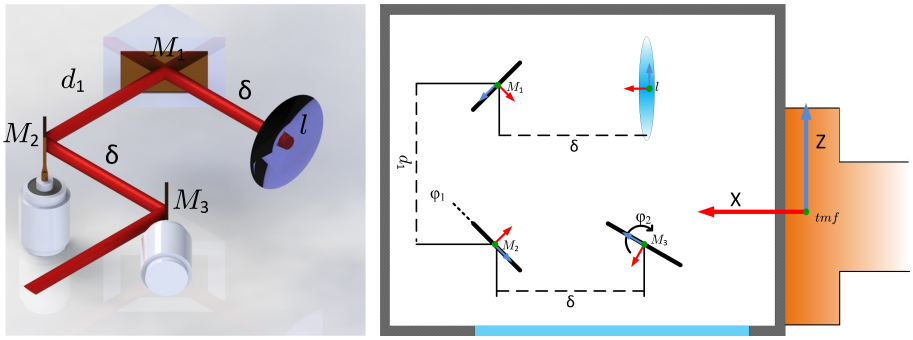


(a) Shows a cad drawing of the conceptual cutting head shown in II.2(b).

(b) Shows a diagram of the first cutting head concept

**Fig. II.2:** Shows a simplified cad model and a diagram of the first cutting head concept. Notice the frame assignment in the cutting head on figure II.2(b)

mirrors are denoted $M_1$-$M_3$ then coordinate frames can be attached to each of then in such a way that their normal vectors $\mathbf{n}_1$-$\mathbf{n}_3$ points in the coordinate frame x direction. The transformations between the lens frame and the unrotated mirror frames can be expressed as:

$$ {}^{l}R_{M_1 s} = roty(\frac{3}{4}\pi) = \begin{bmatrix} -\frac{1}{\sqrt{2}} & 0 & \frac{1}{\sqrt{2}} \\ 0 & 1 & 0 \\ -\frac{1}{\sqrt{2}} & 0 & -\frac{1}{\sqrt{2}} \end{bmatrix} \tag{II.8} $$

$$ {}^{l}R_{M_2 s} = roty(\frac{-3}{4}\pi) = \begin{bmatrix} -\frac{1}{\sqrt{2}} & 0 & -\frac{1}{\sqrt{2}} \\ 0 & 1 & 0 \\ \frac{1}{\sqrt{2}} & 0 & -\frac{1}{\sqrt{2}} \end{bmatrix} \tag{II.9} $$

$$ {}^{l}R_{M_3 s} = roty(\frac{1}{4}\pi) = \begin{bmatrix} \frac{1}{\sqrt{2}} & 0 & \frac{1}{\sqrt{2}} \\ 0 & 1 & 0 \\ -\frac{1}{\sqrt{2}} & 0 & \frac{1}{\sqrt{2}} \end{bmatrix} \tag{II.10} $$

$$ \tag{II.11} $$

The transformation between the static transformations from II.11 and the mirror frames can be expressed as:

$$ {}^{l}R_{M_1} = {}^{l}R_{M_1 s} = \begin{bmatrix} -\frac{1}{\sqrt{2}} & 0 & \frac{1}{\sqrt{2}} \\ 0 & 1 & 0 \\ -\frac{1}{\sqrt{2}} & 0 & -\frac{1}{\sqrt{2}} \end{bmatrix} \tag{II.12} $$

$$ {}^{l}R_{M_2} = {}^{l}R_{M_2 s} \cdot rotz(\phi_1) = \begin{bmatrix} -\frac{1}{\sqrt{2}}c(\phi_1) & -\frac{1}{\sqrt{2}}s(\phi_1) & -\frac{1}{\sqrt{2}} \\ -s(\phi_1) & c(\phi_1) & 0 \\ \frac{1}{\sqrt{2}}c(\phi_1) & \frac{1}{\sqrt{2}}s(\phi_1) & -\frac{1}{\sqrt{2}} \end{bmatrix} \tag{II.13} $$

$$ {}^{l}R_{M_3} = {}^{l}R_{M_3 s} \cdot roty(\phi_2) = \begin{bmatrix} \frac{1}{\sqrt{2}}(c(\phi_2) + s(\phi_2)) & 0 & \frac{1}{\sqrt{2}}(-s(\phi_2) + c(\phi_2)) \\ 0 & 1 & 0 \\ -\frac{1}{\sqrt{2}}(-s(\phi_2) + c(\phi_2)) & 0 & \frac{1}{\sqrt{2}}(c(\phi_2) + s(\phi_2)) \end{bmatrix} \tag{II.14} $$

As the normal vectors of the mirrors are defined as the x axis of these frames, they can by extracting the first row:

$$ {}^{l}\mathbf{n}_1 = \begin{bmatrix} -\frac{1}{\sqrt{2}} \\ 0 \\ -\frac{1}{\sqrt{2}} \end{bmatrix} \tag{II.15} $$

$$ {}^{l}\mathbf{n}_2 = \begin{bmatrix} -\frac{1}{\sqrt{2}}c(\phi_1) \\ -s(\phi_1) \\ \frac{1}{\sqrt{2}}c(\phi_1) \end{bmatrix} \tag{II.16} $$

$$ {}^{l}\mathbf{n}_3 = \begin{bmatrix} \frac{1}{\sqrt{2}}(c(\phi_2)+s(\phi_2)) \\ 0 \\ -\frac{1}{\sqrt{2}}(-s(\phi_2)+c(\phi_2)) \end{bmatrix} \tag{II.17} $$

$$ \tag{II.18} $$

Then combining II.2 with II.14 the resulting reflection vector can be found.

$$ {}^{l}\mathbf{r}_1 = \begin{bmatrix} 0 \\ 0 \\ -1 \end{bmatrix} \tag{II.19} $$

$$ {}^{l}\mathbf{r}_2 = \begin{bmatrix} -1/2 - 1/2\,c\left(2\,\phi_1\right) \\ -1/2\,\sqrt{2}s\left(2\,\phi_1\right) \\ -1/2 + 1/2\,c\left(2\,\phi_1\right) \end{bmatrix} \tag{II.20} $$

$$ {}^{l}\mathbf{r}_3 = \begin{bmatrix} -1/2\,c\left(2\,\phi_2\right) + 1/2\,c\left(2\,\phi_1\right)s\left(2\,\phi_2\right) + 1/2\,s\left(2\,\phi_2\right) + 1/2\,c\left(2\,\phi_1\right)c\left(2\,\phi_2\right) \\ -1/2\,\sqrt{2}s\left(2\,\phi_1\right) \\ -1/2\,s\left(2\,\phi_2\right) - 1/2\,c\left(2\,\phi_2\right) + 1/2\,c\left(2\,\phi_1\right)s\left(2\,\phi_2\right) - 1/2\,c\left(2\,\phi_1\right)c\left(2\,\phi_2\right) \end{bmatrix} \tag{II.21} $$

This final reflective vector ${}^{l}\mathbf{r}_3$ points in the direction of the laser beam in the coordinate system specified by the focus lens coordinate frame l. Now it is just a matter of assigning the other axes as well. To create a coordinate frame it is however necessary that all axes are perpendicular. To ensure this, the X axis of frame l is used to define the direction of the Y axis by taking the cross product of ${}^{l}\mathbf{r}_3$ with [1;0;0] the new Y axis is found

$$ NewY = {}^{l}\,\mathbf{r}_3 \times Y \tag{II.22} $$

$$ = \begin{bmatrix} 0 \\ 1/2\,s\left(2\,\phi_2\right) + 1/2\,c\left(2\,\phi_2\right) - 1/2\,c\left(2\,\phi_1\right)s\left(2\,\phi_2\right) + 1/2\,c\left(2\,\phi_1\right)c\left(2\,\phi_2\right) \\ -1/2\,\sqrt{2}s\left(2\,\phi_1\right) \end{bmatrix} \tag{II.23} $$

And then finally, by taking the cross product of NewY with ${}^{l}\mathbf{r}_3$ the new X axis is found;

$$ NewX = \begin{bmatrix} 5/8 + 1/2\,c\left(2\,\phi_1\right)c\left(4\,\phi_2\right) - 1/8\,c\left(4\,\phi_1\right)s\left(4\,\phi_2\right) - 1/8\,c\left(4\,\phi_1\right) + 1/8\,s\left(4\,\phi_2\right) \\ 1/4\,\sqrt{2}s\left(2\,\phi_1\right)s\left(2\,\phi_2\right) + 1/8\,s\left(2\,\phi_2\right)\sqrt{2}s\left(4\,\phi_1\right) + 1/8\,\sqrt{2}c\left(2\,\phi_2\right)s\left(4\,\phi_1\right) - 1/4\,\sqrt{2}s\left(2\,\phi_1\right)c\left(2\,\phi_2\right) \\ -1/8\,c\left(4\,\phi_2\right) + 1/8\,c\left(4\,\phi_1\right)c\left(4\,\phi_2\right) + 1/2\,c\left(2\,\phi_1\right)s\left(4\,\phi_2\right) \end{bmatrix} \tag{II.24} $$

The final element that needs to be found is the intersection point of the beam on the last mirror. As all other intersection points are known beforehand it is only necessary to use equation II.3 once. this yields:

$$P_R = \begin{bmatrix} -D(c(\phi_1))^2 + \delta \\ -D\sqrt{2}c(\phi_1)s(\phi_1) \\ -D(s(\phi_1))^2 - d_1 \end{bmatrix} \tag{II.25}$$

where

$$D = \frac{\delta\left(c\left(\phi_2\right) + s\left(\phi_2\right)\right)}{c\left(\phi_2\right)c\left(2\,\phi_1\right) + s\left(\phi_2\right)} \tag{II.26}$$

Due to the complexity of the above equation it has been chosen not to display the final transformation as it is simply a matter of insertion into the matrix described in item 8 in the enumeration presented in section II.

$$T = \begin{bmatrix} NewX & NewY & NewZ & P_R \\ 0 & 0 & 0 & 1 \end{bmatrix} \tag{II.27}$$

Finally, the focus frame can be calculated by finding $d_f$. From the diagram seen in figure II.2 it can be seen that the distance travelled inside the cutting head

$$d_c = \delta + d_1 + \frac{\delta\left(c\left(\phi_2\right) + s\left(\phi_2\right)\right)}{c\left(\phi_2\right)c\left(2\,\phi_1\right) + s\left(\phi_2\right)} \tag{II.28}$$

From this it can be seen that the focus adjustment variable $\delta$ is included in the expression twice. Once by its own and once multiplied by a set of trigonometric functions. This is due to the beam path which includes a static mirror, this gives a gearing of the focus adjustment by a factor of 2 compared to other designs, such as the one described in II.3.

## II.2 Case 2: Mirror 3 offset

The second scenario is, as scenario 1, composed of three mirrors, but this time in another configuration than before. Here the two rotating mirrors rotate around axes perpendicular to each other. A schematic description of this setup can be seen from Fig. II.3(a).
If these three mirrors are denoted $M_1$-$M_3$ then coordinate frames can be attached to each of them in such a way that their normal vectors $\mathbf{n}_1$-$\mathbf{n}_3$ points in the coordinate frame x direction. The static rotational relationship between

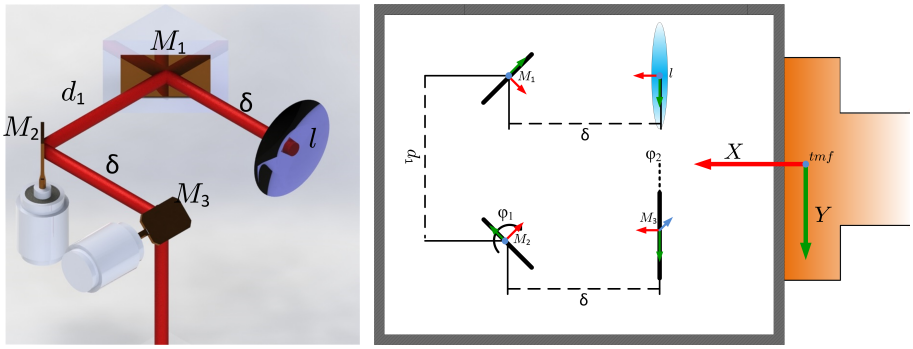


(a) Shows a cad drawing of the conceptual cutting head shown in II.3(b).

(b) Shows a diagram of the first cutting head concept

**Fig. II.3:** Shows a simplified cad model and a diagram of the second cutting head concept. Notice the frame assignment in the cutting head on figure II.3(b)

these normal vectors and the focus lens coordinate frame can be expressed as:

$$ {}^{l}R_{M_1 s} = rotz(\frac{3}{4}\pi) = \begin{bmatrix} -\frac{1}{\sqrt{2}} & -\frac{1}{\sqrt{2}} & 0 \\ \frac{1}{\sqrt{2}} & -\frac{1}{\sqrt{2}} & 0 \\ 0 & 0 & 1 \end{bmatrix} \tag{II.29} $$

$$ {}^{l}R_{M_2 s} = rotz(\frac{-3}{4}\pi) = \begin{bmatrix} -\frac{1}{\sqrt{2}} & \frac{1}{\sqrt{2}} & 0 \\ -\frac{1}{\sqrt{2}} & -\frac{1}{\sqrt{2}} & 0 \\ 0 & 0 & 1 \end{bmatrix} \tag{II.30} $$

$$ {}^{l}R_{M_3 s} = roty(\frac{1}{4}\pi) = \begin{bmatrix} \frac{1}{\sqrt{2}} & 0 & \frac{1}{\sqrt{2}} \\ 0 & 1 & 0 \\ -\frac{1}{\sqrt{2}} & 0 & \frac{1}{\sqrt{2}} \end{bmatrix} \tag{II.31} $$

$$ \tag{II.32} $$

The transformation between the static transformations from II.32 and the rotated mirror coordinate frames can be expressed as:

$$ {}^{l}R_{M_1} = {}^{l}R_{M_1 s} = \begin{bmatrix} -\frac{1}{\sqrt{2}} & -\frac{1}{\sqrt{2}} & 0 \\ \frac{1}{\sqrt{2}} & -\frac{1}{\sqrt{2}} & 0 \\ 0 & 0 & 1 \end{bmatrix} \tag{II.33} $$

$$ {}^{l}R_{M_2} = {}^{l}R_{M_2 s} \cdot rotz(\phi_1) = \begin{bmatrix} -\frac{1}{\sqrt{2}}c(\phi_1) - \frac{1}{\sqrt{2}}s(\phi_1) & -\frac{1}{\sqrt{2}}s(\phi_1) + \frac{1}{\sqrt{2}}c(\phi_1) & 0 \\ -\frac{1}{\sqrt{2}}c(\phi_1) + \frac{1}{\sqrt{2}}s(\phi_1) & -\frac{1}{\sqrt{2}}c(\phi_1) - \frac{1}{\sqrt{2}}s(\phi_1) & 0 \\ 0 & 0 & 1 \end{bmatrix} \tag{II.34} $$

$$ {}^{l}R_{M_3} = {}^{l}R_{M_3 s} \cdot roty(\phi_2) = \begin{bmatrix} \frac{1}{\sqrt{2}}c(\phi_2) + \frac{1}{\sqrt{2}}s(\phi_2) & 0 & -\frac{1}{\sqrt{2}}s(\phi_2) + \frac{1}{\sqrt{2}}c(\phi_2) \\ 0 & 1 & 0 \\ -\frac{1}{\sqrt{2}}c(\phi_2) + \frac{1}{\sqrt{2}}s(\phi_2) & 0 & \frac{1}{\sqrt{2}}c(\phi_2) + \frac{1}{\sqrt{2}}s(\phi_2) \end{bmatrix} \tag{II.35} $$

This entails that the normal vectors can be found as being the first row of these rotational matrices:

$$ {}^{l}\mathbf{n}_1 = \begin{bmatrix} -\frac{1}{\sqrt{2}} \\ \frac{1}{\sqrt{2}} \\ 0 \end{bmatrix} \tag{II.36} $$

$$ {}^{l}\mathbf{n}_2 = \begin{bmatrix} -\frac{1}{\sqrt{2}}c(\phi_1) - \frac{1}{\sqrt{2}}s(\phi_1) \\ -\frac{1}{\sqrt{2}}c(\phi_1) + \frac{1}{\sqrt{2}}s(\phi_1) \\ 0 \end{bmatrix} \tag{II.37} $$

$$ {}^{l}\mathbf{n}_3 = \begin{bmatrix} \frac{1}{\sqrt{2}}c(\phi_2) + \frac{1}{\sqrt{2}}s(\phi_2) \\ 0 \\ -\frac{1}{\sqrt{2}}c(\phi_2) + \frac{1}{\sqrt{2}}s(\phi_2) \end{bmatrix} \tag{II.38} $$

$$ \tag{II.39} $$

Then combining II.2 with II.14 the resulting normal vector can be found.

$$ {}^{l}\mathbf{r}_1 = \begin{bmatrix} 0 \\ 1 \\ 0 \end{bmatrix} \tag{II.40} $$

$$ {}^{l}\mathbf{r}_2 = \begin{bmatrix} -c\,(2\,\phi_1) \\ s\,(2\,\phi_1) \\ 0 \end{bmatrix} \tag{II.41} $$

$$ {}^{l}\mathbf{r}_3 = \begin{bmatrix} c\,(2\,\phi_1)\,s\,(2\,\phi_2) \\ s\,(2\,\phi_1) \\ -c\,(2\,\phi_1)\,c\,(2\,\phi_2) \end{bmatrix} \tag{II.42} $$

This final reflective vector ${}^{l}\mathbf{r}_3$ points in the direction of the laser beam in the coordinate system specified by the focus lens coordinate frame l. Now it is just a matter of assigning the other axes as well. To create a coordinate frame it is however necessary that all axes are perpendicular. To ensure this, the X axis of frame l is used to define the direction of the Y axis. By taking the cross product of ${}^{l}\mathbf{r}_3$ with [1;0;0] the new Y axis is found.

$$ NewY =^{l} \mathbf{r}_3 \times Y = \begin{bmatrix} 0 \\ c\,(2\,\phi_1)\,c\,(2\,\phi_2) \\ s\,(2\,\phi_1) \end{bmatrix} \tag{II.43} $$

And then finally, by taking the cross product of NewY with ${}^{l}\mathbf{r}_3$ the new X axis is found;

$$ NewX =^{l} \mathbf{r}_3 \times NewY = \begin{bmatrix} -\left(c\,(2\,\phi_1)\right)^2 \left(s\,(2\,\phi_2)\right)^2 + 1 \\ -1/2\,s\,(4\,\phi_1)\,s\,(2\,\phi_2) \\ 1/2\,\left(c\,(2\,\phi_1)\right)^2 s\,(4\,\phi_2) \end{bmatrix} \tag{II.44} $$

This again entails that all axes in the new coordinate frame have been defined. Now the intersection point in the final mirror is calculated by using equation II.3.

$$ D = \frac{\delta}{c\,(2\,\phi_1)} \tag{II.45} $$

$$ P_R = \begin{bmatrix} 0 \\ \frac{\delta s(2\,\phi_1)}{c(2\,\phi_1)} + d_1 \\ 0 \end{bmatrix} \tag{II.46} $$

This again entails that the final transformation can be calculated as:

$$T = \begin{bmatrix} -\left(c\left(2\,\phi_1\right)\right)^2\left(s\left(2\,\phi_2\right)\right)^2+1 & 0 & -c\left(2\,\phi_1\right)s\left(2\,\phi_2\right) & 0 \\ -1/2\,s\left(4\,\phi_1\right)s\left(2\,\phi_2\right) & c\left(2\,\phi_1\right)c\left(2\,\phi_2\right) & -s\left(2\,\phi_1\right) & \frac{\delta s(2\,\phi_1)}{c(2\,\phi_1)}+d_1 \\ 1/2\,\left(c\left(2\,\phi_1\right)\right)^2 s\left(4\,\phi_2\right) & s\left(2\,\phi_1\right) & c\left(2\,\phi_1\right)c\left(2\,\phi_2\right) & 0 \\ 0 & 0 & 0 & 1 \end{bmatrix} \tag{II.47}$$

Finally, the focus frame can be calculated by finding $d_f$. From the diagram seen in figure II.3(a) it can be seen that the distance traveled inside the cutting head is equal to

$$d_c = \delta + d_1 + \frac{\delta}{c\left(2\,\phi_1\right)} \tag{II.48}$$

From this equation it can be seen that the focus adjustment variable delta is again included in the expression twice. The derived expressions are however also simpler due to the smaller coupling between the mirrors.

## II.3 Case 3: Mirror 3 offset focus Lens adjustment

In the third scenario the static 45° mirror has been removed from the second scenario. Now the focus adjustment is conducted by moving the focusing lens by a linear actuator. This removes the gearing from scenario 1 and 2 but as it contains one less mirror it is cheaper, it requires less maintenance and the resulting equations are shorter due to one less reflection.
It is clear that in the above schematic there are two mirrors. If these mirrors are denoted $M_1$-$M_2$ then coordinate frames can be attached to each of then in such a way that their normal vectors $\mathbf{n}_1$-$\mathbf{n}_2$ points in the coordinate frame x direction. The rotational static relationship between these normal vectors and the focus lens coordinate frame can be expressed as:

$${}^{l}R_{M_1 s} = rotz(\frac{3}{4}\pi) = \begin{bmatrix} -\frac{1}{\sqrt{2}} & -\frac{1}{\sqrt{2}} & 0 \\ \frac{1}{\sqrt{2}} & -\frac{1}{\sqrt{2}} & 0 \\ 0 & 0 & 1 \end{bmatrix} \tag{II.49}$$

$${}^{l}R_{M_2 s} = rotz(-\frac{1}{2}\cdot\pi)\cdot roty(\frac{1}{4}\cdot\pi) = \begin{bmatrix} 0 & 1 & 0 \\ -\frac{1}{\sqrt{2}} & 0 & -\frac{1}{\sqrt{2}} \\ -\frac{1}{\sqrt{2}} & 0 & \frac{1}{\sqrt{2}} \end{bmatrix} \tag{II.50}$$

The transformation between the static transformations from II.50 and the rotated mirror coordinate frames can be expressed as:

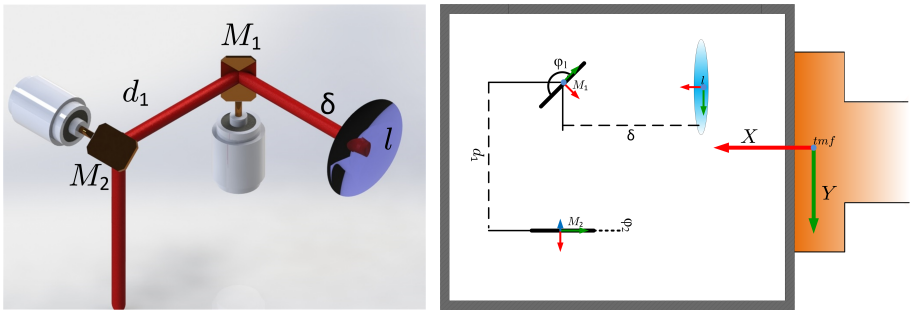


(a) Shows a cad drawing of the conceptual cutting head shown in II.4(b).

(b) Shows a diagram of the third cutting head concept

**Fig. II.4:** Shows a simplified cad model and a diagram of the third cutting head concept. Notice the frame assignment in the cutting head on figure II.4(b)

$$ {}^{l}R_{M_1} = {}^{l}R_{M_1 s} \cdot rotz(\phi_1) = \begin{bmatrix} -\frac{1}{\sqrt{2}}c(\phi_1) + \frac{1}{\sqrt{2}}s(\phi_1) & -\frac{1}{\sqrt{2}}c(\phi_1) - \frac{1}{\sqrt{2}}s(\phi_1) & 0 \\ \frac{1}{\sqrt{2}}c(\phi_1) + \frac{1}{\sqrt{2}}s(\phi_1) & -\frac{1}{\sqrt{2}}c(\phi_1) + \frac{1}{\sqrt{2}}s(\phi_1) & 0 \\ 0 & 0 & 1 \end{bmatrix} \tag{II.51} $$

$$ {}^{l}R_{M_2} = {}^{l}R_{M_2 s} \cdot roty(\phi_2) = \begin{bmatrix} 0 & 1 & 0 \\ -\frac{1}{\sqrt{2}}c(\phi_2) - \frac{1}{\sqrt{2}}s(\phi_2) & 0 & -\frac{1}{\sqrt{2}}c(\phi_2) + \frac{1}{\sqrt{2}}s(\phi_2) \\ -\frac{1}{\sqrt{2}}c(\phi_2) + \frac{1}{\sqrt{2}}s(\phi_2) & 0 & \frac{1}{\sqrt{2}}c(\phi_2) + \frac{1}{\sqrt{2}}s(\phi_2) \end{bmatrix} \tag{II.52} $$

(II.53)

This entails that the normal vectors can be found as being the first row of these rotational matrices:

$$ {}^{l}\mathbf{n}_1 = \begin{bmatrix} -\frac{1}{\sqrt{2}}c(\phi_1) + \frac{1}{\sqrt{2}}s(\phi_1) \\ \frac{1}{\sqrt{2}}c(\phi_1) + \frac{1}{\sqrt{2}}s(\phi_1) \\ 0 \end{bmatrix} \tag{II.54} $$

$$ {}^{l}\mathbf{n}_2 = \begin{bmatrix} 0 \\ -\frac{1}{\sqrt{2}}c(\phi_2) - \frac{1}{\sqrt{2}}s(\phi_2) \\ -\frac{1}{\sqrt{2}}c(\phi_2) + \frac{1}{\sqrt{2}}s(\phi_2) \end{bmatrix} \tag{II.55} $$

Then combining II.2 with II.14 the resulting normal vector can be found.

$$ {}^{l}\mathbf{r}_1 = \begin{bmatrix} s\,(2\,\phi_1) \\ c\,(2\,\phi_1) \\ 0 \end{bmatrix} \tag{II.56} $$

$$ {}^{l}\mathbf{r}_2 = \begin{bmatrix} s\,(2\,\phi_1) \\ -c\,(2\,\phi_1)\,s\,(2\,\phi_2) \\ -c\,(2\,\phi_1)\,c\,(2\,\phi_2) \end{bmatrix} \tag{II.57} $$

$$ \tag{II.58} $$

This final reflective vector ${}^{l}\mathbf{r}_2$ points in the direction of the laser beam in the coordinate system specified by the focus lens coordinate frame l. Now it is just a matter of assigning the other axes as well. To create a coordinate frame it is however necessary that all axes are perpendicular. To ensure this, the X axis of frame l is used to define the direction of the Y axis by taking the cross product of ${}^{l}\mathbf{r}_2$ with [1;0;0] the new Y axis is found

$$ NewY =^{l} \mathbf{r}_2 \times Y = \begin{bmatrix} 0 \\ c\,(2\,\phi_1)\,c\,(2\,\phi_2) \\ -c\,(2\,\phi_1)\,s\,(2\,\phi_2) \end{bmatrix} \tag{II.59} $$

And then finally, by taking the cross product of NewY with ${}^{l}\mathbf{r}_3$ the new X axis is found;

$$ NewX =^{l} \mathbf{r}_2 \times NewY = \begin{bmatrix} (c\,(2\,\phi_1))^2 \\ 1/2\,s\,(4\,\phi_1)\,s\,(2\,\phi_2) \\ 1/2\,c\,(2\,\phi_2)\,s\,(4\,\phi_1) \end{bmatrix} \tag{II.60} $$

This means that the three axes of the final transformation have been found, now only the intersection point should be found before the transformation can be derived. This is again done by using equation II.3. This yields the following intersection distance D and the intersection point:

$$ D = \frac{d_1}{c\,(2\,\phi_1)} \tag{II.61} $$

$$ P_R = \begin{bmatrix} \delta + \frac{d_1 s(2\,\phi_1)}{c(2\,\phi_1)} \\ d_1 \\ 0 \end{bmatrix} \tag{II.62} $$

These can, as described in the previous scenarios, be inserted into a corresponding rotational matrix to yield the complete transformation matrix

$$T = \begin{bmatrix} 1/2\,c\,(4\,\phi_1) + 1/2 & 0 & -s\,(2\,\phi_1) & \delta + \frac{d_1 s(2\,\phi_1)}{c(2\,\phi_1)} \\ 1/2\,s\,(4\,\phi_1)\,s\,(2\,\phi_2) & c\,(2\,\phi_1)\,c\,(2\,\phi_2) & c\,(2\,\phi_1)\,s\,(2\,\phi_2) & d_1 \\ 1/2\,c\,(2\,\phi_2)\,s\,(4\,\phi_1) & -c\,(2\,\phi_1)\,s\,(2\,\phi_2) & c\,(2\,\phi_1)\,c\,(2\,\phi_2) & 0 \\ 0 & 0 & 0 & 1 \end{bmatrix} \tag{II.63}$$

Finally, the focus frame can be calculated by finding $d_f$. From the diagram seen in figure II.2 it can be seen that the distance traveled inside the cutting head

$$d_c = \delta + \frac{d_1}{c\,(2\,\phi_1)} \tag{II.64}$$

It is seen that the expressions are simpler than the ones derived for configuration 1 in section II.1 and in section II.2. It is however also seen that the focus adjustment variable $\delta$ is only included once in the expression which entails that the gearing described in the previous sections have been lost due to the simpler configuration.

# Appendix III

# Work, travel and Z rotation angular decomposition

It has been chosen to use Euler angles as a minimum representation the orientation of the laser beam. Internally the robotics toolbox does however use quaternions and transfer matrices for orientation representation. As described in [125] and in section it 4.2.1 it has been chosen to determine the allowable incident angles for the RFC process based on Work and travel angles. These work and travel angles are then used as a permutation on path points to sample feasible configurations. As the Work and travel angle is defined as the deviation from the plane normal in the cutting direction and perpendicular to the cutting direction it is necessary to define how a transformation can be derived from these two angles. It is clear that this definition does not match with the definition of Euler angles. The permutation is defined as a rotation matrix R which can be defined as a set of three vectors spanning an orthogonal basis:

$$R = \begin{bmatrix} \hat{X_n} & \hat{Y_n} & \hat{Z_n} = \end{bmatrix} = \begin{bmatrix} r_{11} & r_{12} & r_{13} \\ r_{21} & r_{22} & r_{23} \\ r_{31} & r_{32} & r_{33} \end{bmatrix} \tag{III.1}$$

When such a rotation matrix has been designed it is possible to derive an Euler angle representation that can be used in the kinematics. In the following section these three vectors will be defined and expressions for deriving the work and travel angle and z rotation from a given transformation matrix will be given.

## III.1 Defining an orthogonal basis

The orthogonal basis shown in equation III.1 should be derived by the definition of the work and travel angle summarised in the paper [125]. To ease the

readability and reduce the size of the matrices in the following section $c$ and $s$ will be used as a substitution for sine and cosine. From this definition it can be seen that as the work and travel angle is defined as deviations from the plane normal in the cutting direction and perpendicular direction. This again entails that the in fact give the direction of a normal vector that points in the direction of the beam. This beam vector forms the $\hat{Z_n}$ vector from equation III.1. If two vectors are created in the direction of the original X and Y axis these need to be tilted by the Work and travel angle respectively.

$$\hat{X} = \begin{bmatrix} c(\alpha) \\ 0 \\ s(\alpha) \end{bmatrix} \tag{III.2}$$

$$\hat{Y} = \begin{bmatrix} 0 \\ c(\beta) \\ s(\beta) \end{bmatrix} \tag{III.3}$$

$$\tag{III.4}$$

Here it should be noted that these two vectors expand a plane defined by a normal vector that can be found by taking the cross product. This normal vector forms the Z vector of the orthogonal basis that is used in the following.

$$\hat{Z_n} = \hat{X} \times \hat{Y} = \begin{bmatrix} c(\alpha) \\ 0 \\ s(\alpha) \end{bmatrix} \times \begin{bmatrix} 0 \\ c(\beta) \\ s(\beta) \end{bmatrix} = \begin{bmatrix} 0 - s(\alpha)c(\beta) \\ 0 - c(\alpha)s(\beta) \\ c(\alpha)c(\beta) - 0 \end{bmatrix} \tag{III.5}$$

This vector defines 1/3 of the III.1. As $\hat{X}$ and $\hat{Y}$ are not orthogonal due to the tilting of the axes defined in equation III.4 it has been chosen to defined $\hat{X_n}$ $=\hat{X}$ as the other vector and finally defined the $\hat{Y_n}$ as:

$$\hat{Y_n} = \hat{Z_n} \times \hat{X_n} = \begin{bmatrix} -s(\alpha)c(\beta) \\ -c(\alpha)s(\beta) \\ c(\alpha)c(\beta) - 0 \end{bmatrix} \times \begin{bmatrix} c(\alpha) \\ 0 \\ s(\alpha) \end{bmatrix} \tag{III.6}$$

$$= \begin{bmatrix} -s(\alpha)c(\alpha)s(\beta) \\ s(\alpha)s(\alpha)c(\beta) + c(\alpha)c(\alpha)c(\beta) \\ c(\alpha)c(\alpha)s(\beta) - 0 \end{bmatrix} \tag{III.7}$$

$$= \begin{bmatrix} s(\alpha)c(\alpha)s(\beta) \\ c(\beta)(s^2(\alpha) + c^2(\alpha) \\ c^2(\alpha)s(\beta) \end{bmatrix} \tag{III.8}$$

$$= \begin{bmatrix} -s(\alpha)c(\alpha)s(\beta) \\ c(\beta) \\ c^2(\alpha)s(\beta) \end{bmatrix} \tag{III.9}$$

And by inserting these found vectors in III.1 a rotation matrix is found.

$$R_{Ort} = \begin{bmatrix} \hat{X_n} & \hat{Y_n} & \hat{Z_n} \end{bmatrix} = \begin{bmatrix} c(\alpha) & -s(\alpha)c(\alpha)s(\beta) & -s(\alpha)c(\beta) \\ 0 & -c(\beta) & c(\alpha)s(\beta) \\ s(\alpha) & c^2(\alpha)s(\beta) & c(\alpha)c(\beta) \end{bmatrix} \quad \text{(III.10)}$$

This represents a rotation around the work and travel angle, but as a z rotation is needed this is right hand side multiplied to the expression.

$$Rt = R_{Ort} \cdot \begin{bmatrix} c(\xi) & -s(\xi) & 0 \\ s(\xi) & c(\xi) & 0 \\ 0 & 0 & 1 \end{bmatrix} = \quad \text{(III.11)}$$

$$\begin{bmatrix} c(\alpha)c(\xi) - s(\alpha)c(\alpha)s(\beta)s(\xi) & -c(\alpha)s(\xi) - s(\alpha)c(\alpha)s(\beta)c(\xi) & -s(\alpha)c(\beta) \\ c(\beta)s(\xi) & c(\beta)c(\xi) & -c(\alpha)s(\beta) \\ s(\alpha)c(\xi) + (c(\alpha))^2 s(\beta)s(\xi) & -s(\alpha)s(\xi) + (c(\alpha))^2 s(\beta)c(\xi) & c(\alpha)c(\beta) \end{bmatrix} \quad \text{(III.12)}$$

This final expression denotes the rotation matrix derived from the work and travel angle decomposition.

On the other hand, if the work and travel angle needs to be found from a given transformation it is necessary to derive expressions which isolates $\beta$,$\alpha$ and $\xi$ respectively. This can be done by seeing that it is possible to combine pairs of sine and cosine of the angles multiplied by cosine of another angle. This cosine of another angle can be seen as a scale factor that doesn't influence the angle.

$$\alpha = atan2(-r_{13}, r_{33}) = atan2(s(\alpha)c(\beta), c(\alpha)c(\beta)) \quad \text{(III.13)}$$

$$\beta = atan2(-r_{23}, r_{33}) = atan2(c(\alpha)s(\beta), c(\alpha)c(\beta)) \quad \text{(III.14)}$$

$$\xi = atan2(r_{21}, r_{22}) = atan2(c(\beta)s(\xi), c(\beta)c(\xi)) \quad \text{(III.15)}$$

This entails that the three angles can be reformed by using the above formulae. It should however be noted that when the these equations break down when $\beta = \pm 90°$ and $\alpha = \pm 90°$. When this happens the cosine factors are 0 and atan2 is undefined. This is however of no consequence as no laser processes can run with an incident angle of 90°.

# Appendix IV

# The maximum joint velocities for the industrial robot and scanner cutting head

To evaluate if the repositioning between two robot configurations in a given period of time saturates the joint speeds of the kinematic system it is necessary to find the maximum allowable joint speeds for the individual joints on the entire kinematic chain. As described in section 3.3.2 two mechanical components defines the kinematic chain; An industrial robot, a scanner mirror driven Cutting head. As the cutting head is not yet purchased the maximum joint velocities depend on the final configuration of the head and the purchased components. The industrial robot is however acquired and described in section I. To ensure a uniform naming convention the variables describing the joint states are named as in section 3.3.2.

- $\theta_i$ - The joint angle associated with joint i of the industrial robot
- $\psi$ -The DOE rotation angle
- $\phi_k$ - The deflection angle from the deflection mirrors, where k is the scanner mirror number
- $\delta$ - focus adjustment distance

If the maximum velocity of these joints are named the following way;

- $\dot{\theta}_{i_{max}}$ - The maximum joint velocity associated with joint i of the industrial robot

- $\dot{\psi}_{max}$ - The maximum angular velocity of the DOE rotator
- $\dot{\phi}_{k_{max}}$ - The maximum angular velocity of the rotation of the deflection mirrors, where k is the scanner mirror number
- $\dot{\delta}_{max}$ - focus adjustment linear velocity

As the Industrial robot is already specified the maximum angular velocities are given by: The beam rotator is based on a faulhaber 4490H048B motorwhich,

| i | 1 | 2 | 3 | 4 | 5 | 6 |
|---|---|---|---|---|---|---|
| $\dot{\theta}_{i_{max}}$ | 136°/s | 130°/s | 120°/s | 292°/s | 258°/s | 284°/s |

at rated voltage runs at around 9700 RPM unloaded. If it is assumed that it runs unloaded due to the small inertia of the DOE and if the gearing ration of 1:30 is taken into account and a conversion between seconds and minuts is applied the maximum angular velocity is found to be:

$$\dot{\psi}_{max} = 1940°/s \tag{IV.1}$$

(IV.2)

When considering the remaining values $\dot{\phi}_{k_{max}}$ and $\dot{\delta}_{max}$ it is clear that as they still on a concept level they are unspecified. However for an assessment of the maximum speed the datasheets for the Cambrdige optics Lightning LXP scanning head has been used [119]. Here it is seen that the maximum jump velocity is 16 m/s with typical operation speed of 6.5m/s. If 500 mm focal length after the final mirror is assumed this gives a maximum speed of 1833°/s

| i | 1 | 2 |
|---|---|---|
| $\dot{\phi}_{k_{max}}$ | 1833°/s | 1833°/s |

When considering $\dot{\delta}_{max}$ solutions exist that offers very high speed focus shifts. Some of which offers focus shift speeds of up to 30m/s [107, 119]. It is however unclear to what extent these solutions are applicable when considering that ROBOCUT uses a DOE in the collimated beamopath. This is due to the fact that often these products work by enlarging the diameter of the collimated beam. This is however compatible with ROBOCUT as the DOEs are designed for specific beamwidths. This has entailed that it has been chosen to operate with a focus shift speed that operates at a rate of 1 m/s which generally can be obtained by a traditional linear actuator.

$$\dot{\delta}_{max} = 1m/s \tag{IV.3}$$

(IV.4)

| $\dot{\theta}_{1_{max}}$ | $\dot{\theta}_{2_{max}}$ | $\dot{\theta}_{3_{max}}$ | $\dot{\theta}_{4_{max}}$ | $\dot{\theta}_{5_{max}}$ |
|---|---|---|---|---|
| 136°/s | 130°/s | 120°/s | 292°/s | 258°/s |
| $\dot{\theta}_{6_{max}}$ | $\dot{\psi}_{max}$ | $\dot{\phi}_{1_{max}}$ | $\dot{\phi}_{2_{max}}$ | $\dot{\delta}_{max}$ |
| 284°/s | $1940°/s$ | 1833°/s | 1833°/s | 1m/s |

All of these maximum joint variables are summarised in the following table:

It should however be noted the chosen values should be reviewed when a system is acquired. It should also be noted that it is assumed that the speed in the maximum velocity in the positive direction equals the maximum velocity in the negative direction for all joints

# Papers

# Paper A

# Flexible Laser Metal Cutting - An Introduction to the ROBOCUT Laser Cutting Technique

Sigurd Villumsen, Steffen Nordahl Joergensen and Morten Kristiansen

The paper has been published in the
*Proceedings of the 7th World Conference on Mass Customization* pp. 217-228, 2014.

# Paper B

# Optimizing Tracking Performance of XY Repositioning System with ILC

Sigurd Villumsen and Casper Schou

The paper has been published in the
*Recent Advances in Mechanism Design for Robotics.Proceedings of the 3rd IFToMM Symposium on Mechanism Design for Robotics* vol.33, pp. 207-217, 2015.

# Paper C

# Angular Stability Margins for the Remote Fusion Cutting Process

Sigurd Villumsen and Morten Kristiansen

The paper has been published in the
*Physics Procedia (2015) 15th Nordic Laser Materials Processing Conference*
vol.78 , pp. 89 - 98, 2015.

# Paper D

# Theoretical Limits of Accuracy of Industrial Robots With Scanner Heads for Remote Laser Cutting

Sigurd Villumsen and Morten Kristiansen

The paper has been published in the
*Proceedings of the 2nd AAU Workshop on Robotics 2013*

# Paper E

# Modelling of the Remote Fusion Cutting Process Based on Experiments

Morten Kristiansen, Sigurd Villumsen and Flemming O. Olsen

The paper has been published in the
*Physics Procedia (2015) 15th Nordic Laser Materials Processing Conference*
vol.78, pp. 110 - 119, 2015.

# Paper F

# PRM based path planning along end effector path for redundant robotic laser processing machinery with scanner mirrors

Sigurd Lazic Villumsen, Stephen F. Smith, Morten Kristiansen

Scheduled for later publication

# Paper G

# A framework for task sequencing for redundant robotic remote laser processing equipment based on redundancy space sampling

Sigurd Lazic Villumsen, Stephen F. Smith, Morten Kristiansen

Scheduled for later publication

# Paper H

# On the stability of remote laser cutting with customized beam patterns

Sigurd Lazic Villumsen, Morten Kristaiansen and Flemming O. Olsen

Abstract accepted at the 9th international conference on Photonic Technologies 2016 (LANE 2016)

# References


[1] Al-Sulaiman, F., Yilbas, B., and Ahsan, M. Co 2 laser cutting of a carbon/carbon multi-lamelled plain-weave structure. *Journal of materials processing technology 173*, 3 (2006), 345–351.

[2] Alatartsev, S. *Robot Trajectory Optimization for Relaxed Effective Tasks*. PhD thesis, Otto-von-Guericke-Universität Magdeburg, 2015.

[3] Allen-Bradley. Rockwell automation, kinetix 3 component servo drives. `http://literature.rockwellautomation.com/idc/groups/literature/documents/um/2071-um001_-en-p.pdf`. Accessed: 20-December-2015.

[4] Angel, E., and Shreiner, D. *Interactive Computer Graphics: A Top-Down Approach with Shader-Based OpenGL*, 6th ed. Addison-Wesley Publishing Company, USA, 2011.

[5] ANORAD. Rockwell automation, lc series linear motors user manual. `http://literature.rockwellautomation.com/idc/groups/literature/documents/um/lc-um001_-en-p.pdf`. Accessed: 20-December-2015.

[6] Applegate, D. L., Bixby, R. E., Chvatal, V., and Cook, W. J. *The Traveling Salesman Problem: A Computational Study (Princeton Series in Applied Mathematics)*. Princeton University Press, Princeton, NJ, USA, 2007.

[7] Arimoto, S., Kawamura, S., and Miyazaki, F. Bettering operation of robots by learning. *Journal of Robotic Systems 1*, 2 (1984), 123–140.

[8] Åström, K. J., and Hägglund, T. The future of pid control. *Control engineering practice 9*, 11 (2001), 1163–1175.

[9] Beckhoff. Beckhoff ads structure. `http://www.beckhoff.com/`. Accessed: 14-December-2015.

[10] Berenson, D., and Srinivasa, S. S. Probabilistically complete planning with end-effector pose constraints. In *Robotics and Automation (ICRA), 2010 IEEE International Conference on* (2010), IEEE, pp. 2724–2730.

[11] Berenson, D., Srinivasa, S. S., Ferguson, D., and Kuffner, J. J. Manipulation planning on constraint manifolds. In *Robotics and Automation, 2009. ICRA'09. IEEE International Conference on* (2009), IEEE, pp. 625–632.

[12] Bertsekas, D. P. *Dynamic Programming and Optimal Control*, 2nd ed. Athena Scientific, 2000.

[13] Chen, S. The effects of gas composition on the $co_2$ laser cutting of mild steel. *Journal of Materials Processing Technology 73*, 1–3 (1998), 147 – 159.

[14] Chiaverini, S., Oriolo, G., and Walker, I. Kinematically redundant manipulators. In *Springer Handbook of Robotics*, B. Siciliano and O. Khatib, Eds. Springer Berlin Heidelberg, 2008, pp. 245–268.

[15] Cohen, J. D., Lin, M. C., Manocha, D., and Ponamgi, M. I-collide: An interactive and exact collision detection system for large-scale environments. In *Proceedings of the 1995 symposium on Interactive 3D graphics* (1995), ACM, pp. 189–ff.

[16] Conkur, E. S., and Buckingham, R. Clarifying the definition of redundancy as used in robotics. *Robotica 15* (1997), 583–586.

[17] Corke, P. I. *Robotics, Vision & Control: Fundamental Algorithms in Matlab*. Springer, 2011.

[18] Dewil, R., Vansteenwegen, P., Cattrysse, D., Laguna, M., and Vossen, T. An improvement heuristic framework for the laser cutting tool path problem. *International Journal of Production Research 53*, 6 (2015), 1761–1776.

[19] Dowden, J. *The Theory of Laser Materials Processing: Heat and Mass Transfer in Modern Technology*. Springer Series in Materials Science. Springer Netherlands, 2009.

[20] Durbin, R. An analogue approach to the travelling salesman. *Nature 326* (1987), 16.

[21] E. Rohmer, S. P. N. Singh, M. F. V-rep: a versatile and scalable robot simulation framework. In *Proc. of The International Conference on Intelligent Robots and Systems (IROS)* (2013).

[22] Edan, Y., Flash, T., Peiper, U. M., Shmulevich, I., and Sarig, Y. Near-minimum-time task planning for fruit-picking robots. *Robotics and Automation, IEEE Transactions on 7*, 1 (1991), 48–56.

[23] Edwards, C. H., and Penney, D. E. *Calculus and analytic geometry / C.H. Edwards, Jr., David E. Penney*, 6th edition ed. ed. Prentice-Hall Englewood Cliffs, N.J, 2002.

[24] Ehmann, S. A., and Lin, M. C. Accelerated proximity queries between convex polyhedra by multi-level voronoi marching. In *Intelligent Robots and Systems, 2000.(IROS 2000). Proceedings. 2000 IEEE/RSJ International Conference on* (2000), vol. 3, IEEE, pp. 2101–2106.

[25] Erdős, G., Kemény, Z., Kovács, A., and Váncza, J. Planning of remote laser welding processes. *Procedia CIRP 7* (2013), 222–227.

[26] Erdős, G., Kardos, C., Kemény, Z., Kovács, A., and Váncza, J. Process planning and offline programming for robotic remote laser welding systems. *International Journal of Computer Integrated Manufacturing 0*, 0 (0), 1–20.

[27] Eriksson, I., Powell, J., and Kaplan, A. F. H. Measurements of fluid flow on keyhole front during laser welding. *Science and Technology of Welding and Joining 16*, 7 (2011), 636–641.

[28] Farrokhi, F., Nielsen, S., Schmidt, R., Pedersen, S., and Kristiansen, M. Effect of cut quality on hybrid laser arc welding of thick section steels. *Physics Procedia 78* (2015), 65–73.

[29] Farrokhi, F., Nielsen, S., Schmidt, R., Pedersen, S., and Kristiansen, M. Effect of cut quality on hybrid laser arc welding of thick section steels. *Physics Procedia 78* (2015), 65 – 73. 15th Nordic Laser Materials Processing Conference, Nolamp 15.

[30] Fomin, V., Gapontsev, V., Shcherbakov, E., Abramov, A., Ferin, A., and Mochalov, D. 100 kw cw fiber laser for industrial applications. In *Laser Optics, 2014 International Conference* (June 2014), pp. 1–1.

[31] Foulloy, L., Kechemair, D., Burg, B., Lamotte, E., and Zavidovique, B. A rule based decision system for the robotization or metal laser cutting. In *Robotics and Automation. Proceedings. 1985 IEEE International Conference on* (Mar 1985), vol. 2, pp. 192–197.

[32] Glass, K., Colbaugh, R., Lim, D., and Seraji, H. Real-time collision avoidance for redundant manipulators. *Robotics and Automation, IEEE Transactions on 11*, 3 (1995), 448–457.

[33] GmbH, K. R. kr120 datasheet. http://www.kuka-robotics.com/en/products/industrial_robots/high/pro/kr120_r2500_pro/. Accessed: 14-December-2015.

[34] Grundfos. Project partner "grundfos". https://www.grundfos.com/. Accessed: 14-December-2015.

[35] Gueta, L. B., Chiba, R., Ota, J., Ueyama, T., and Arai, T. Coordinated motion control of a robot arm and a positioning table with arrangement of multiple goals. In *Robotics and Automation, 2008. ICRA 2008. IEEE International Conference on* (2008), IEEE, pp. 2252–2258.

[36] Hace, A., Rodic, M., Terbuc, M., and Jezernik, K. Robust motion control and trajectory planning for planar laser cutting system. In *5th International Workshop on Advanced Motion Control* (1998), pp. 53 –58.

[37] Hamamatsu. Lcos-slm (liquid crystal on silicon - spatial light modulator datasheet). http://www.hamamatsu.com/jp/en/X10468-07.html. Accessed: 20-December-2015.

[38] Hansen, K., Kristiansen, M., and Olsen, F. Beam shaping to control of weldpool size in width and depth. *Physics Procedia 56* (2014), 467–476.

[39] Hansen, K., Kristiansen, M., and Olsen, F. Beam shaping to control of weldpool size in width and depth. *Physics Procedia 56* (2014), 467 – 476. 8th International Conference on Laser Assisted Net Shape Engineering {LANE} 2014.

[40] Hansen, K., Olsen, F., Kristiansen, M., and Madsen, O. Design of measurement equipment for high power laser beam shapes. In *The 14th Nordic Laser Materials Processing Conference NOLAMP 14* (2013), pp. 293–304.

[41] Hansen, K. S., Olse, F. O., Kristiansen, M., and Madsen, O. Design of measurement equipment for high power laser beam shapes. In *Proceedings of The 14th Nordic Laser Materials Processing Conference NOLAMP 14* (2013), A. Kaplan and H. Engström, Eds.

[42] Hatwig, J., Minnerup, P., Zaeh, M., and Reinhart, G. An automated path planning system for a robot with a laser scanner for remote laser cutting and welding. In *Mechatronics and Automation (ICMA), 2012 International Conference on* (Aug 2012), pp. 1323–1328.

[43] Hatwig, J., Reinhart, G., and Zaeh, M. F. Automated task planning for industrial robots and laser scanners for remote laser beam and cutting. *Production Engineering. Research and Development* (1 July 2010).

[44] Hatwig, J., Reinhart, G., and Zaeh, M. F. Automated task planning for industrial robots and laser scanners for remote laser beam welding and cutting. *Production Engineering 4*, 4 (2010), 327–332.

[45] Helsgaun, K. An effective implementation of the lin–kernighan traveling salesman heuristic. *European Journal of Operational Research 126*, 1 (2000), 106 – 130.

[46] Helsgaun, K. Solving the equality generalized traveling salesman problem using the lin–kernighan–helsgaun algorithm. *Mathematical Programming Computation 7*, 3 (2015), 269–287.

[47] Herwig, P., and Wetzig, A. *REMOTE LASER CUTTING OF METALLIC MATERIALS*. Fraunhofer Institute for Material and Beam Technology IWS.

[48] Hollerbach, J. M., and Suh, K. C. Redundancy resolution of manipulators through torque optimization. *Robotics and Automation, IEEE Journal of 3*, 4 (1987), 308–316.

[49] Homburg, O., Bayer, A., Mitra, T., Meinschien, J., and Aschke, L. Beam shaping of high power diode lasers benefits from asymmetrical refractive micro-lens arrays. In *Lasers and Applications in Science and Engineering* (2008), International Society for Optics and Photonics, pp. 68760B–68760B.

[50] II, B. J. P. Mass customization: The new frontier in business competition, boston. *Harvard Business School Press* (1993).

[51] Industri, I. A. Project partner "ib andresen industri". `http://www.iai.dk/`. Accessed: 14-December-2015.

[52] innovation foundation, D. Danish innovation foundation (previously known as højteknologifonden). `http://innovationsfonden.dk`. Accessed: 14-December-2015.

[53] IPU. Project partner "ipu". `http://www.ipu.dk/`. Accessed: 14-December-2015.

[54] ISO, E. 9283: 1998. *Manipulating industrial robots-Performance criteria and related test methods* (1998).

[55] Ivarson, A., Powell, J., and Magnusson, C. The role of oxidation in laser cutting stainless and mild steel. *Journal of Laser Applications 3*, 3 (1991), 41–45.

[56] Kaakkunen, J. J. J., Laakso, P., and Kujanpää, V. Adaptive multibeam laser cutting of thin steel sheets with fiber laser using spatial light modulator. *Journal of Laser Applications 26*, 3 (2014).

[57] Kah, P., Lu, J., Martikainen, J., and Suoranta, R. Remote laser welding with high power fiber lasers. *journal of Engineering 5*, 9 (2013), 700 – 706.

[58] Karaman, S., and Frazzoli, E. Incremental sampling-based algorithms for optimal motion planning. *arXiv preprint arXiv:1005.0416* (2010).

[59] Kim, C., Kim, J., Lim, H., and Kim, J. Investigation of laser remote welding using disc laser. *Journal of materials processing technology 201*, 1 (2008), 521–525.

[60] Kolakowska, E. *Integrated Planning and Scheduling in Fully Automatic Robot System: PhD Thesis*. Aalborg Universitet, Institut for Produktion., 2009.

[61] Kovács, A. Task sequencing for remote laser welding in the automotive industry. In *23rd International Conference on Automated Planning and Scheduling (ICAPS)* (2013), A. Press, Ed.

[62] Kovács, A. Integrated task sequencing and path planning for robotic remote laser welding. *International Journal of Production Research* (2015), 1–15.

[63] Kristiansen, M., Selchau, J., Olse, F. O., and Hansen, K. S. Quality and performance of laser cutting with a high power sm fiber laser. In *NOLAMP 14* (2013), A. Kaplan and H. Engström, Eds.

[64] Kristiansen, M., Selchau, J., Olse, F. O., and Hansen, K. S. Quality and performance of laser cutting with a high power sm fiber laser. In *Proceedings of The 14th Nordic Laser Materials Processing Conference NOLAMP 14* (2013), A. Kaplan and H. Engström, Eds., pp. 109–120.

[65] Kristiansen, M., Selchau, J., Olsen, F., and Hansen, K. Quality and performance of laser cutting with a high power sm fiber laser. In *The 14th Nordic Laser Materials Processing Conference NOLAMP 14* (2013), pp. 109–120.

[66] Kristiansen, M., Villumsen, S., and Olsen, F. O. Modelling of the remote fusion cutting process based on experiments. *Physics Procedia 78* (2015), 110 – 119. 15th Nordic Laser Materials Processing Conference, Nolamp 15.

[67] Kuffner, J. J., and LaValle, S. M. Rrt-connect: An efficient approach to single-query path planning. In *Robotics and Automation, 2000. Proceedings. ICRA'00. IEEE International Conference on* (2000), vol. 2, IEEE, pp. 995–1001.

[68] Kuryntsev, S., and Gilmutdinov, A. The effect of laser beam wobbling mode in welding process for structural steels. *The International Journal of Advanced Manufacturing Technology* (2015), 1–9.

[69] Kuryntsev, S., and Gilmutdinov, A. Heat treatment of welded joints of steel 0.3c–1cr–1si produced by high-power fiber lasers. *Optics and Laser Technology 74* (2015), 125 – 131.

[70] Kuryntsev, S., and Gilmutdinov, A. Welding of stainless steel using defocused laser beam. *Journal of Constructional Steel Research 114* (2015), 305 – 313.

[71] LANE. international conference on photonic technologies (lane). `http://www.lane-conference.org/`. Accessed: 20-December-2015.

[72] laserfocusworld.com, S. U. Fiber laser revenues boost the 2013 laser market. `http://www.industrial-lasers.com/articles/print/volume-29/issue-1/features/fiber-laser-revenues-boost-the-2013-laser-market.html`. Accessed: 14-December-2015.

[73] Laskin, A., and Laskin, V. Controllable beam intensity profile for the tasks of laser material processing. paper 707. In *Proceeding of the Laser Materials Processing Conference 2012, Icaleo, LIA* (2012), pp. 270–276.

[74] LaValle, S. M. *Planning algorithms*. Cambridge university press, 2006.

[75] Li, L., and Mazumder, J. A study of the mechanism of laser cutting of wood. *Forest products journal (USA)* (1991).

[76] Mahrle, A., Luetke, M., and Beyer, E. Fibre laser cutting: beam absorption characteristics and gas-free remote cutting. *Proceedings of the Institution of Mechanical Engineering Part C-Journal of Mechanical Engineering Science 224*, C5, Sp. Iss. SI (2010), 1007–1018.

[77] MATLAB. Matlab programming documentation. `http://se.mathworks.com/help/`. Accessed: 20-December-2015.

[78] Mayer, A. Laser materials processing market reaches record high. *Advanced Optical Technologies 1*, 1 (2012).

[79] Mehta, J., and Bhirud, S. Image stitching techniques. In *Thinkquest 2010*, S. Pise, Ed. Springer India, 2011, pp. 74–80.

[80] Mersmann, O., Bischl, B., Bossek, J., Trautmann, H., Wagner, M., and Neumann, F. Local search and the traveling salesman problem: A feature-based characterization of problem hardness. In *Learning and Intelligent Optimization*. Springer, 2012, pp. 115–129.

[81] Michalos, G., Makris, S., Papakostas, N., Mourtzis, D., and Chryssolouris, G. Automotive assembly technologies review: challenges and outlook for a flexible and adaptive approach. *{CIRP} Journal of Manufacturing Science and Technology 2*, 2 (2010), 81 – 91.

[82] Müller, A., Goecke, S.-F., Sievi, P., Albert, F., and Rethmeier, M. Laser beam oscillation strategies for fillet welds in lap joints. *Physics Procedia 56* (2014), 458 – 466. 8th International Conference on Laser Assisted Net Shape Engineering {LANE} 2014.

[83] Musiol, J., Luetke, M., Schweier, M., Hatwig, J., Wetzig, A., Beyer, E., and Zaeh, M. F. Combining remote ablation cutting and remote welding: opportunities and application areas. In *Proc. SPIE* (2012), vol. 8239, pp. 82390Q–82390Q–14.

[84] Nakamura, Y., Hanafusa, H., and Yoshikawa, T. Task-priority based redundancy control of robot manipulators. *The International Journal of Robotics Research 6*, 2 (1987), 3–15.

[85] Noon, C. E., and Bean, J. C. An efficient transformation of the generalized traveling salesman problem. *INFOR 31*, 1 (1993), 39.

[86] Olse, F. O. Laser cutting from CO2-laser to disc- or fibre laser - possiblities and challenges. In *ICALEO* (2011).

[87] Olse, F. O. An evaluation of the cutting potential of different types of high power lasers. In *ICALEO 2006 Congress Proceeding* (November 2006).

[88] Olsen, F. O. Laser metal cutting with tailored beam patterns. In *Industrial Laser Solutions 17-19* (2011).

[89] Olsen, F. O., Hansen, K. S., and Nielsen, J. S. Multibeam fiber laser cutting. *Journal of Laser Applications 21*, 3 (Aug. 2009), 133–138.

[90] O'Neill, W., and Gabzdyl, J. New developments in laser-assisted oxygen cutting. *Optics and Lasers in Engineering 34*, 4–6 (2000), 355 – 367. Laser Material Processing.

[91] O'Neill, W., and Gabzdyl, J. New developments in laser-assisted oxygen cutting. *Optics and Lasers in Engineering 34*, 4–6 (2000), 355 – 367. Laser Material Processing.

[92] Oriolo, G., and Mongillo, C. Motion planning for mobile manipulators along given end-effector paths. In *Robotics and Automation, 2005. ICRA 2005. Proceedings of the 2005 IEEE International Conference on* (2005), IEEE, pp. 2154–2160.

[93] Oriolo, G., Ottavi, M., and Vendittelli, M. Probabilistic motion planning for redundant robots along given end-effector paths. In *Intelligent Robots and Systems, 2002. IEEE/RSJ International Conference on* (2002), vol. 2, IEEE, pp. 1657–1662.

[94] Padberg, M., and Rinaldi, G. A branch-and-cut algorithm for the resolution of large-scale symmetric traveling salesman problems. *SIAM review 33*, 1 (1991), 60–100.

[95] personvagnar, V. Project partner "volvo personvagnar". `http://www.volvocars.com/se`. Accessed: 14-December-2015.

[96] Pihlava, A., Purtonen, T., Salminen, A., Kujanpää, V., and Savinainen, T. Quality aspects in remote laser cutting. *Welding in the World 57*, 2 (2013), 179–187.

[97] Poole, H. H. *Fundamentals of robotics engineering*. Springer Science & Business Media, 2012.

[98] Powell, J., and Kaplan, A. A technical and commercial comparison of fiber laser and co2 laser cutting. In *Proceedings of ICALEO 2012* (2012), L. institute of america, Ed., Laser Institute of America.

[99] Powell, J., Petring, D., Kumar, R. V., Al-Mashikhi, S., Kaplan, A. F. H., and Voisey, K. T. The energy generated by the oxidation reaction during laser-oxygen cutting of mild steel. In *I ICALEO, 27th International Congress on Applications of Lasers and Electro-Optics* (October 20 - 23 2008), pp. 628–636.

[100] Reinelt, G. TSPLIB- a traveling salesman problem library. *ORSA Journal of Computing 3*, 4 (1991), 376–384.

[101] Reinhart, G., Munzert, U., and Vogl, W. A programming system for robot-based remote-laser-welding with conventional optics. *CIRP Annals - Manufacturing Technology 57*, 1 (2008), 37 – 40.

[102] Rexroth. Bosch-rexroth, indradrive cs technical specification. `http://www.boschrexroth.com/dcc/Vornavigation/Vornavi.cfm?Language=EN&PageID=p146994`. Accessed: 20-December-2015.

[103] roboter gmbh, K. Project partner "kuka roboter gmbh". `http://www.kuka-robotics.com/`. Accessed: 14-December-2015.

[104] Rosenkrantz, D. J., Stearns, R. E., and Philip M. Lewis, I. An analysis of several heuristics for the traveling salesman problem. *SIAM Journal on Computing 6*, 3 (1977), 563–581.

[105] Salvador, F., Holan, P. M. D., and Piller., F. Cracking the code of mass customization. *MIT Sloan Management Review 50*, 3 (2009), 70–79.

[106] Salvagnini. L3 laser cutter performance. `http://www.salvagninigroup.com/product/fiber-laser/l3/performances`. Accessed: 14-December-2015.

[107] ScanLab. Scanlab adjustable z axis for mounting on scanner system. `http://www.scanlab.de/en/products/z-axes-3d-add-ons/z-axis`. Accessed: 20-December-2015.

[108] Schäfer, P. Cutting at a distance. *ATZproduktion worldwide 3*, 2 (2010), 8–11.

[109] Schulz, W. E., Simon, G. G., Urbassek, H. M., and Decker, I. On laser fusion cutting of metals. *Journal of Physics D: Applied Physics 20*, 4 (1987).

[110] Seifert, M., Brenner, B., Tietz, F., and Beyer, E. Pioneering laser scanning system for hardening of turbine blades. In *Proceeding of the Laser Materials Processing Conference, Icaleo, LIA* (1999), vol. 87, pp. 252–261.

[111] Serway, R. A. *Physics for Scientists & engineers with Modern Physics*, fourth edition ed. Saunders College publishing, 1996.

[112] Siciliano, B. Kinematic control of redundant robot manipulators: A tutorial. *Journal of Intelligent and Robotic Systems 3*, 3 (1990), 201–212.

[113] Sobih, M., Crouse, P. L., and Li, L. Elimination of striation in laser cutting of mild steel. *Journal of Physics D: Applied Physics* (2007).

[114] SolidCam. Solidcam. `http://www.solidcam.com/`. Accessed: 14-December-2015.

[115] Steen, W., Watkins, K. G., and Mazumder, J. *Laser material processing*. Springer Science & Business Media, 2010.

[116] Stemmann, J., and Zunke, R. Robot task planning for laser remote welding. In *Operations Research Proceedings 2005*, H.-D. Haasis, H. Kopfer, and J. Schönberger, Eds., vol. 2005 of *Operations Research Proceedings*. Springer Berlin Heidelberg, 2006, pp. 729–734.

[117] Sullivan, A. B. D., and Houldcroft, P. T. Metal cutting by oxygen - assisted laser. *Optics Technology* (1967).

[118] Tabuchi, M., Watanabe, T., Kubo, K., Matsui, M., Kinugawa, J., and Abe, F. Creep crack growth behavior in the {HAZ} of weldments of w containing high cr steel. *International Journal of Pressure Vessels and Piping 78*, 11–12 (2001), 779 – 784.

[119] technology, C. Cambridge technology lxp$^{TM}$ scan heads. `http://www.camtech.com/index.php`. Accessed: 20-December-2015.

[120] Tönshoff, H., and Emmelmann, C. Laser cutting of advanced ceramics. *CIRP Annals-Manufacturing Technology 38*, 1 (1989), 219–222.

[121] `http://www.laserfocusworld.com`, S. U. Laser marketplace 2015: Lasers surround us in the year of light. `http://www.laserfocusworld.com/articles/print/volume-51/issue-01/features/laser-marketplace-2015-lasers-surround-us-in-the-year-of-light.html`. Accessed: 14-December-2015.

[122] VICTOR, B., FARSON, D., REAM, S., and WALTERS, C. Custom beam shaping for high-power fiber laser welding. *Welding journal 90*, 6 (2011).

[123] Villumsen, S., Joergensen, S., and Kristiansen, M. Flexible laser metal cutting: An introduction to the robocut laser cutting technique. In *Proceedings of the 7th World Conference on Mass Customization, Personalization, and Co-Creation (MCPC 2014), Aalborg, Denmark, February 4th - 7th, 2014*, T. D. Brunoe, K. Nielsen, K. A. Joergensen, and S. B. Taps, Eds., Lecture Notes in Production Engineering. Springer International Publishing, 2014, pp. 217–228.

[124] Villumsen, S., and Kristiansen, M. Theoretical limits of accuracy of industrial robots with scanner heads for remote laser cutting. In *AAU workshop on robotics* (2013).

[125] Villumsen, S., and Kristiansen, M. Angular stability margins for the remote fusion cutting process. *Physics Procedia 78* (2015), 89 – 98. 15th Nordic Laser Materials Processing Conference, Nolamp 15.

[126] Villumsen, S., and Kristiansen, M. A framework for task sequencing for redundant robotic remote laser processing equipment based on redundancy space sampling. In *Unpublished* (2016).

[127] Villumsen, S., and Kristiansen, M. Prm based pathplanning along end effector path for redundant robotic laser processing machinery with scanner mirrors. In *Unpublished* (2016).

[128] Villumsen, S., Kristiansen, M., and Olsen, F. O. On the stability of remote laser cutting with customised beam patterns. In *Unpublished - Abstract accepted for presentation at the 9th international conference on Photonic Technologies 2016 (LANE 2016)* (2016).

[129] Villumsen, S., and Schou, C. Optimizing tracking performance of xy repositioning system with ilc. In *Recent Advances in Mechanism Design for Robotics*, S. Bai and M. Ceccarelli, Eds., vol. 33 of *Mechanisms and Machine Science*. Springer International Publishing, 2015, pp. 207–217.

[130] Wandera, C., Salminen, A., and Kujanpaa, V. Inert gas cutting of thick-section stainless steel and medium-section aluminum using a high power fiber laser. *Journal of laser applications 21*, 3 (2009), 154–161.

[131] Wessel, J. K. *The handbook of advanced materials: enabling new designs*. John Wiley & Sons, 2004.

[132] Yang, H., and Shao, H. Distortion-oriented welding path optimization based on elastic net method and genetic algorithm. *Journal of Materials Processing Technology 209*, 9 (2009), 4407 – 4412.

[133] Zaeh, M. F., Hatwig, J., Musiol, J., Roesch, O., and Reinhart, G. Analysis of the accuracy of industrial robots and laser scanners for remote laser beamwelding and cutting. In *Robotics (ISR), 2010 41st International Symposium on and 2010 6th German Conference on Robotics (ROBOTIK)* (June 2010), pp. 1–8.

[134] Zaeh, M. F., Moesl, J., Musiol, J., and Oefele, F. Material processing with remote technology revolution or evolution? *Physics Procedia 5, Part A*, 0 (2010), 19 – 33. Laser Assisted Net Shape Engineering 6, Proceedings of the LANE 2010, Part 1.

[135] Zhou, K., Khargonekar, P. P., Stoustrup, J., and Niemann, H. H. Robust performance of systems with structured uncertainties in state space. *Automatica 31*, 2 (1995), 249–255.

[136] Ziegler, J. G., and Nichols, N. B. Optimum settings for automatic controllers. *trans. ASME 64*, 11 (1942).

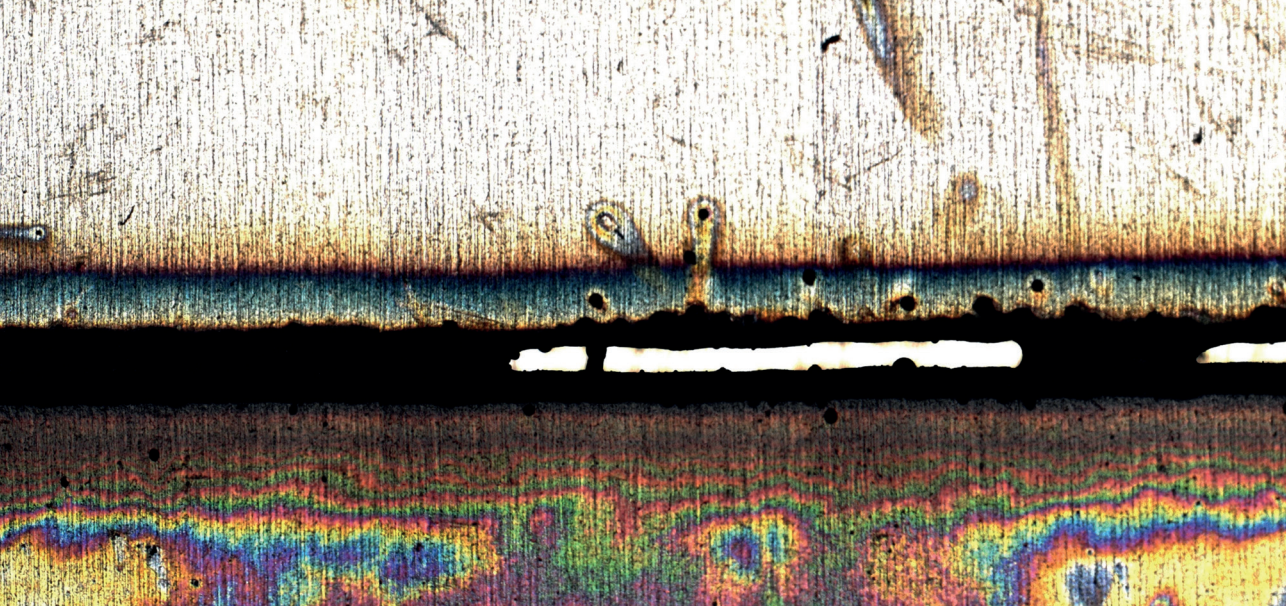

# SUMMARY

This dissertation is written as a part of the ROBOCUT project which concerns the development of a new laser cutting technology that seeks to increase the performance of traditional and remote laser cutting by using beam shaping technologies. The resulting customized beam patterns are obtained by using a diffractive optical element (DOE).

The main work of this dissertation falls within three areas of focus.

The first area of focus covers the development of a flexible laser processing laboratory for DOE cutting. A laboratory was created with a single mode fiber laser used for DOE cutting and an industrial robot and XY table for positioning the laser beam.

The second area of focus covers the establishment of a benchmark with which the performance of the ROBOCUT technology could be evaluated. It was chosen to use remote fusion cutting as a benchmark for this evaluation. It was shown through several experimental series that ROBOCUT cutting performed significantly better when concerning stability than RFC.

The third and final area of focus concerns the development of a framework for task sequencing and path planning for remote laser processing. The developed framework was based on sampling the redundant axes of the laser cutting system and transforming the sequencing problem into a generalized traveling salesman problem (GTSP).

ISSN (online): 2246-1248
ISBN (online): 978-87-7112-539-9

AALBORG UNIVERSITY PRESS